Design and Control Considerations for a Skid-to-Turn Unmanned Aerial Vehicle

A Thesis
Presented to the Faculty of
California Polytechnic State University
San Luis Obispo

In Partial Fulfillment
Of the Requirements for the Degree of
Master of Science in Aerospace Engineering

By
Tanner Austin Sims
May 2009

Approval Page

TITLE: Design and Control Considerations for a Skid-to-Turn Unmanned Aerial Vehicle

AUTHOR: Tanner Austin Sims

DATE SUBMITTED: May 2009

COMMITTE CHAIR : Daniel Biezad, PhD

COMMITTEE MEMBER: Eric Mehiel, PhD

COMMITTEE MEMBER: Jordi Puig-Suari, PhD

COMMITTEE MEMBER: Alberto Jimenez, PhD

Abstract

Design and Control Considerations for a Skid-to-Turn Unmanned Aerial Vehicle

Tanner Austin Sims

The use of Unmanned Aerial Vehicles (UAVs) are rapidly expanding and taking on new roles in the military. In the area of training and targeting vehicles, control systems are expanding the functionality of UAVs beyond their initially designed purpose. Aeromech Engineering's NXT UAV is a high speed target drone that is intended to simulate a small aircraft threat. However, in the interest of increasing functionality, enabling NXT to accomplish wings level skidding turns provides the basis for a UAV that can simulate a threat from a missile. Research was conducted to investigate the aerodynamic and performance characteristics of a winged vehicle performing high acceleration skidding turns. Initially, a linear model was developed using small disturbance theory. The model was further improved by developing a six degree of freedom simulation. A controller using four loop closures and utilizing both rudder and aileron for control was developed. Any outside guidance system that navigates using a heading command can easily be integrated into this controller design. Simulations show this controller enables the NXT UAV to accomplish up to 3 G wings level skidding turns. Further testing, showed that the controller was able to tolerate significant turbulence, sensor noise, loop failures and changes within the plant dynamics. This research shows how it is possible for a winged UAV to easily maneuver using wings level skid turns.

Acknowledgements

The idea for this research was provided by Aeromech Engineering. I want to thank them for their cooperation in this project. I would especially like to thank two engineers, Patrick Stewart and Nick Brake, for their assistance.

I want to express my deepest appreciation to my advisor, Dr. Biezad, for his guidance and support in this research. His unique personality and unconventional teaching style provided a real life prospective of engineering that simply cannot be taught from a textbook. I would also like to thank the rest of my committee for their input into this project.

Finally, I want to thank my family for their never ending support. I have two remarkable parents and a brother that have shown me how to work hard and explore the world around me. Only with their help, has it been possible for this farm kid from Kansas to embrace the many adventures that life brings.

Table of Contents

Table of Tables

Table of Figures

Nomenclature

A – Plant Matrix
AR – Aspect Ratio
AVL – Athena Vortex Lattice
a – Acceleration
B – Control Matrix
BTT – Bank-to-Turn
b – Reference Wing Span
C – Coefficient
– Output Matrix
c – Reference Chord Length
D – Feed-forward Matrix
e – Efficiency Factor
G – Dynamic System
g – Acceleration Due to Gravity
I – Moment of Inertia
L – Dimensional Rolling Moment Stability Derivative
l – Rolling Moment along $\hat{i}$ in Body Coordinates
M – Dimensional Pitching Moment Stability Derivative
m – Pitching Moment along $\hat{j}$ in Body Coordinates
– Mass of the Vehicle
N – Dimensional Yawing Moment Stability Derivative
n – Yawing Moment along $\hat{i}$ in Body Coordinates
PD – Proportional-Derivative
PI – Proportional-Integral
PID – Proportional-Integral-Derivative
p – Roll Rate along $\hat{i}$ in Body Coordinates
Q – Dynamic Pressure
q – Pitch Rate along $\hat{j}$ in Body Coordinates
r – Pitch Rate along $\hat{k}$ in Body Coordinates
S – Reference Wing Area
STT – Skid-to-Turn
s – Variable in the Frequency Domain
u – Velocity along $\hat{i}$ in Body Coordinates
– Control Vector
V – Velocity
v – Velocity along $\hat{j}$ in Body Coordinates
w – Velocity along $\hat{k}$ in Body Coordinates
X – Force along $\hat{i}$ in Body Coordinates
– Dimensional Force Stability Derivative

x – State Vector
Y – Force along $\hat{j}$ in Body Coordinates
– Dimensional Force Stability Derivative
Z – Force along $\hat{k}$ in Body Coordinates
– Dimensional Force Stability Derivative
α – Angle of Attack
β – Sideslip Angle
Δ – Perturbation
δr – Rudder Deflection
δa – Aileron Deflection
δc – Control Deflection
δha – Horizontal Stabilizer Aileron Deflection
δLHZ – Left Horizontal Tail Control Flap Deflection
δLW – Left Wing Control Flap Deflection
δRHZ – Right Horizontal Tail Control Flap Deflection
δRW – Right Wing Control Flap Deflection
δV – Vertical Tail Control Flap Deflection
δwa – Wing Aileron Deflection
ζ – Damping ratio
η – Load Factor
θ – Pitch Angle
λ – Eigenvalue
τ – Time Constant
ϕ – Bank Angle
ψ – Heading Angle
ω – Frequency

Subscripts
0 – Initial or Constant Value
c – Compensator
comm – Commanded Value
D – Drag
d – Damped Frequency
f – Filter
L – Lift
l – Rolling Moment
m – Pitching Moment
n – Natural Frequency
– Yawing Moment
p – Partial Derivative with Respect to Rolling Moment
r – Partial Derivative with Respect to Yaw Rate
roll – Roll Mode

spiral – Spiral Mode
STT – Skid-to-Turn
v – Partial Derivative with Respect to Side Velocity
x – In the X Direction
Y – Side Force
y – In the Y Direction
z – In the Z Direction
δa – Partial Derivative with Respect to Aileron Deflection
δr – Partial Derivative with Respect to Rudder Deflection

Chapter 1: Introduction

1.1 Background

The modern aerial battlefield is progressively being dominated by the rapid expansion of unmanned aerial vehicles (UAVs). These unique systems are providing capabilities that are slowly reducing and replacing the need for certain types of manned aircraft. Aspects of aerial warfare, such as reconnaissance, strike and even pilot training have evolved to incorporate the use of these systems. Unmanned aerial vehicles combine the technologies developed by the Wright Brothers, Sperry and Marconi.

Elmer Sperry was the first to realize that an autonomous aircraft would require some form of gyroscopic stabilization. In the summer of 1916 Sperry and Peter Hewitt successfully demonstrated the concept of an unmanned autonomous bomb to both the United States Navy and Army.[1] This proved to be the first steps toward guided munitions that dominate modern war.

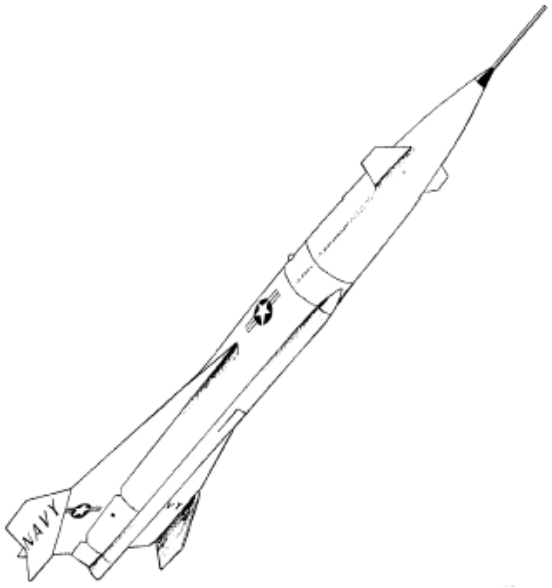

Figure 1-1: AQM-37C Rocket Powered Target Drone[2]

Advances in aerial threats throughout the decades always necessitate new tools to train the military in combating these weapons. Unmanned aerial technology also provides an excellent platform to simulate the dynamics of emerging threats. One of the more advanced target drones that is used to simulate high speed missiles is the AQM-37C. Initially developed in 1962 by the Navy, this rocket propelled target drone is capable of altitudes up to 100,000 ft. with flight speeds ranging from Mach 0.7 to Mach 4.0.[2] A significant disadvantage of this system is that it is non- recoverable and is a single role vehicle.

In today's military, cost effectiveness and multiuse platforms are highly desired both as weapons and training devices. Cold War era weapons programs are being phased out in favor of more adaptable technology. In the field of target drones, unmanned aircraft are being deployed to provide a larger array of training possibilities. An example of a potentially cost effective multi-role training UAV would be a recoverable drone that has the capability of simulating both aircraft and missile threats. Such a design would require the vehicle capable of flight dynamics that are not usually performed by aircraft.

1.2 Turning Aerodynamic Vehicles

A majority of aerodynamic vehicles use the basic principle of banking the wings to rotate the lift vector towards the center of rotation during a turn. Rudder is simultaneously applied to produce a condition where the projection of the vector sum of forces, both aerodynamic and gravitational, is zero in the spanwise direction of the aircraft. This particular condition is known as coordination. Operating an aircraft in this manner produces a highly efficient means of maneuverability to ridged aerodynamic

vehicles. Coordination allows the velocity vector to remain tangent to the curvature of the flight path which subsequently minimizes drag during the turn.

Rudder deflections depend on the aerodynamic forces generated from the aircraft's geometry. Aircraft using ailerons for roll control experience a condition where the outside wing in a turn produces more drag, due to the downward control deflection, subsequently creating an adverse yawing moment to the direction of the turn. Conversely, spoiler controlled aircraft generate a proverse yawing moment, more drag on the inside wing, which yaws the aircraft towards the inside of the turn. When the velocity vector is directed towards the outside of the turn, the aircraft is said to be in a slipping condition. Opposite of a slip, when the velocity vector is directed towards the inside of the turn, the airplane is in a skidding condition. Normally, appropriate rudder deflection is applied to maintain coordination.

1.3 Cross Coordination

Situations arise where aircraft must use uncoordinated maneuvers to safely operate. The two most common cross coordinated maneuvers are a forward slip and a sideslip (Figure 1-2). In a forward slip, the pilot applies a large amount of rudder to yaw the aircraft at an angle to the relative wind. Opposite aileron is applied to provide enough bank angle to counteract any turning tendency and maintain the original ground track. By presenting a larger cross sectional area to the oncoming flow, an aircraft in a forward slip significantly increases drag. This maneuver is used as a method to rapidly descend without increasing airspeed.

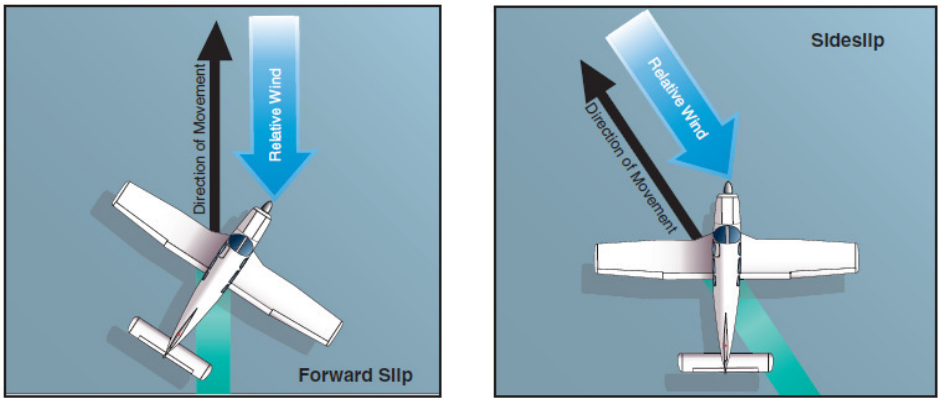

Figure 1-2: Aircraft in a Forward Slip (Left) and Sideslip (Right)[3]

The second cross coordinated maneuver is the sideslip which is used to combat crosswinds during landing. For this procedure, the pilot banks the aircraft into the wind such that the resulting lift vector cancels out the crosswind component. Opposite rudder is used to counteract a turn and maintain the aircraft's fuselage centerline parallel to the runway.

There is an additional uncoordinated maneuver, a skid turn, which can be performed. In a skidding turn, the pilot applies rudder with enough opposite aileron to maintain wings level. While all aircraft use bank-to-turn (BTT) maneuvering schemes, missiles (non-ballistic) do not necessarily use bank-to-turn control. In general, smaller tactical missiles such as the AIM-7 Sparrow use a skid-to-turn (STT) control scheme[4].

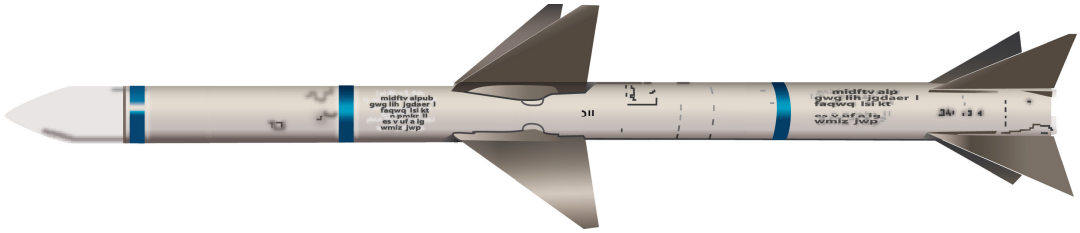

Figure 1-3: AIM-7 Sparrow Missile[5]

These types of weapons are intended for short range air-to-air or air-to-ground attack. Tactical missiles do not have a need for large wings because of their short distance

mission profile. The lack of a large primary lifting surface negates the need for a tactical missile to bank during its turns. Instead, these missiles use a combination of aerodynamic surfaces and thrust vectoring to yaw the missile onto its intended trajectory. Even some BTT missiles use a hybrid BTT and STT control scheme with smaller heading corrections using the STT control scheme[6].

1.4 NXT Unmanned Aerial Vehicle

Aeromech Engineering has developed a high speed UAV, called NXT, that is being used as a research vehicle to develop low cost targeting solutions (Fig. 1-4). The intended use of the NXT is to carry a laser based targeting counter that can track the number and accuracy of kills made on the vehicle. This type of UAV is suitable to simulate an aerial threat from a UAV or a larger aircraft that has a lower radar cross sectional area. A small reusable UAV, such as the NXT, provides a very cheap platform for this type of work.

TOGW	200	lbs
Empty Weight	90	lbs
Payload	30	lbs
Fuel Load	100	lbs
Wing Span	5	ft
Length	8.4	ft
Cruise Speed	300-350	kts
Endurance	1.25	hr
Dash Speed	400	kts
Service Ceiling	25,000	ft

Table 1-1: NXT Specifications and Performance

One area of research for this particular vehicle is to extend its capabilities by having NXT fly like a tactical missile. As designed, the NXT uses the Cloud Cap Piccolo autopilot for maneuvering with BTT control laws. By implementing a set of STT control laws, NXT would have the capability to fly like a UAV and a missile. This provides a single reusable system that has a multifunctional role.

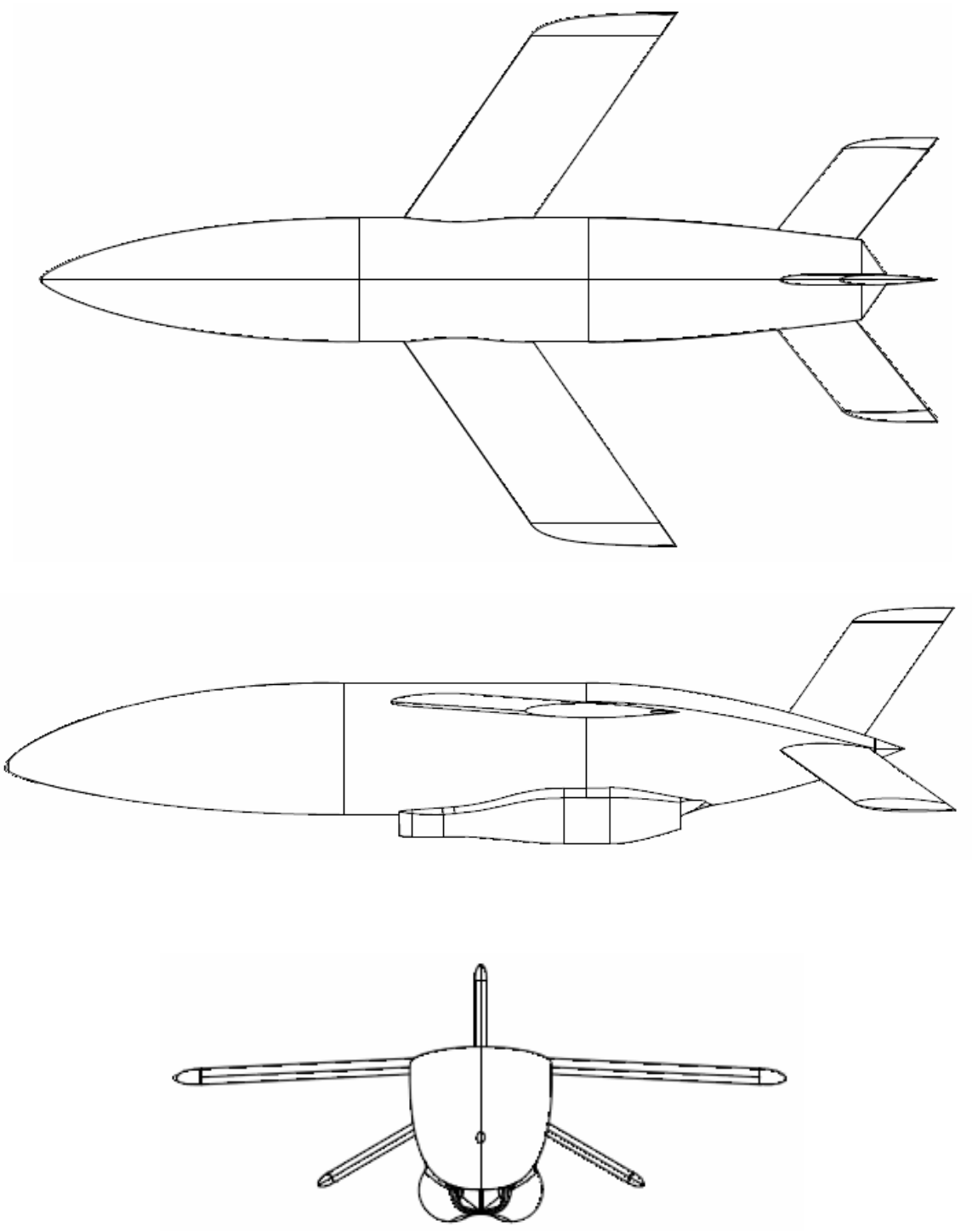

Figure 1-4: NXT Target Vehicle Three View

1.5 Objective

Aeromech Engineering's NXT is a highly agile and capable vehicle that performs well as an aircraft. Extending the envelope of capabilities to make NXT perform like a tactical missile will require extensive modeling and simulation before any STT control laws can be implemented into the autopilot system. Additionally, very little research has been applied towards taking 'airplane like' vehicles and maneuvering them in high G skidding turns.

The purpose of this thesis is to investigate the dynamics and performance characteristics, from a controls standpoint, of high speed UAVs in skidding turns and generate a set of control laws to accomplish these turns. As a case study, the NXT vehicle will be used as the UAV of interest, with the control laws being specifically designed for NXT.

The first objective is to look at the dynamics of a skidding turn and develop a set of design equations and performance metrics. This requires taking the six degree of freedom (6DOF) equations for rigid body mechanics, making appropriate assumptions and simplifying them to form the equations for skid turns. The second objective is to analyze the current capabilities of the NXT to perform a skidding turn to provide baseline data. Simple trade studies can then used to enhance the performance of the vehicle in an attempt to meet the design requirements. The next objective is to take a modified design of the NXT UAV and develop a set of classical control laws to enable STT guidance and control. Lastly, a nonlinear 6DOF flight dynamics simulation will be used to validate the control laws, refine the design, and allow for robustness analysis.

1.6 Design Requirements and Limitations

Before any design based project can begin, a set of requirements and limitations must be used to determine when the vehicle meets the desired characteristics. However, these requirements presented below are not intended to be used to judge the success or failure of the research, but rather provide upper end performance goals. In discussions with Aeromech Engineering, the only suggested guidelines were to remain within a specified bank angle tolerance while attempting up to an eight G skidding turn using the existing autopilot. These few requirements provided a framework but more substantial goals and tolerances are addressed in the following paragraphs.

Manned aircraft requirements have a firmly established precedence in performance and handling qualities research. The primary document governing these requirements is the Department of Defense publication, *Flying Qualities of Piloted Aircraft,* MIL-STD-1797[7]. While piloted aircraft requirements have been developed over the years of flight testing, UAVs are a new enough technology that basic requirements have not been developed. It is hard to define broad handling quality specifications for unmanned aircraft since the degree of autonomy varies between platforms. In the case of the NXT, full autonomous flight is possible; however, there could be situations where a pilot might have to fly in the loop. Because of this possibility, manned aircraft handling quality specifications will be applied along with customer requirements and the physical limitations of the system.

Handling quality specifications define aircraft in four different classes, operating in three different flight phases. The NXT UAV flying a ‘missile-like’ mission profile will be

categorized as a Class IV aircraft flying in a Category A flight phase. Table 1-2 below defines these flying quality classifications.

Class IV Aircraft	High-maneuverability airplanes, such as fighter/interceptor, attack, tactical reconnaissance, observation and trainer for Class IV.
Category A Flight Phase	Non-terminal flight phase that requires rapid maneuvering, precision tracking, or precise flight path-control.

Table 1-2: NXT Flying Quality Classification[8]

Using the appropriate aircraft classification, MIL-STD-1797 provides guidance for the flight dynamic requirements. It is worth noting that the wings-level turning requirement uses a different definition of bandwidth (see Appendix A). The list below outlines the requirements for the design and tolerances of the physical system itself.

I. Flight Dynamics and Handling Qualities[7]
   a. Dutch Roll Mode
      i. $\zeta >= 0.19$
      ii. $\zeta * \omega n >= 0.35$ rad/sec
      iii. $\omega d >= 1$ rad/sec
   b. Roll Mode
      i. $\tau <= 1.0$ sec
   c. Spiral Mode
      i. Stable or Time to Double $<= 12$
   d. Bandwidth
      i. For precision tracking and wings-level turn 1.25 rad/sec

II. Customer Requirements
   a. Bank Angle ± 5º during STT
   b. Shall Accomplish up to 8 G skid turn
   c. Capable of pilot or automatic STT

III. Physical Limitations

a. Gyroscopes[9]

i. Range ± 300 º/s

ii. Scale Factor Error <3º/s

iii. Noise <+/- 0.7º/s

iv. Resolution 0.0155º/sec

v. Bandwidth 100 rad/sec

b. Accelerometers[9]

i. Range +/-10G

ii. Scale Factor Error < 100mG

iii. Noise <+/- 12 mG

iv. Bandwidth 100 rad/sec

c. Servo[10]

i. Rate Limit 0.17sec/60º --or-- 353º/sec

d. Control Surfaces

i. ± 20º of Throw Angle

e. Ground Station[11]

i. 0.1s Uplink / Downlink Latency

Chapter 2: Skid-to-Turn Performance and Dynamics

2.1 Skid-to-Turn Rigid Body Dynamics

Fully understanding the dynamics of the STT problem requires starting with the 6DOF equations of rigid body motion. With all dynamics problems, the base coordinate system (**x y z**), positive body forces (**X Y Z**) and positive velocities (**u v w**) must be established. The angular rates (**p q r**) and body moments (**l m n**) are defined by positive rotations about the coordinate axes. Figure 2-1 below shows the basic definition of the body centered coordinate system. The angle of attack (α) is defined such that positive α occurs with positive u and w velocity components:

$$\alpha = \tan^{-1}\frac{w}{u} \tag{2-1}$$

where positive sideslip angle (β) occurs with a positive u, v and w components:

$$\beta = \sin^{-1}\frac{v}{\sqrt{u^2 + v^2 + w^2}} \tag{2-2}$$

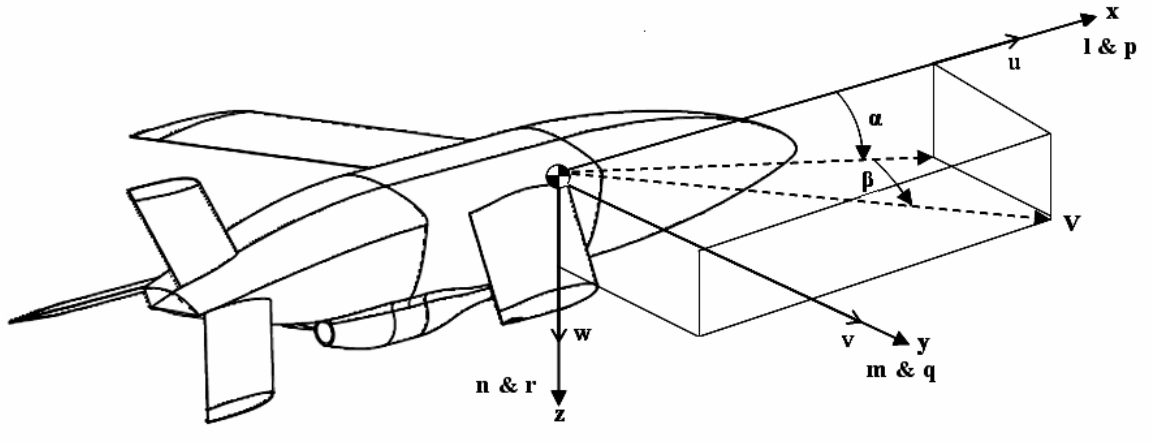

Figure 2-1: Body Coordinate, Angle of Attack and Sideslip Definition

Since the derivation of the 6DOF equations of motion are readily available, the equations, as developed by Nelson[8], will be used as a starting point. The equations of force acting on the body are as follows:

$$X = m(\dot{u} + qw - rv) + m\,g\sin\theta \quad \textbf{(2-3)}$$

$$Y = m(\dot{v} + ru - pw) - m\,g\cos\theta\sin\phi \quad \textbf{(2-4)}$$

$$Z = m(\dot{w} + pv - qu) - m\,g\cos\theta\cos\phi \quad \textbf{(2-5)}$$

The equations of moments acting on the body:

$$l = I_x\dot{p} - I_{xz}\dot{r} + qr(I_z - I_y) - I_{xz}pq \quad \textbf{(2-6)}$$

$$m = I_y\dot{q} - rp(I_x - I_z) + I_{xz}(p^2 - r^2) \quad \textbf{(2-7)}$$

$$n = -I_{xz}\dot{p} + I_z\dot{r} + pq(I_y - I_x) - I_{xz}qr \quad \textbf{(2-8)}$$

Finally, the body angular velocities in terms of Euler angles and Euler Rates:

$$p = \dot{\phi} - \dot{\psi}\sin\theta \quad \textbf{(2-9)}$$

$$q = \dot{\theta}\cos\phi + \dot{\psi}\cos\theta\sin\phi \quad \textbf{(2-10)}$$

$$r = \dot{\psi}\cos\theta\cos\phi - \dot{\theta}\sin\phi \quad \textbf{(2-11)}$$

Since we are initially interested in steady state STT performance of the vehicle the following is true in a steady state skid turn:

$$\dot{u} = \dot{v} = \dot{w} = \dot{p} = \dot{q} = \dot{r} = \dot{\phi} = 0$$

During a steady state skid turn, it is desired to keep the wings level and the pitch angle small. By keeping the pitch angle small, the vehicle maneuvers in the local x-y plane.

$$\phi = \theta = 0$$

With the alignment of the principle axis and the body axis from the assumptions above, the product of inertia terms become zero.

$$I_{xy} = I_{xz} = I_{yz} = 0$$

It is also assumed that the roll rate and pitch rate will be zero during a skid turn.

$$p = q = 0$$

Applying these assumptions to equations (2-3) through (2-8), the force equations become:

$$X = m(-r\,v) \tag{2-12}$$

$$Y = m(r\,u) \tag{2-13}$$

$$Z = -m\,g \tag{2-14}$$

with the moment equations becoming:

$$l = 0 \tag{2-15}$$

$$m = 0 \tag{2-16}$$

$$n = 0 \tag{2-17}$$

and finally the angular rate equations:

$$r = \dot{\psi} \tag{2-18}$$

It may seem counterintuitive for $\dot{v}$ to be zero during a skid turn, as stated in the assumption above, since lateral G's will be applied to the aircraft. However, consider that during a skidding turn, the aircraft's sideslip angle remains at a steady state condition. If this were not the case, then the aircraft would spin like a top during the turn. By using equation (2-2) and assuming a descent rate of zero, the small angle approximation of β is:

$$\beta \approx \frac{v}{u} \tag{2-19}$$

Since beta must remain constant, the only possible way for that to occur is for $\dot{v}$ to equal zero with u remaining constant as the freestream velocity.

$$\dot{\beta} = \frac{d}{dt}\beta = \frac{1}{u}\frac{d}{dt}v = 0 \quad \rightarrow \quad \dot{v} = 0$$

Now that the steady state kinematic condition has been established, the forces and moments must now be considered. Aircraft pose a significant challenge in modeling these due to the highly nonlinear nature of the aerodynamics. Small disturbance theory is used to generate a first order Taylor series representation of the forces and moments. Starting with Nelson's[8] approach to small disturbance theory, each variable can be written as a constant plus a perturbation. Starting with equation (2-4) for side force and approximating the variables:

$$Y_0 + \Delta Y \qquad v_0 + \Delta v \qquad r_0 + \Delta r \qquad p_0 + \Delta p$$

$$w_0 + \Delta w \qquad u_0 + \Delta u \qquad \theta_0 + \Delta\theta \qquad \phi_0 + \Delta\phi$$

It is assumed that the reference flight condition will cause the following variables to become zero:

$$Y_0 = v_0 = p_0 = r_0 = w_0 = \phi_0 = 0$$

Since only the lateral-directional properties of the airplane are of interest, it can be assumed that there will be negligible changes in pitch angle and vertical velocity.

$$\Delta\theta = \Delta w = 0$$

Substituting the linearized variables and assumptions into equation (2-4), the linearized side force equation becomes:

$$\Delta Y + mg\cos\theta_0\Delta\phi = m\left(\frac{d}{dt}\Delta v + \Delta r(u_0 + \Delta u)\right) \qquad \textbf{(2-20)}$$

The equation can be reduced even further by realizing that a small perturbation Δ multiplied by another perturbation is a smaller number.

$$\Delta Y + mg\cos\theta_0\Delta\phi = m\left(\frac{d}{dt}\Delta v + \Delta r\, u_0\right) \qquad \textbf{(2-21)}$$

A perturbation in the side force ΔY can be expressed as a first order function of the remaining variables and the rudder deflection δr .

$$\frac{\partial Y}{\partial v}\Delta v \qquad \frac{\partial Y}{\partial p}\Delta p \qquad \frac{\partial Y}{\partial r}\Delta r \qquad \frac{\partial Y}{\partial \delta r}\Delta \delta r$$

The mass of the vehicle can be divided through equation (2-21). By doing this the newly formed stability derivatives above become:

$$Y_v = \frac{\partial Y}{\partial v}\frac{\Delta v}{m} \qquad Y_p = \frac{\partial Y}{\partial p}\frac{\Delta p}{m} \qquad Y_r = \frac{\partial Y}{\partial r}\frac{\Delta r}{m} \qquad Y_{\delta r} = \frac{\partial Y}{\partial \delta r}\frac{\Delta \delta r}{m}$$

Substituting and factoring the linearized side force is shown below in equation (2-22). A similar derivation, not shown here, is applied to the rolling and yawing moment equations. The complete set of linearized lateral-directional equations are shown below.

$$\left(\frac{d}{dt} - Y_v\right)\Delta v - Y_p\,\Delta p + (u_0 - Y_r)\,\Delta r - (g\cos\theta_0)\Delta\phi = Y_{\delta r} \qquad \textbf{(2-22)}$$

$$-L_v\Delta v + \left(\frac{d}{dt} - L_p\right)\Delta p - \left(\frac{I_{xz}}{I_x}\frac{d}{dt} + L_r\right)\Delta r = L_{\delta a}\Delta\delta a + L\Delta\delta r \qquad \textbf{(2-23)}$$

$$-N_v\Delta v - \left(\frac{I_{xz}}{I_z}\frac{d}{dt} + N_p\right)\Delta p + \left(\frac{d}{dt} - N_r\right)\Delta r = N_{\delta a}\Delta\delta a + N_{\delta r}\Delta\delta r \qquad \textbf{(2-24)}$$

The equations above can then be rearranged and written in state space form:

$$\begin{bmatrix}\dot{v}\\ \dot{p}\\ \dot{r}\\ \dot{\phi}\end{bmatrix} = \begin{bmatrix} Y_v & Y_p & -(u_0 - Y_r) & g\cos\theta \\ L_v & L_p & L_r & 0 \\ N_v & N_p & N_r & 0 \\ 0 & 1 & 0 & 0 \end{bmatrix}\begin{bmatrix} v\\ p\\ r\\ \phi\end{bmatrix} + \begin{bmatrix} 0 & Y_{\delta r} \\ L_{\delta a} & L_{\delta r} \\ N_{\delta a} & N_{\delta r} \\ 0 & 0 \end{bmatrix}\begin{bmatrix}\delta a\\ \delta r\end{bmatrix} \qquad \textbf{(2-25)}$$

2.2 Skid-to-Turn Performance Considerations

A principle quantity in defining the performance of a skidding turn is the number of G's that is pulled during the maneuver, also called lateral load factor η_{STT} . To better understand the definition of lateral load factor, the acceleration term of equation (2-4)

should be considered. By applying the assumptions for a skidding turn the lateral acceleration becomes:

$$a_y = \dot{v} + ru - pw \quad \rightarrow \quad a_y = ru \tag{2-26}$$

Since the number of G's applied to airframe is desired, the lateral load factor is defined by dividing the body acceleration by gravity.

$$\eta_{STT} = \frac{ru}{g} \tag{2-27}$$

One of the most important considerations during a skidding turn is the effect that the yaw rate of the aircraft has on the lateral axis. During a sustained skid turn, the aircraft is yawing at a constant rate. This causes the vehicle to rotate about its center of gravity and subsequently applies a velocity gradient along the span of the wing as seen in Figure 2-2.

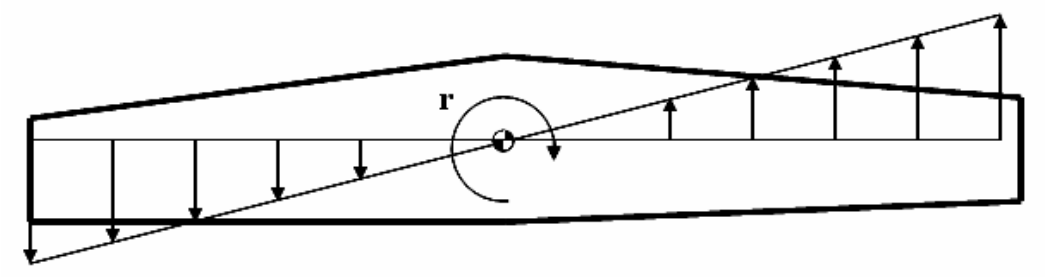

Figure 2-2: Velocity Gradient on a Yawing Wing

The outside wing sees a greater induced velocity since it is rotating at a higher angular rate and subsequently produces more lift. Asymmetric lift on the wing generates an induced roll rate that must be canceled out by the ailerons. Figure 2-3 shows that an increase in either yaw rate or aspect ratio produces an exponential increase in the induced roll rate. It is then desirable to minimize the aspect ratio on a vehicle that is being designed for skidding turns. This in turn minimizes the required aileron deflection to maintain a wings level attitude.

If there is too large of yaw rate during a skidding turn, the ailerons can saturate and the aircraft will roll. As the bank angle increases the rudder acts more like an elevator, yawing the aircraft into an extremely nose low attitude. Such a condition would prove catastrophic for NXT while flying at 400 knots.

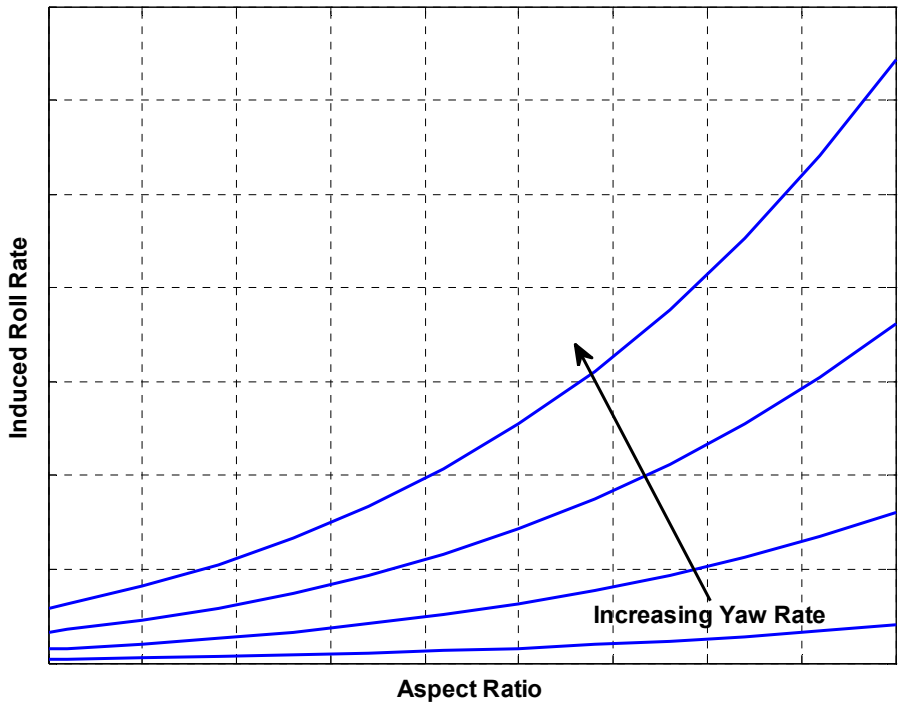

Figure 2-3: Effect on Induced Roll Rate with Increasing AR and Yaw Rate

Now that the two important factors in steady state STT performance have been established, the previously derived equations must be arranged to provide this information. Performance analysis can then be conducted on the NXT using these equations. Starting with the state space form of the lateral directional equations (2-25), the assumptions for the kinematic condition for steady state skid turn is applied. By rearranging the system of equations to solve for side velocity, yaw rate and aileron deflection given a rudder deflection and bank angle, the new set of equations are given below.

$$\begin{bmatrix} Y_v & -(u_0 - Y_r) & 0 \\ L_v & L_r & L_{\delta a} \\ N_v & N_r & N_{\delta a} \end{bmatrix} \begin{bmatrix} v \\ r \\ \delta a \end{bmatrix} = \begin{bmatrix} -Y_{\delta r} & -g\cos\theta \\ -L_{\delta r} & 0 \\ -N_{\delta r} & 0 \end{bmatrix} \begin{bmatrix} \delta r \\ \phi \end{bmatrix} \quad \textbf{(2-28)}$$

This set of linear, time invariant equations will become the basis for the preliminary design studies to analyze and modify NXT to try and meet the requirements outlined in the previous chapter.

2.3 Aircraft Lateral Directional Modes

The analysis has primarily dealt with the steady state performance during a skid turn. However, the transient response will ultimately play a significant factor in the final control law design. To better understand the dynamics of the problem, the three lateral-directional dynamic modes of the aircraft will be discussed briefly; with emphasis on the Dutch roll mode.

The simplest and least problematic of the dynamic modes is the roll mode. This can generally be characterized by a single degree of freedom rolling motion that is influenced by viscous damping. Equation[8] (2-29) below shows a simple and reasonably accurate approximation to this first order response.

$$\lambda_{roll} = -\frac{1}{\tau} = L_p \quad \textbf{(2-29)}$$

A highly damped roll mode is beneficial for STT performance. Increased damping means that there will be less transient demand on the ailerons at the beginning of a wings level skidding turn.

Spiral mode is a condition where the aircraft experiences an initial disturbance that causes divergence from the desired flight path. The airplane's bank angle slowly increases which causes the sideslip angle to increase; subsequently tightening the turn.

Usually this mode has a very large time to double and can easily be corrected by the pilot. The spiral mode can be roughly approximated as[8]:

$$\lambda_{spiral} = \frac{L_\beta N_r - L_r N_\beta}{L_\beta}$$

Aileron is generally the best control to stabilize this mode, which becomes problematic for an aircraft performing skid turns. This reduces the amount of available aileron throw that can be used during STT maneuvers which reduces the maximum yaw rate that the aircraft can handle.

The most influential lateral mode that affects the dynamics of a skidding turn is Dutch roll. This mode is characterized by second order oscillations in both the roll and yaw axis. As an aircraft yaws, the vehicle rolls in the direction of the yawing motion. The vertical stabilizer then generates a yawing moment in the opposite direction. Since the lateral axis is lightly damped, the aircraft yaws through and to a sideslip angle in the opposite direction of the intended turn. Once again, the new yawing motion rolls the aircraft in the opposite direction of the first oscillation. A rough mathematical approximation for the dynamics of the Dutch roll is described with the following equations[8]:

$$\omega_n = \sqrt{\frac{Y_\beta N_r - N_\beta Y_r + u_0 N_\beta}{u_0}}$$

$$\zeta = -\frac{1}{2\omega_n}\left(\frac{Y_\beta + u_0 N_r}{u_0}\right)$$

Dutch roll can be very problematic for an aircraft performing a sudden high G skid turn. This mode causes very large yaw and roll rates with large deflections of the rudder. During this transitory phase, enormous demand is placed on the ailerons to

neutralize rolling motion. Every time the aircraft starts yawing in a new direction, the ailerons must completely reverse their position in a very short period of time. The effects of Dutch roll are a driving factor in the development of STT control laws.

Chapter 3: Aerodynamic Modeling

3.1 Athena Vortex Lattice Program

One of the biggest challenges in this project is to generate aerodynamic data that can be used in performance analysis. Normally flight test or wind tunnel data is used to aid in the development of an aerodynamics model for a project such as this. However, at the beginning of this research, the NXT was still in the design phase and no actual flights had taken place. Even to date, there has been no useful flight test data to support this project. From the beginning, this research has been designed around computer generated aerodynamic data and flight simulation to provide a basis for the control laws.

In years past, the most traditional way to estimate stability derivatives was to use the USAF Data Compendium (DATCOM). This document is a collection of empirical formulas that was generated through extensive flight testing and modeling. DATCOM can produce reasonable estimates of stability derivatives for aircraft that lie within the parameters of the equations. However, the NXT design lies on the fringes of the validity of the DATCOM methods. Several attempts were made to estimate the characteristics of NXT using DATCOM; however, none were successful at generating a reasonable model.

Another method of stability derivative generation is the use of vortex-lattice code. Professor Mark Drela, PhD at the Massachusetts Institute of Technology created a simple but industry accepted computer program called Athena Vortex Lattice (AVL) that uses the an expanded vortex-lattice method to generate stability derivatives[12]. AVL's method of analysis takes geometric and mass input files, places horseshoe vortexes on a series of panels defined by the geometry and calculates the resulting force using the Kutta-

Joukowski theorem[12]. A particular flight condition can be specified and a set of stability derivatives about that trim point is generated.

The AVL program has wide acceptance in industry and academia for the conceptual and preliminary design phases. Cloud Cap Technologies, makers of the Piccolo Autopilot[11], use AVL as a basis to generate an initial set of gains for their autopilots. Since this research is intended to be a conceptual design or proof of concept study, AVL will provide aerodynamic data that is of high enough fidelity.

AVL does have its limitations which should be noted. Vortex-lattice calculations produce linear solutions at a given trim point. Since the solution is inviscid, stall cannot be determined or modeled. Limits also exist on the Mach number at which calculations are valid. AVL should not be used for any computations where transonic or supersonic flow is suspected. Once again, the geometry and flight regime that the NXT flies in pushes the upper limits of the validity of the solution. However, since the solution from AVL is semi-analytical, there is likely to be better modeling accuracy using this method rather than the empirical methods of DATCOM.

3.2 NXT AVL Modeling

Accurately modeling NXT within AVL was challenging. The wings on this aircraft are small enough that the fuselage provides a significant contribution to the aerodynamic forces. To model these forces, flat plates are used to simulate the maximum cross sectional area of the fuselage. Initially, the fuselage was modeled using two of these flat plates in a cruciform shape. One problem encountered using this technique was erroneous results from the coupling between the two fuselage plates.

In order to eliminate this error, the fuselage could only be modeled using one flat plate at a time. The equations established in Chapter 2 separates the longitudinal and lateral dynamics. Additionally, the performance equations derived only need stability derivatives relating to the lateral-directional axes. Taking advantage of this decoupling, two separate geometry files can be used to fully model the aircraft. Each of the two geometry files placed the fuselage plate at the location of maximum cross sectional area for the respective case. Figure 3-1 below shows lateral – directional AVL geometry that was used. While not needed for the initial performance analysis, the model shown in Figure 3-2 is needed to generate the longitudinal stability derivatives for the nonlinear simulation. Appendix B contains the lateral-directional AVL geometry for NXT.

As a side note, AVL uses its own axis definition that is different than the body axis defined in Figure 2-1. This new coordinate system places the positive x direction pointed towards the tail, positive y out the right wing and positive z vertically through the fuselage.

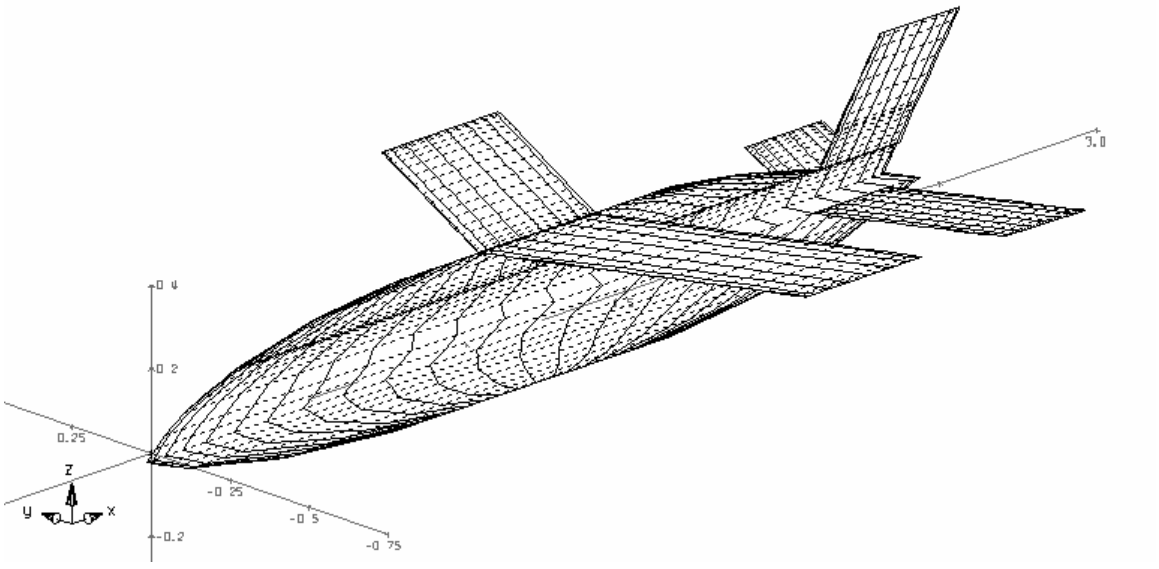

Figure 3-1: NXT Lateral – Directional AVL Model

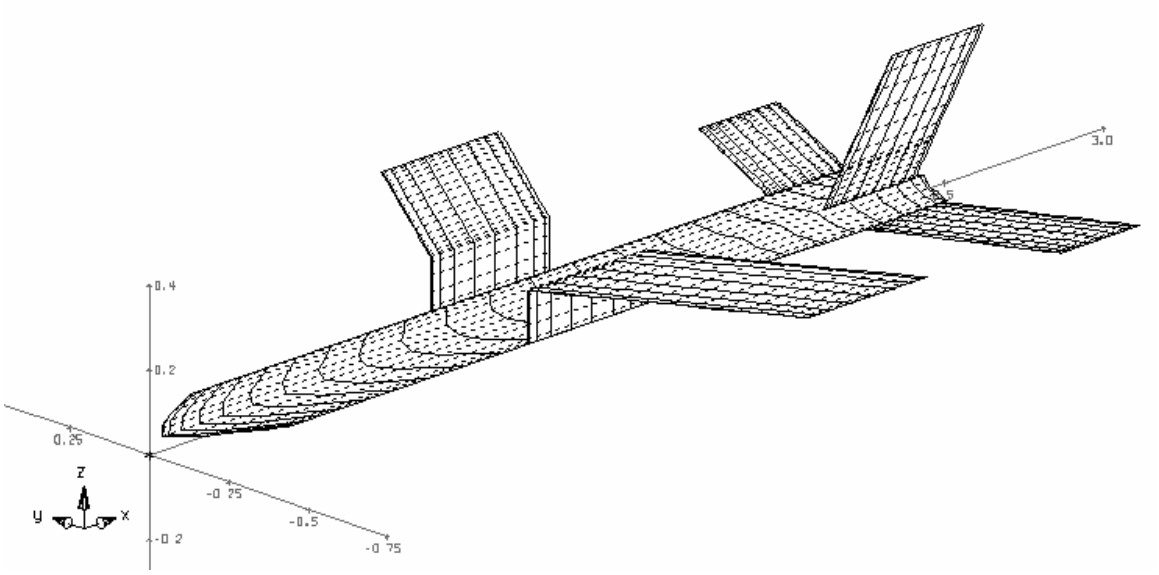

Figure 3-2: NXT Longitudinal AVL Model

As explained in Chapter 1, the NXT uses the horizontal stabilizer control surfaces for both roll and pitch control, with yaw being controlled by the rudder. AVL allows for arbitrary control surface definitions with the option of cross linking surfaces for the purpose of trim analysis. To better model the NXT, it was desired to keep each control flap independent. This allows for post process control mixing into any configuration desired. For performance analysis, the five independent control surfaces (left and right wing flaps, left and right horizontal stabilizers flaps, and the rudder) were mixed into four coupled surfaces (elevator, wing ailerons, horizontal stabilizer ailerons and rudder) using a matrix.

$$\begin{bmatrix} \delta e \\ \delta wa \\ \delta ha \\ \delta r \end{bmatrix} = \begin{bmatrix} 0 & -1 & 0 & 0 \\ 0 & 1 & 0 & 0 \\ 1 & 0 & -1 & 0 \\ 1 & 0 & 1 & 0 \\ 0 & 0 & 0 & 1 \end{bmatrix} \cdot \begin{bmatrix} \delta LW \\ \delta RW \\ \delta LHZ \\ \delta RHZ \\ \delta V \end{bmatrix}$$

AVL supports user defined run cases. These specify the vehicle's mass and inertial properties as well as the flight condition. They also specify which surfaces shall be actuated to trim out the undesirable moments. Since the NXT model is defined with independent control surfaces, a compromise must be made in the trim analysis. Only one of the horizontal tail surfaces can be used to trim out the pitch moment, with the other being used to cancel out the roll moment. In reality, both surfaces are mixed to provide both roll and pitch control. This is a reasonable assumption since both angle of attack and sideslip angle are close to zero in the flight regime used for linearization.

Lastly, a standardized flight condition must be established for all performance computations. A standard atmosphere with NXT flying at sea level and 400 knots will provide the best baseline flight condition for all computations. The reasoning behind this is that the UAV will spend most of its missions at lower altitudes. Flying at a speed of 400 knots is the fastest that NXT is capable of flying and subsequently the closest that it can come to missile flight speeds.

Chapter 4: Linear Analysis and Design of NXT

4.1 NXT1 Steady State Performance

The original NXT design must be analyzed to provide a baseline understanding of the current performance. Using the method of aerodynamic modeling as discussed in Chapter 3, the state space equation for lateral directional motion is shown below. (Note that the data is relative to the AVL geometric coordinate system.)

$$\begin{bmatrix} \dot{v} \\ \dot{p} \\ \dot{r} \\ \dot{\phi} \end{bmatrix} = \begin{bmatrix} -0.9033 & -2.8637 & 204.2756 & 9.81 \\ 2.8263 & -8.8438 & 0.9378 & 0 \\ -0.4945 & -0.0011 & -3.1405 & 0 \\ 0 & -1 & 0 & 0 \end{bmatrix} \begin{bmatrix} v \\ p \\ r \\ \phi \end{bmatrix} + \begin{bmatrix} 0.5922 & -0.3802 \\ 8.8580 & 2.5 \\ 2.9320 & -1.9080 \\ 0 & 0 \end{bmatrix} \begin{bmatrix} \delta a \\ \delta r \end{bmatrix} \quad \textbf{(4-1)}$$

Taking this data and applying the kinematic condition for a steady state skid turn a new set of linear equations is formed.

$$\begin{bmatrix} -0.9033 & 204.2756 & 0.5922 \\ 2.8263 & 0.9378 & 8.8580 \\ -0.4945 & -3.1405 & 2.9320 \end{bmatrix} \begin{bmatrix} v \\ r \\ \delta a \end{bmatrix} = \begin{bmatrix} 0.3802 & -9.81 \\ -2.5 & 0 \\ 1.9080 & 0 \end{bmatrix} \begin{bmatrix} \delta r \\ \phi \end{bmatrix} \quad \textbf{(4-2)}$$

Since the maximum throw of the rudder is 20º and it is assumed that the wings will remain perfectly level, the solution to equation (4-2) becomes:

$$\begin{bmatrix} v \\ r \\ \delta a \end{bmatrix} = \begin{bmatrix} 0.6614 & {}^{m}/_{s} \\ 0.0026 & {}^{rad}/_{s} \\ -0.1128 & rad \end{bmatrix}$$

Most importantly the lateral load factor and the required aileron deflection for the baseline NXT design are:

$$\begin{bmatrix} \eta_{STT} \\ \delta a \end{bmatrix} = \begin{bmatrix} 0.05 & G's \\ -6.5 & \text{deg} \end{bmatrix}$$

The calculated performance values for the NXT vehicle seem somewhat reasonable for the size and shape of the aircraft. It is good that the required aileron deflection is relatively low since these surfaces will have to allow for additional throw to control pitch and transient roll responses. However, the lateral load factor of only 0.05 G's is far from the desired target value of 8 G's.

4.2 NXT Dynamic Performance

The next step in analyzing the design is to look at the open loop dynamics of the UAV. This will show how closely the system is designed relative to the requirements described in Chapter 1. Most importantly, the eigenvalues of the system will give a broad description of the dynamics. These eigenvalues from equation (4-1) are shown below.

$$\lambda = \begin{bmatrix} -2.07 + 10.32i \\ -2.07 - 10.32i \\ -8.655 \\ -0.086 \end{bmatrix}$$

As designed, the NXT is stable in all modes. This is good since it will not require dedicated control bandwidth just to stabilize the system. The roll and spiral modes each have a time constant of 0.12 sec and 11.63 sec respectively. Both of these fall into Level I handling quality specifications. Dutch roll has a damping ratio of 0.197, natural frequency of 10.53 rad/sec, and a damped frequency of 10.32 rad/sec. This too places Dutch roll within the Level I criteria.

There are three step responses of the open loop system that provide some insight into the behavior of the UAV in relation to skidding turns. The first is the aileron to roll rate response as given in equation (4-3). For the uncompensated system, the Dutch roll is very prevalent in the transient response with the system returning to a role rate of zero

over a long period of time. However, the key piece of information is the speed at which the roll rate responds to an aileron input. This is directly related to the roll mode of the system. A fast response is desired as it will be easier to control the roll angle within the required tolerances.

$$\frac{p}{\delta a} = \frac{8.858\ s\ (s^2 + 4.543s + 295.8)}{(s + 8.655)(s + 0.08612)(s^2 + 4.14s + 110.7)} \qquad \textbf{(4-3)}$$

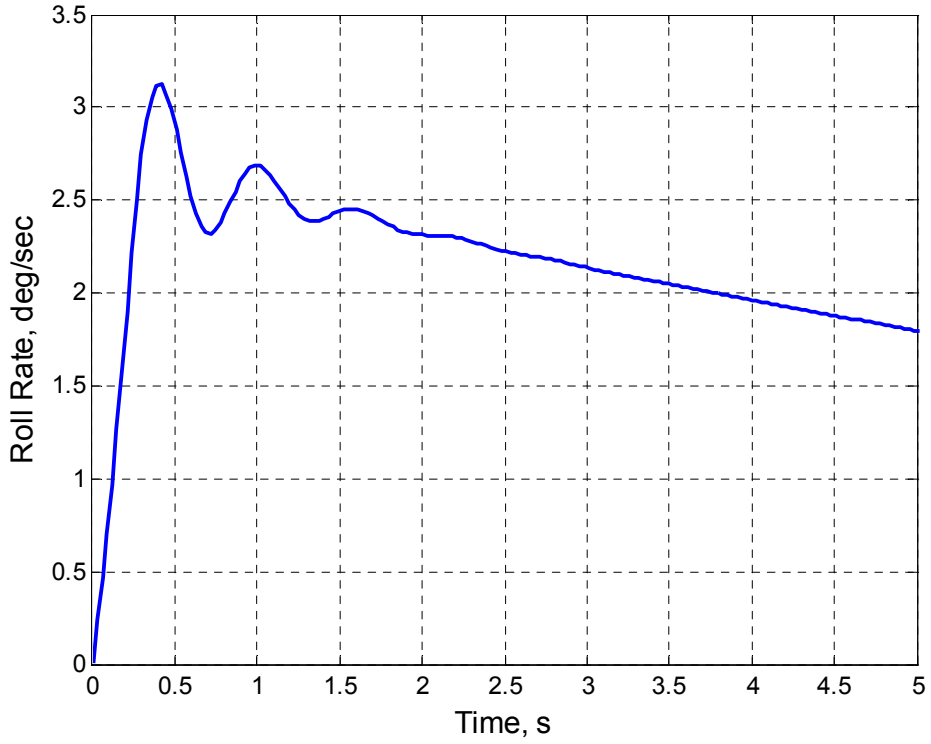

Figure 4-1: Step Response for p/δa Transfer Function

A step response of the rudder to the roll rate, as seen in Figure 4-2 and equation (4-4), shows two main characteristics. At the very beginning of the response, the aircraft actually rolls in the opposite direction of the turn. This is caused by the rolling moment from the lift generated on the vertical tail that initially rotates the airplane in the opposite direction. The roll rate then quickly increases in the direction of the turn. Once again, this is the effect that was described in Chapter 2.2. What is surprising is that the induced

roll rate from the rudder is close to one third of the roll rate as produced by the aileron in Figure 4-1. This shows how effective the rudder is in producing a rolling moment.

$$\frac{p}{\delta r} = \frac{-2.932\ s\ (s^2 + 1.7851s + 5.398)}{(s + 8.655)(s + 0.08612)(s^2 + 4.14s + 110.7)} \quad \textbf{(4-4)}$$

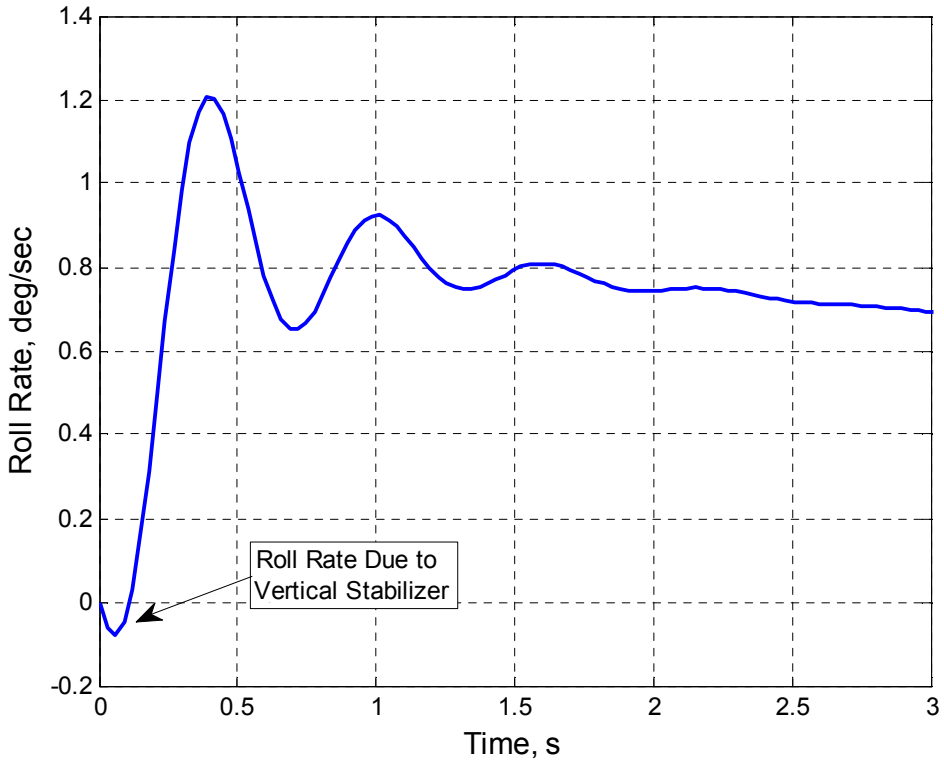

Figure 4-2: Step Response for p/δr Transfer Function

The last response is the yaw rate from a rudder input given by equation (4-5). Most importantly to note is the initial oscillation that is due to Dutch roll. Even with only a small input, large oscillations occur which may become detrimental to designing a STT control system.

$$\frac{r}{\delta r} = \frac{1.908(s + 8.358)\ (s^2 + 1.7851s + 5.398)}{(s + 8.655)(s + 0.08612)(s^2 + 4.14s + 110.7)} \quad \textbf{(4-5)}$$

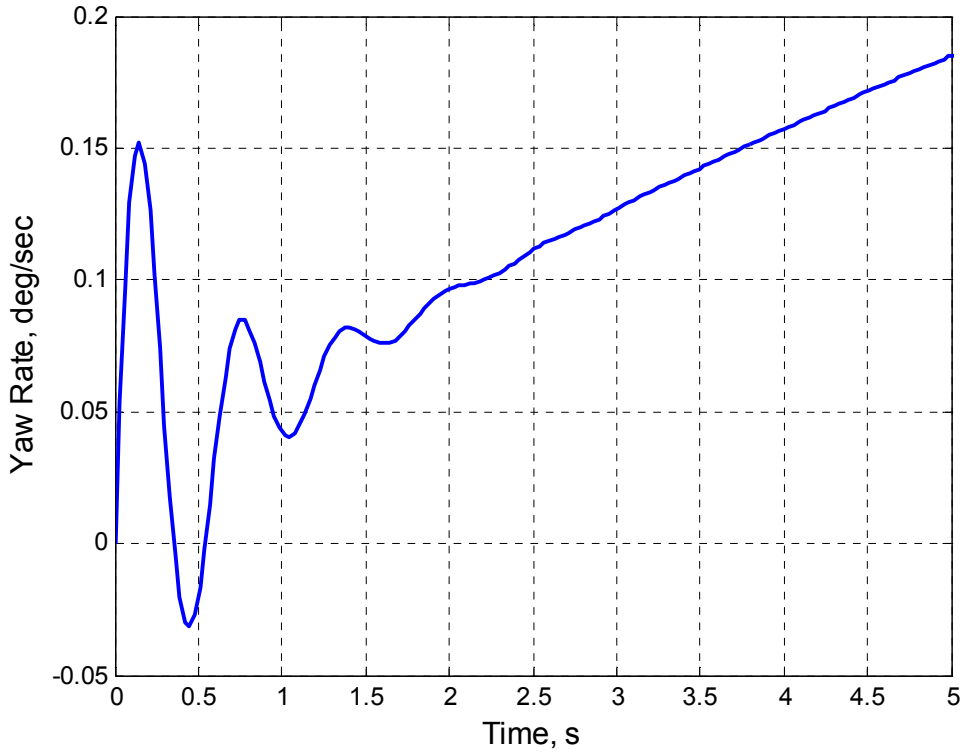

Figure 4-3: Step Response to r/δr Transfer Function

4.3 Improving Skid-to-Turn Performance

Linear analysis of NXT provides a good starting point to consider design modifications that would allow NXT to perform skidding turns better. Equation (2-27) shows that in order to increase the lateral load factor of an aircraft performing a skid turn, the yaw rate must be increased. Missiles use a mixture of four primary configurations to accomplish this increase in yaw rate. Three of these methods are aerodynamic with the last being a propulsive solution.

Not only is it desirable to increase the maximum lateral load factor of the UAV, it is also essential that the Cloud Cap autopilot system has the capability to handle the bare airframe dynamics. Presenting the autopilot or a ground based pilot with a UAV that is highly unstable is not a feasible option for this particular research. The only unstable

dynamics that will be tolerated is a spiral mode that conforms to Level I handling qualities as specified by MIL-STD-1797.

The fundamental control architecture of the current Cloud Cap autopilot uses a series of feedback control loops based on linear theory. While not currently capable of supporting skidding turns, any modifications to the existing control architecture should be minimized. Having a highly unstable airframe might require extensive reengineering of all controls laws in the autopilot. By minimizing the natural instabilities of the system, less autopilot function has to be dedicated to stability augmentation. Additionally, the autonomy level of the NXT still necessitates that a pilot needs be ready to assume control over the vehicle as necessary. In the event of autopilot failure, the vehicle should still be flyable by a pilot from a ground control station.

One of the most common means for maneuvering missiles is using a set of canards placed at the nose of the fuselage. An example of a missile utilizing canard control is the AIM-9 Sidewinder as seen in Figure 4-4.

Figure 4-4: AIM-9 Sidewinder Missile[5]

The basic principle behind this method of control, as with most aerodynamically controlled vehicles, is using the canards to generate a moment on the body. In the case of skidding turns, the canards are used to generate a large yawing moment. The aft fins on the missile remain stationary and are simply there to provide minimal stability.

A fundamental problem with canard control is that the aerodynamic surfaces are forward of the center of gravity; thus they are destabilizing to static stability. As the missile yaws and the sideslip angle is increased, more lift is generated on the canard. The resulting increase in lift produces an even larger moment; yawing the missile further. Only a very slim margin of static stability is maintained by the tail.

Application of this method of control on NXT would create significant stability challenges. As stated earlier, stability is a critical issue for this UAV. An additional problem from this configuration is the wake produced by the canard. Subsequently, the entire fuselage and tail do not receive clean airflow. In the case of the NXT, placement of a forward canard will also disrupt the flow being ingested into the engine on the underside of the aircraft. From a structural standpoint, canards mounted on the nose will be damaged during the nose low ground impact during parachute recovery.

The next alternative is placing dorsal fins at roughly the center of gravity. Figure 4-5 shows the AGM-88 HARM missile that utilizes this method of control.

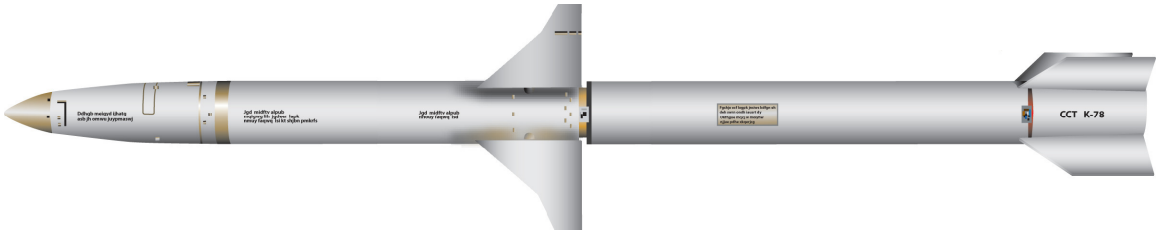

Figure 4-5: AGM-88 HARM Missile[5]

Once again the aft tail is fixed and only used for static stability purposes, whereas the dorsal fins are actuated to initiate a maneuver. This method of control relies on applying a force directly at the center of gravity towards the center of the turn. The stabilizing tail yaws the fuselage in an attempt to correct for the inherent sideslip of the maneuver. A

benefit of this configuration is that dorsal fins are usually a neutrally stable addition to the airframe.

Adding dorsal fins to NXT might initially seem like a feasible solution since it does not have the stability issues like canards. However, dorsal fins would structurally and operationally impact NXT. The center of gravity for this particular UAV is located near the engine. It would be impractical to try and mount the bottom fin underneath the engine nacelle. Operationally, NXT is catapulted from a rail launcher during takeoff. A dorsal fin mounted on the underside of the fuselage would interfere with this equipment.

The last aerodynamic option is to continue to use the aft tail for control. A few of the slower missiles, such as the AGM-65 Maverick, and every aircraft utilize this control method.

Figure 4-6: AGM-65 Maverick Missile[5]

Aerodynamically this is not the most efficient means for control, but it is the most stable. To produce a yawing moment, the vertical tail must apply a force to the outside of the turn. This can cause the missile to initially translate outwards before yawing in the intended direction of the turn. From a controls standpoint, this is a significant problem as it produces right half plane zeros.[4] Stabilizing control loops on these states could require unrealistic compensation to keep the poles in the left half of the complex plane.

A final, non-aerodynamic option is to use thrust vectoring control. Many missiles take advantage of rotating their high force thrust vector to provide significant moments

for maneuvering. Tactical missiles have the advantage of being propelled by solid rocket motors that can easily be actuated for thrust vectoring. Conversely, the NXT uses a lower thrust turbojet engine for its propulsion.

The two ways that thrust vectoring could be accomplished on NXT would be to physically swivel the engines or introduce a rotating vane into the exhaust. A potential downside to swiveling the engine, besides the obvious structural changes, is the resultant loss of thrust to counteract drag. Skidding turns are a high drag maneuver and the current thrust of the engines would struggle to compensate for the drag rise. This would result in an altitude or airspeed loss. The second option of adding a vane into the exhaust flow might be feasible; however, the vane could interfere with the catapult equipment or easily become damaged upon recovery.

Design Proposal	Pros	Cons
Canards	- Smaller Surfaces - Large Increase in Maneuverability	- Destabilizing - Downwash Along Entire Vehicle - Payload Interference
Dorsal Fins	- Neutrally Stable	- Engine & Launch Catapult Interference
Aft Tail	- Stabilizing	- Increased Damping
Thrust Vectoring	- Increase in Maneuverability	- Decrease of Forward Thrust Component

Table 4-1: Summary of Design Modifications

4.4 NXT2 Design

After considering the potential options for improving the STT performance, it was decided to stay with the current method of aft control. Using the existing aft tail configuration on the NXT would be beneficial as this would reduce redesign and manufacturing. Given the scope of this research and the goal to minimize the changes of the UAV, it was decided that continuing to use an aft control system would be the most practical. Additionally, the NXT must still be capable to function like a traditional UAV.

Maintaining the current control system would not require redesigning the control loop architecture for flight as an aircraft.

As the liner analysis of the original NXT design shows, the vehicle is only capable of performing a 0.05 G skid turn. To get higher lateral G's, larger control forces must be generated. A solution to this could be increasing the size of the control flap of the rudder from 20% of the chord. However, flow separation problems do exist by making the control surface a greater chord percentage. One way to mitigate flow separation might be to create full chord control surfaces. Without the discrete jump in geometry at the control hinge, the flow is more likely to stay attached at the higher Reynolds numbers of the baseline flight condition. The larger surface also requires less control deflection for a desired force. If properly mounted, the control servos should not have to overcome any hinge moments from control deflection.

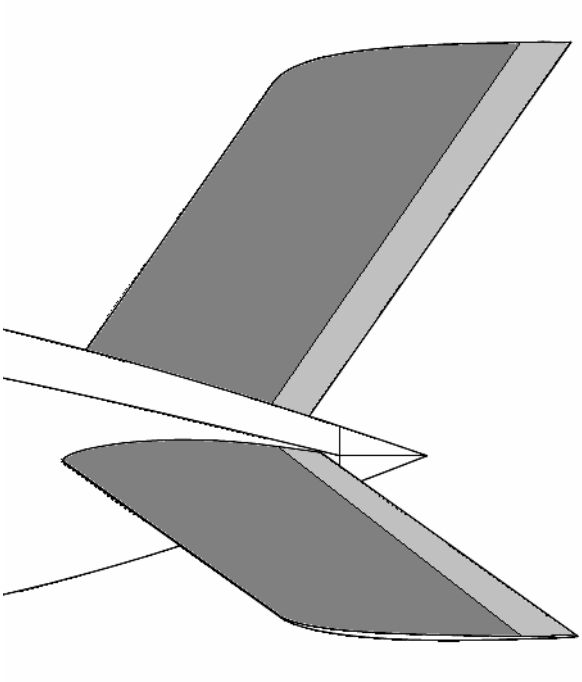

Figure 4-7: NXT Tail Section with Proposed Increase in Control Surfaces

It was decided to include a full span rudder in an attempt to increase lateral G's. More control power from the rudder also necessitates lager control power from the ailerons to overcome the induced rolling moment. Making the horizontal stabilizer a full moving control surface would greatly increase both roll and pitch control power.

Another potential modification is rotating the inverted V tail to make it a true horizontal tail. The inverted V is a remnant of a prior design iteration that provides no benefit for STT operations. Since the control surfaces on the inverted V are not used to control yaw, they simply inhibit the maximum yaw rate attainable. In other words, they provide no control force and extract energy out of the maneuver as shown in Figure 4-8. It is possible that the vertical tail might have to be increased to account for the slight loss in static lateral stability provided by the inverted V configuration. Another potential drawback is the possibility that the spiral mode will become slightly unstable from this new geometry configuration.

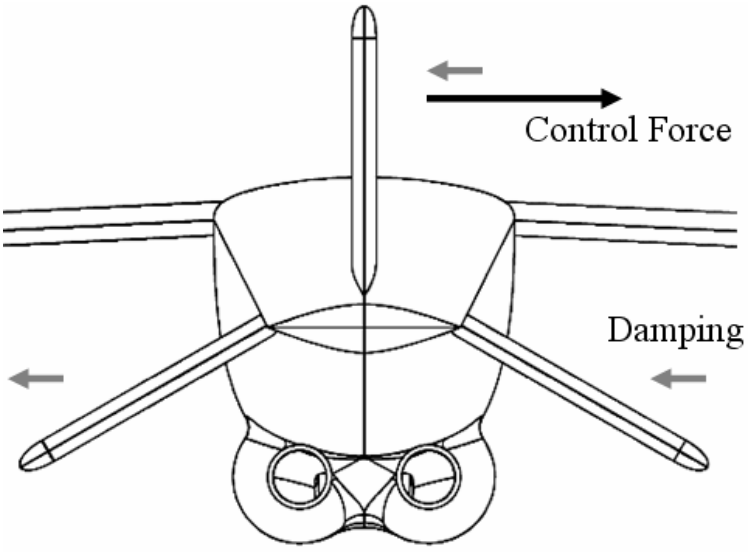

Figure 4-8: Control and Damping Forces on the Inverted V Tail while Yawing

4.5 NXT2 Linear Design Analysis

The various design modifications suggested in the previous section should provide an increase in the maximum lateral load factor of the NXT. These new design changes will be designated as the NXT2 to distinguish from the original design. In an attempt to maximize the performance and to gain insight into the effects of the vertical tail on skid turns, analysis using the linearized equations of Chapter 2 is used.

Analysis of the tail controlled configuration is accomplished by creating a set of geometry cases that are run in AVL. The primary feature of interest is the area of the vertical stabilizer. Nineteen different cases were modeled with tail areas ranging from 0.03 m^2 (about ½ original size) to 0.21 m^2 (3x original size) were analyzed. To maintain aerodynamic similarity, aspect ratio of the vertical tail was preserved for the run cases. Figure 4-9 below graphically shows the variation of tail area.

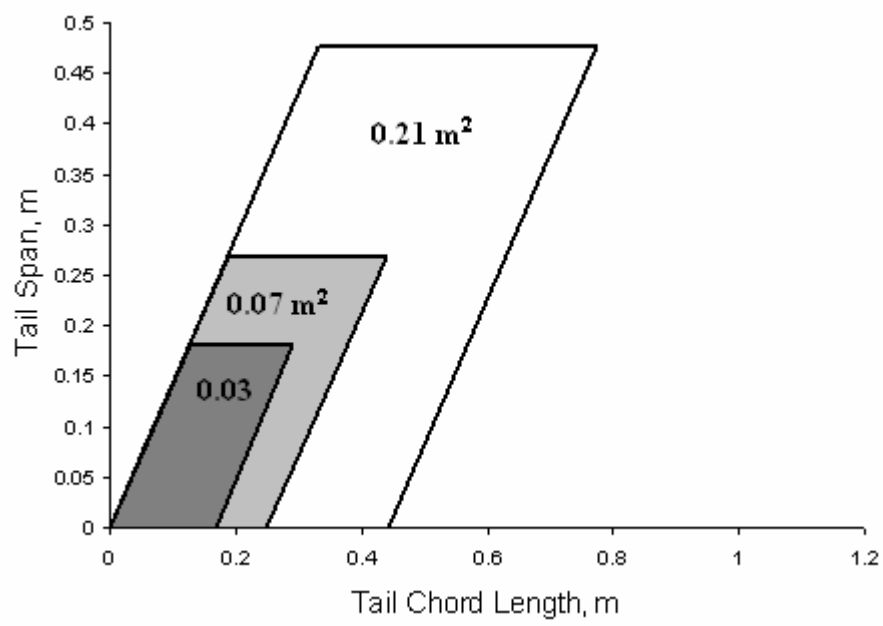

Figure 4-9: Variation of Vertical Tail Area

Additionally, the inverted V tail was made horizontal by rotating the surfaces about the fuselage centerline. The resulting stability derivatives from a 20º rudder deflection and a bank angle of zero were used to determine the steady state skid turn parameters.

Initial results from the linear study show that the lateral load factor was increased by making the vertical stabilizer a fully moving surface. Although, two unique and problematic phenomena were apparent as the area of the tail was adjusted. Figure 4-10 shows the lateral load factor as the tail area is varied.

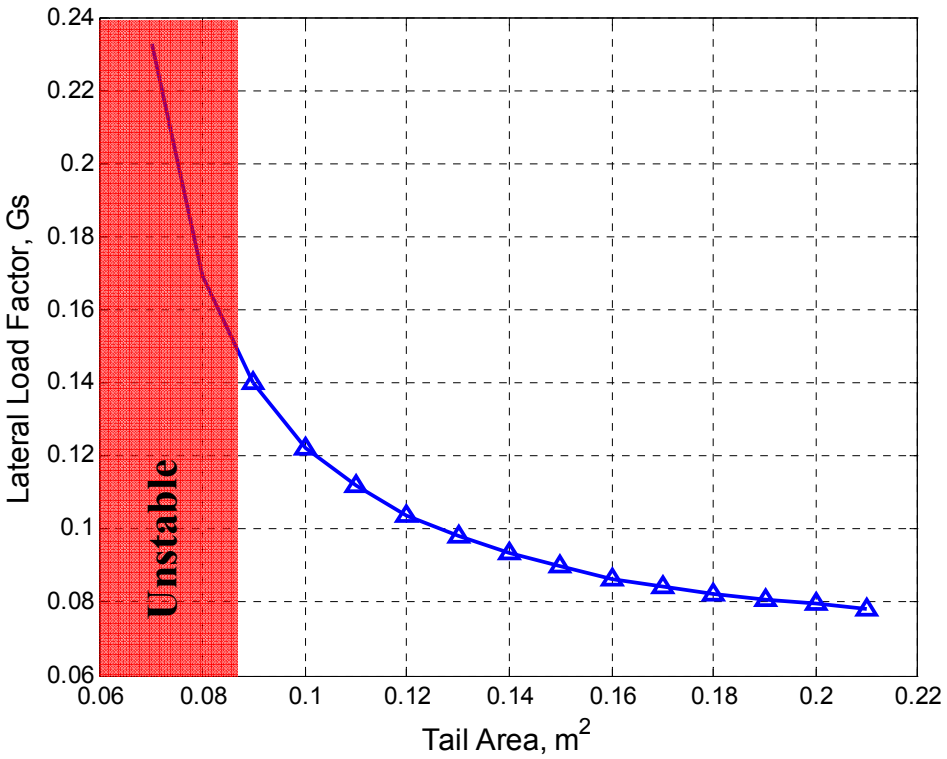

Figure 4-10: Steady State Lateral Load Factor Variation with Tail Area

The first problem, and most serious, is that the UAV becomes unstable as the area decreases below a critical value. This is unfortunate since the lateral load factor is actually increased by decreasing the tail area. Decreasing tail area allows the fuselage to become more dominant and overpower the stabilizing moment from the tail. It proves that the fuselage alone is unstable with sideslip angle. If just the fuselage is considered,

the center of pressure during sideslip is forward of the center of gravity, producing an adverse yawing moment.

Another way to analyze this effect is to look at the $C_{n\beta}$ stability derivative for the entire UAV, or in body coordinates the C_{nv} derivative. Figure 4-11 shows how the dimensional N_v derivative becomes negative when the system is unstable. Theoretically, the vertical tail's contribution to N_v should be positive; therefore when N_v is zero, the fuselage's instability is equally canceling out the stabilizing effects of the tail. Some amount of instability can be tolerated by both the autopilot and the pilot at the ground station. It might be beneficial to decrease the size of the vertical tail and make the vehicle laterally unstable to gain additional STT performance.

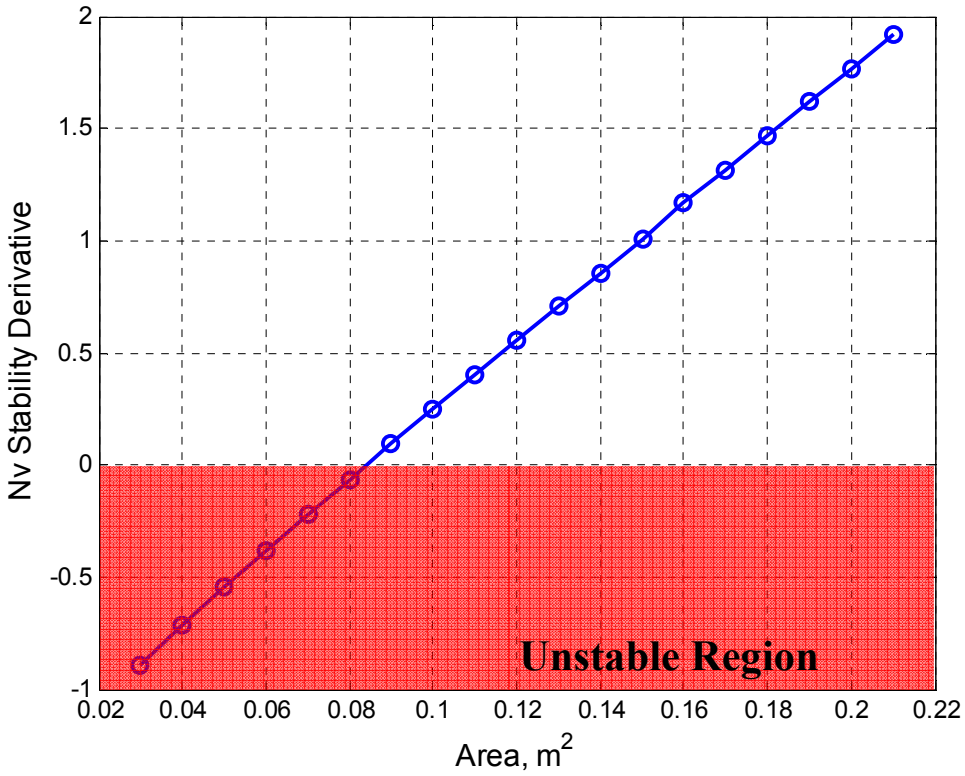

Figure 4-11: Nv Stability Derivative Variation with Tail Area

However, the lateral modes of the system must be investigated to better understand the dynamics involved. Both the roll subsidence mode and the spiral mode remain virtually unchanged as the tail area is varied. Conversely, the Dutch roll mode shows dramatic changes as shown in Figure 4-12. The Dutch roll root turns unstable at the same time that the N_v stability derivative becomes negative. This level of instability is not acceptable due to the sensitivity of the Dutch roll mode. Intentionally making the system unstable in this way is not feasible.

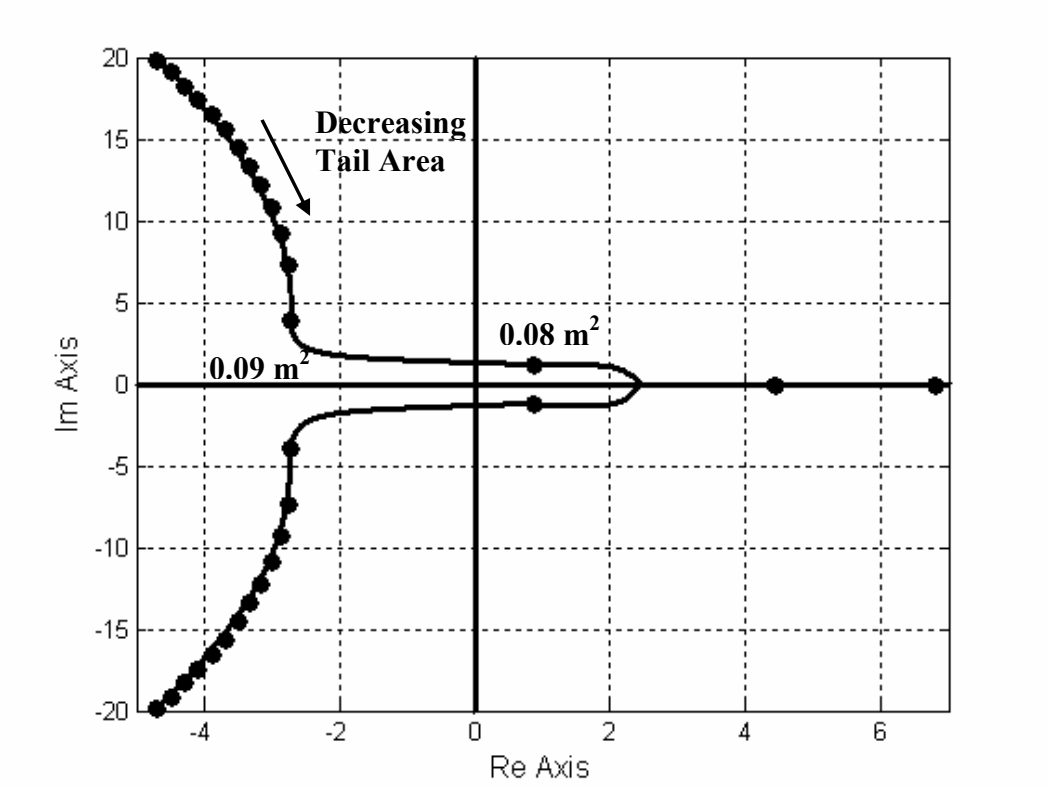

Figure 4-12: Variation of Dutch Roll Roots with Tail Area

The second problem that was encountered from the analysis was the unpredicted effect that the lateral load factor would decrease as the vertical tail size increased. With the rudder being a full moving vertical tail, increasing the tail size will increase the control power of the rudder. However, increasing area also means that there is more cross

sectional area that subsequently increases the damping due to yaw rate (Figure 4-8). Quantitatively, this is shown in Figure 4-13 by comparing the N_r (yaw rate damping) and $Y_{\delta r}$ (rudder control power) stability derivatives. As the tail area is increased, the damping derivative increases at a faster rate than the control derivative. Any gains in control power are quickly lost to an increase in damping.

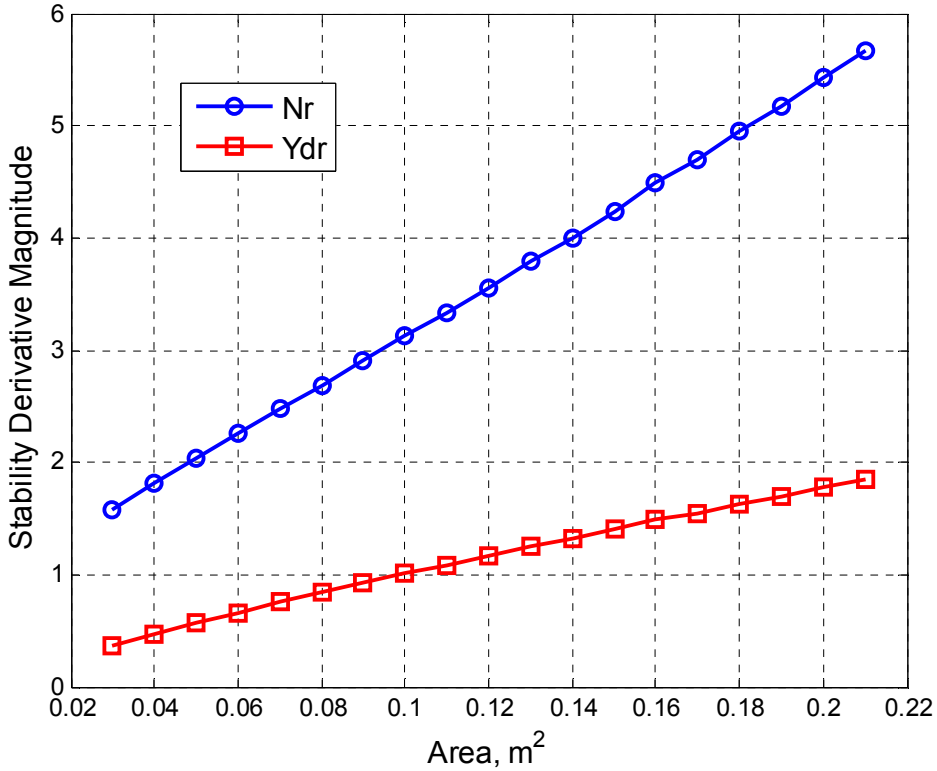

Figure 4-13: Nr and Yδr Stability Derivative Variation with Tail Area

The final design of the NXT2, as suggested by the linear analysis, shows that there should be few changes to maximize performance. One of the biggest changes that should be considered is creating full chord aileron/elevator and rudder control surfaces. This provides the biggest improvement in performance. The second suggestion would be to make the inverted V tail into a true horizontal stabilizer. However, since lateral static stability is reduced, the vertical stabilizer should be increased from 0.07 m^2 to 0.09 m^2.

These recommendations are based on linear analysis and should be analyzed in a nonlinear environment. The large changes in state that occur during STT maneuvers exceed the capabilities of a linear model, although the trends will be the same between both. While it is necessary to use a linear model to design classical control laws, a nonlinear model should be used to increase accuracy of performance and control calculations.

Chapter 5: Non-Linear Flight Simulation Development

5.1 Non-Linear Simulation Development

Proper flight dynamics and controls analysis must include some level of nonlinear simulation before any modifications or control laws are implemented on a flying vehicle. The problem with creating the nonlinear simulation is getting data to drive the flight dynamics. A mix of computational, experimental and flight test data is preferred to generate a good simulation of the flight dynamics. Unfortunately, the NXT has no usable flight test or experimental (wind tunnel) data. Once again, AVL will have to be used to generate the required data for the simulation. By running sweeps of both angle of attack and sideslip angle, tables of stability derivatives can be generated for any desired flight regime.

The simulator was designed to be flexible and non-aircraft specific. It was also implemented in Simulink to aid in control law analysis and design. There are four main subsystems that contain specific functions within the simulation (Figure 5-1): forces/moments, equations of motion, control laws and data processing. The equations of motion subsystem used is a default block from Simulink. A simple flat earth, 6DOF model that uses an Euler angle representation was chosen. Since this simulation was intended to be a test bed for control laws, a flat earth model is accurate enough. Extreme attitude angles are not intended to be modeled; as a result Euler angles should not pose a problem.

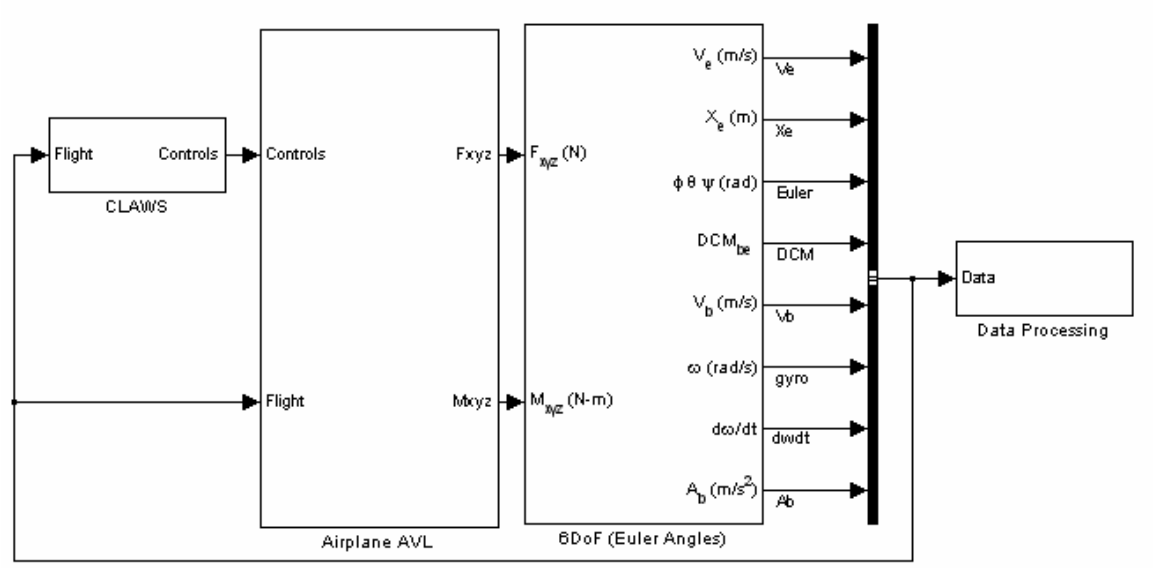

Figure 5-1: Root Level View of the Simulation Program

The forces and moments block is what makes the simulation unique to a specific aircraft. These forces and moments are calculated by taking a summation of the linearized aerodynamics coefficients (non-dimensional stability derivatives). Table lookups are used to hold the nonlinear coefficients as a function of angle of attack or sideslip angle. All of the forces and moments were calculated in stability coordinates using the AVL geometry coordinate system. A rotation from this axis to the standard body coordinate system was made before applying the equations of motion. Appendix C shows the Simulink diagrams used in the nonlinear simulation. The equations used to compute the forces and moments in the simulation are as follows:

Equation for lift:

$$C_L = C_{L0} + C_{L\alpha}\alpha + C_{L\delta c}\delta c + \frac{c}{2V_a}\left(C_{Lq}q\right) \tag{5-1}$$

$$L = QSC_L \tag{5-2}$$

Equation for drag:

$$C_D = C_{D0} + \frac{(C_L - C_{L0})^2}{\pi e A R} + C_{D\delta c}\delta c \tag{5-3}$$

$$D = QSC_D \tag{5-4}$$

Equation for sideforce:

$$C_Y = C_{Y\beta}\beta + C_{Y\delta c}\delta c + \frac{b}{2V_a}\left(C_{Yp} + C_{Yr}r\right) \tag{5-5}$$

$$Y = QSC_Y \tag{5-6}$$

Equation for rolling moment:

$$C_l = C_{l\beta}\beta + C_{l\delta c}\delta c + \frac{b}{2V_a}\left(C_{lp}p + C_{lr}r\right) \tag{5-7}$$

$$l = QSbC_l \tag{5-8}$$

Equation for pitching moment:

$$C_m = C_{m0} + C_{m\alpha}\alpha + C_{m\delta c}\delta c + \frac{c}{2V_a}\left(C_{mq}q\right) \tag{5-9}$$

$$m = QScC_m \tag{5-10}$$

Equation for yawing moment:

$$C_n = C_{n\beta}\beta + C_{n\delta c}\delta c + \frac{b}{2V_a}\left(C_{np}p + C_{nr}r\right) \tag{5-11}$$

$$n = QSbC_n \tag{5-12}$$

5.2 Non-Linear NXT2 Design Analysis

With a nonlinear simulation completed, the NXT2 design can be tested without any STT control laws applied. Alpha and beta sweeps were conducted within AVL to

generate a set of stability derivatives to feed into the simulation. Appendix D has a complete listing of the derivatives used for the initial NXT2 testing. A simple performance test was conducted by hand flying the aircraft with a joystick. Rudimentary control laws were applied to aid in the stabilization of the aircraft to ensure accurate and steady values. The key parameters looked at were steady state lateral load factor, aileron deflection and beta angle.

There are three criteria that must be used to determine the maximum STT capability of the NXT2. First is a limit on the angle of attack and sideslip angle. Since AVL does not have the capability to detect stall, a self imposed limitation of 10º on alpha and beta must be applied. Given the already limited capability of the analysis, maneuvering in the post stall regime should not be explored. Second is a limitation on aileron deflection. If the capabilities of the ailerons were ever exceeded, then the UAV might roll at such a high rate that the vehicle could flip and start tumbling uncontrollably. Finally, if the previous two limits have not been exceeded, the rudder will be limited to a maximum deflection of 20º. In the test, rudder deflection will slowly be increased until any of these limits are exceeded.

Surprising results came from the analysis. It appears that the linear model grossly underestimates the dynamics of the vehicle. After increasing the rudder deflection by only 1 degree, the sideslip angle limitation was hit (Figure 5-3). The resulting steady state lateral load factor reached a value of 2.9 G's (Figure 5-2), versus the 0.14 G's as predicted by linear analysis. Additionally, a smaller aileron deflection of 12.5 degrees was predicted by the nonlinear simulation versus the 26.5 degrees as calculated linearly.

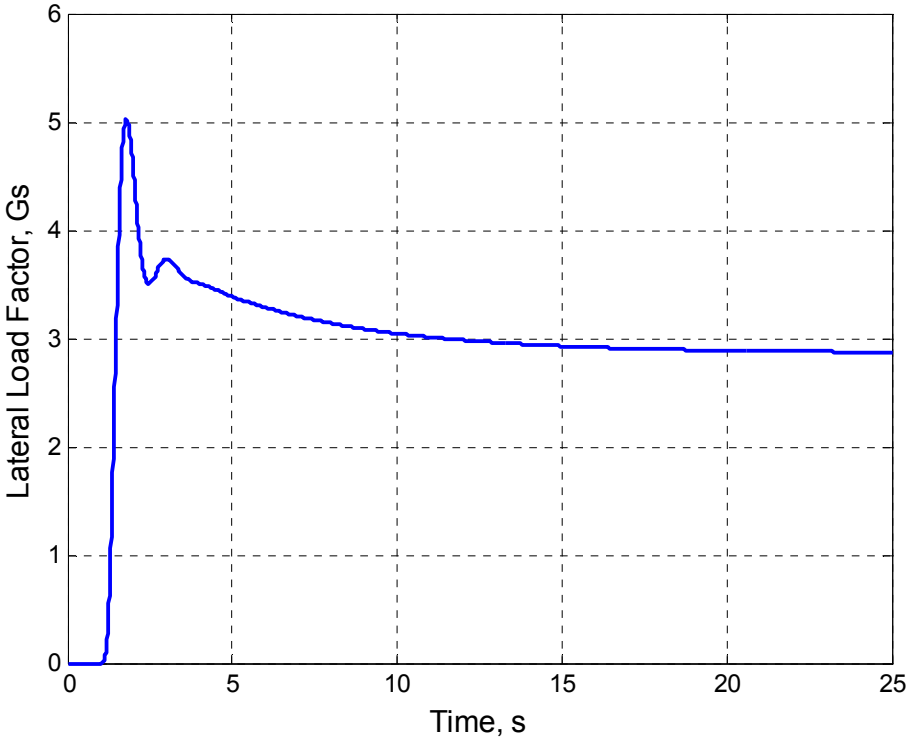

Figure 5-2: Lateral Load Factor vs Time for Initial NXT2 Design

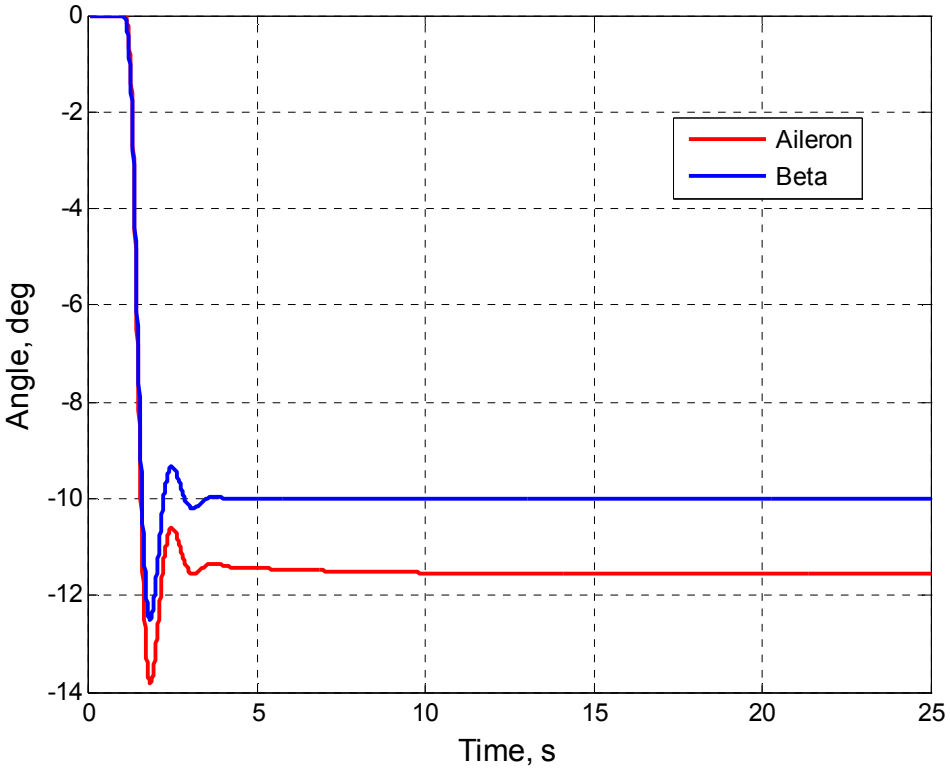

Figure 5-3: Aileron and Sideslip Angle vs Time for Initial NXT2 Design

The results of the previous two figures show that there is a discrepancy between the linear and nonlinear analysis. In reality this is not an unexpected problem. Linearizing the equations of motion makes an assumption that all of the variables are constants plus a very small perturbation. In practice this type of analysis should not be used in situations where large variations of the states are present. Skid-to-turn maneuvering produces exactly these large variations. However, linear analysis does still predict the proper trends and general dynamics that the system will see. It also is far less computationally intensive and more mathematically friendly to use linear analysis to observe the basic dynamic trends along with the fast exploration of many scenarios.

Using this new information from the NXT2 nonlinear simulation, there is a small change to the suggested NXT2 design. The simulation showed that the linear analysis was greatly under predicting the control effectiveness of the surfaces. Because of this, it is recommended that the rudder control surface stay as a 20% chord flap rather than being a full span surface. The rest of the suggested changes should still be implemented. There is a strong need for aileron deflection thus keeping the full chord horizontal stabilizers is necessary. Converting the inverted V tail is also suggested. Besides from the previous argument about damping, the inverted V tail produces more effective ailerons. The final suggested changes to the NXT2 design is summarized below.

1. Replace the inverted V tail with a true horizontal stabilizer of the same area
2. Increase the size of the vertical stabilizer to 0.09 m^2
3. Create full chord control surfaces on the horizontal stabilizer

Chapter 6: NXT2 Skid-to-Turn Controller Design

6.1 Controller Overview

A component of this research is to create simple control laws that enable NXT2 to perform skid-to-turn maneuvers. These control laws should allow easy integration into the existing autopilot architecture. The emphases of this case study will be on maintaining attitude control throughout STT maneuvers with some discussion of rudimentary guidance laws that may be applied.

When designing a set of control laws using linear control theory, it is desirable to try and reduce the problem into a single input – single output system (SISO). This works well for longitudinal control of the aircraft; however, the tight coupling of the lateral and directional axes do not allow such a reduction. In the case of STT control laws, aileron and rudder will be used to control three different states: yaw rate, roll rate and bank angle. This type of system is also known as a multi-input multi-output system (MIMO).

Analysis of MIMO systems using basic loop shaping techniques requires that only one loop at a time can be closed. This allows for that particular loop's controller to be designed to the proper specifications. With each subsequent loop closure, the plant dynamics change and the new dynamics are used for additional loop designs. Since the plant dynamics change with each loop, there is a chance that some iteration is involved with fine tuning gains. A benefit of using SISO loop shaping techniques on a MIMO system is that robustness is ensured with each loop closure and that problems resulting from feedback can more easily be traced to the offending loop.

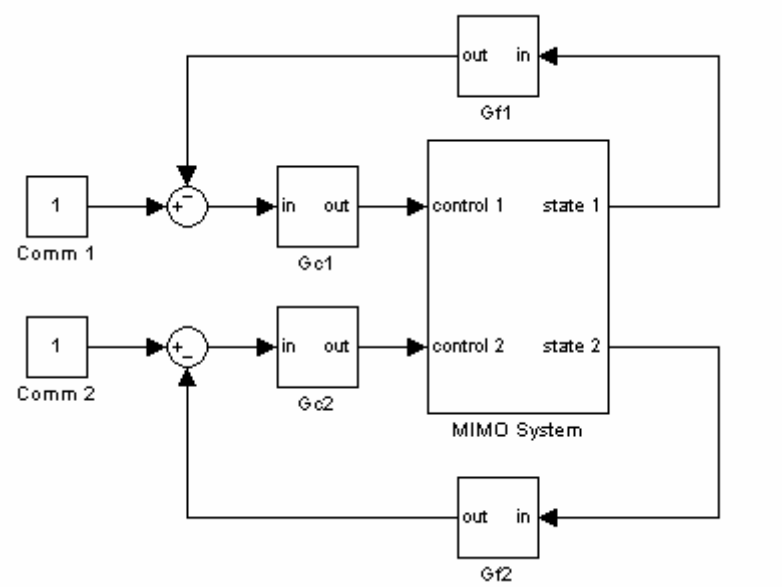

Figure 6-1: General MIMO System

A simple analysis of a generalized MIMO system can be started by looking at a standard state space system.

$$\dot{x} = Ax + Bu \tag{6-1}$$

$$y = Cx + Du \tag{6-2}$$

By taking the Laplace transform of the system and setting the feed forward term to zero, the system becomes:

$$s\,X(s) = A\,x(s) + B\,u(s) \tag{6-3}$$

$$Y(s) = C\,x(s) \tag{6-4}$$

The system in Figure 6-1 above has two feedback loops with sensors G_f. The control signal δ for each loop can be represented using the equation:

$$\begin{aligned} \delta_1 &= G_{c1}(\delta_{1comm} - G_{f1}x_1) \\ \delta_2 &= G_{c2}(\delta_{2comm} - G_{f2}x_2) \end{aligned} = G_c(\delta_{comm} - G_f CX) \tag{6-5}$$

Feeding back the states causes the plant matrix A to now become:

$$A_{fb} = [A - BG_f C] \tag{6-6}$$

Substituting equation (6-5) and (6-6) into equation (6-3)

$$sX = [A - BG_f C]X + B[G_c(\delta_{comm} - G_f CX)] \quad \textbf{(6-7)}$$

Rearranging to solve for $X(s)$, the new set of transfer functions can be defined by:

$$X(s) = [sI - [A - BG_c G_f C]]^{-1} BG_c \delta_{comm} \quad \textbf{(6-8)}$$

Mathematically it is possible to represent the system with multiple loop closures. However, there is no mathematical way that will determine the best order in which the loops should be closed. Ashkenas, Graham and McRuer[13] provide some insight into the best way a MIMO system can be solved using SISO techniques. Care must be taken to close the loops in the most efficient way possible to avoid excessive iterations when fine tuning the gains. Higher bandwidth loops, such as rate feedback, should be closed and tuned first. Lower bandwidth and command loops should be closed last. If there are any adverse dynamics in the system, those modes should be augmented using some form of rate feedback, if possible. Any mode augmentation loops should be tuned and closed before the rest of the loops.

The simplest way to provide STT control to the NXT UAV is through a multi-loop scheme as shown in Figure 6-2. This basic control architecture consists of four loops (A1, A2, R1, R2) to maintain attitude control of the vehicle and provide appropriate compensation for heading commands. The controller can be broken down into two sets (two loops each) with each set controlling the ailerons or rudder.

Control loop R1 is a loop closure of $r \rightarrow \delta r$ with a washout filter placed in the feedback loop. The sole purpose of this loop is to assist in damping the Dutch roll mode. Blackelock[14] recommends this type of loop closure as it is usually the most effective in controlling Dutch roll. Figure 5-2 shows how influential the transient response of this

mode can be on the lateral load factor. It is desired to minimize these oscillations to avoid excessive aileron control actuation. The washout filter uses its attenuation properties at low frequency to effectively open the loop when not needed and close the loop when there is a higher frequency yaw rate command. By closing this loop, the yaw rate is effectively being driven to zero. While not a problem for BTT aircraft, this is a significant problem for STT maneuvering since the intent is to maintain a steady yaw rate. The trick to applying this filter for STT control laws is to set the cutoff frequency lower than the natural frequency of the Dutch roll, but higher than the 1.25 rad/sec bandwidth as required by MIL-STD-1797.

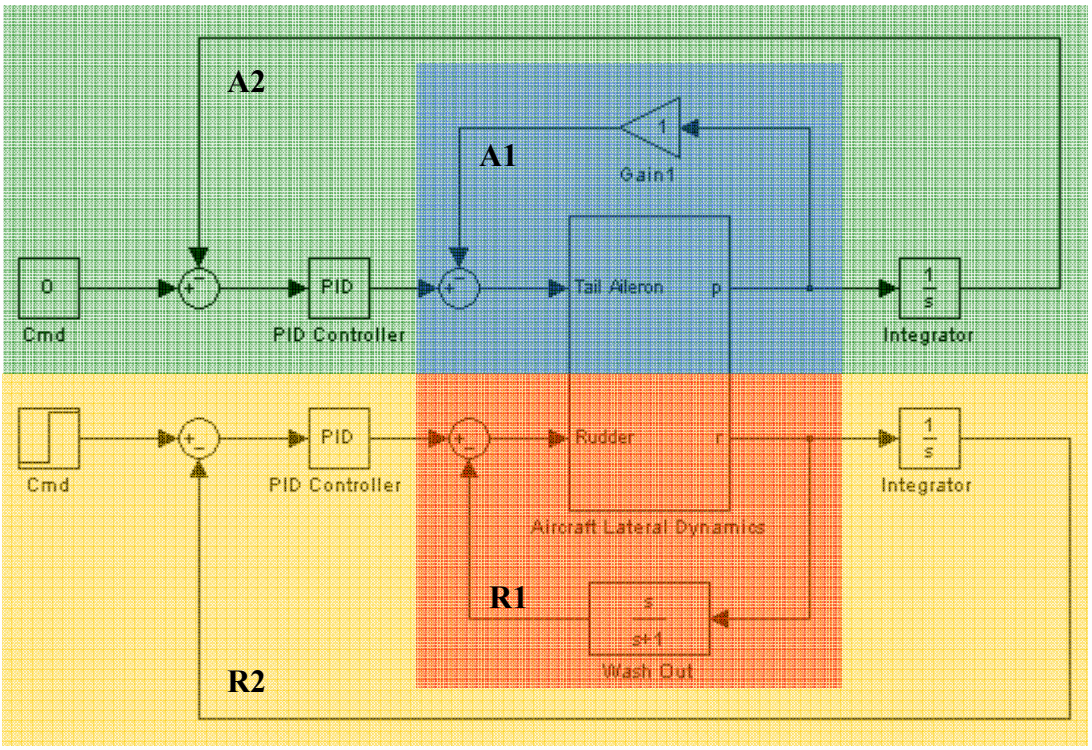

Figure 6-2: Skid-to-Turn Control Laws General Layout

Control loop A1 is a rate feedback of $p \rightarrow \delta a$ and is intended to drive the roll rate to zero as quickly as possible. The ailerons will be able to respond much quicker to sudden commands by using roll rate feedback than if only bank angle control was used.

Unfortunately, the inherent phase delay of the system will still allow some steady state roll angle to exist. Correcting any deviations in roll angle is the outer A2 loop which is a feedback of $\phi \rightarrow \delta a$. This loop is wrapped around the rate feedback and is compensated through some form of a Proportional-Integral-Derivative (PID) controller that will be determined during the analysis.

The final control loop R2 is the outer loop feedback of $\psi \rightarrow \delta r$. This loop is intended to command the vehicle, using the rudder, to turn and maintain a specific heading. Some form of compensation using a PID controller will be used to condition the signal as appropriate for this loop. The R2 heading loop becomes the foundation for any navigational and guidance control laws that may be used to control the UAV through a heading command.

6.2 Linear Control Law Design – Inner R1 Washout Loop

The first loop to be closed and designed is the inner R1 loop that contains the washout filter. As explained in the last section, this loop is used to provide extra damping of the Dutch roll mode. The $r \rightarrow \delta r$ transfer function for the proposed NXT2 system is shown below.

$$\frac{r}{\delta r} = \frac{2.26(s+7.64)(s^2+1.941s+6.073)}{(s+6.20)(s+0.95)(s^2+5.48s+23.16)} \qquad \textbf{(6-9)}$$

By looking at the Bode plot (Figure 6-4) for the $r \rightarrow \delta r$ transfer function, the resonant frequency for the Dutch roll mode is a around 5.25 rad/sec. In order for the washout filter to work, the break frequency of the filter must be less than the resonant, but larger than the required bandwidth.

After a few iterations of analyzing the closed-loop bode and step responses, the final washout filter break frequency was chosen to be 5 rad/sec. A gain of 5 was added to the filter to increase the effectiveness of the damping effects. The final transfer function for the filter is given below along with the block diagram for the system in Figure 6-3:

$$washout = \frac{5s}{s+5}$$

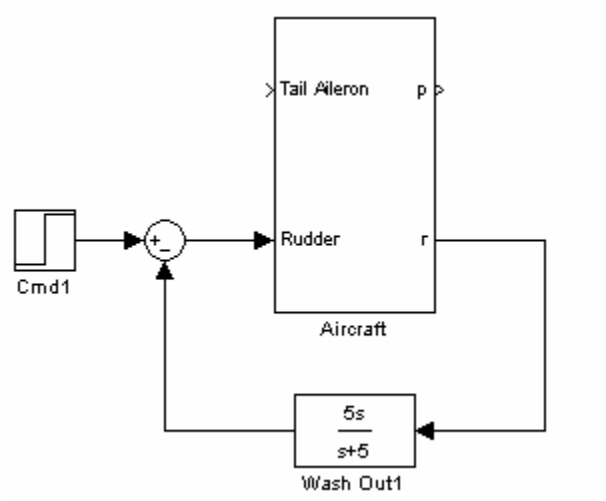

Figure 6-3: Block Diagram for R1 System

By looking at Figure 6-5, the step response shows an improvement during the initial transitory response. This is very important that even this little oscillation is damped out. Any residual oscillations that are still present in the dynamics can quickly become amplified when maximum performance skidding turns are attempted. Unfortunately, the system does respond a little slower; however, this slower response is easily tolerated. Figure 6-4 also shows a visible reduction in the resonant peak between the two systems. It is worth noting that the washout filter does not change the low or high frequency responses of the system, only the mid frequency portion of the Bode plot is altered.

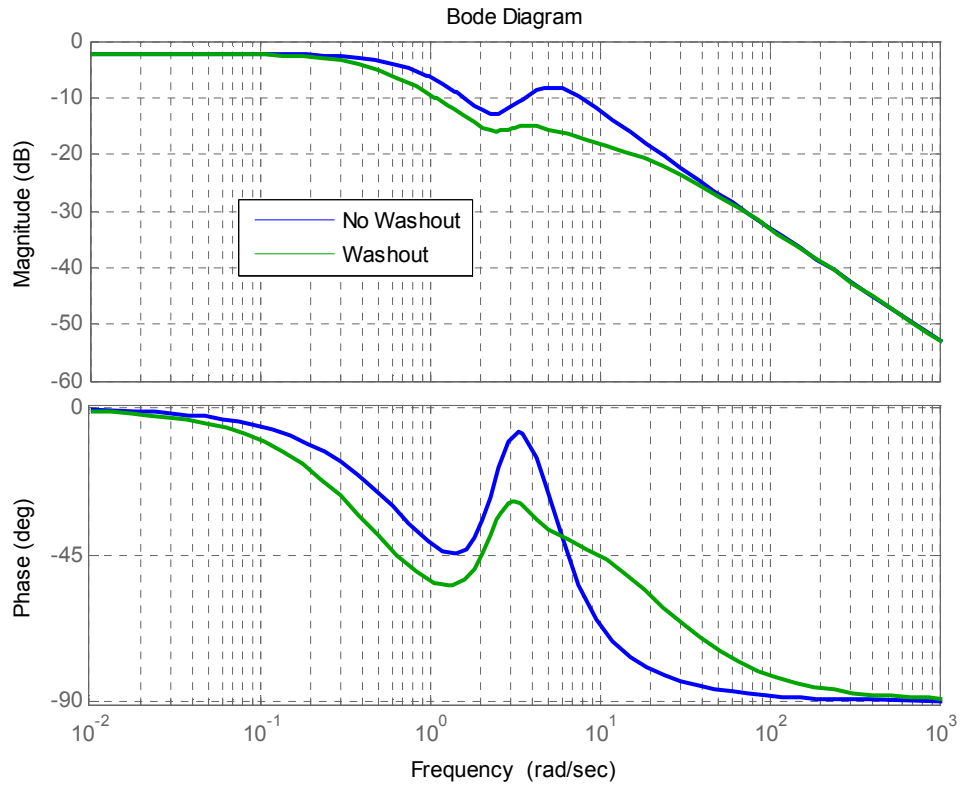

Figure 6-4: Bode Plot of r → δr Transfer Functions

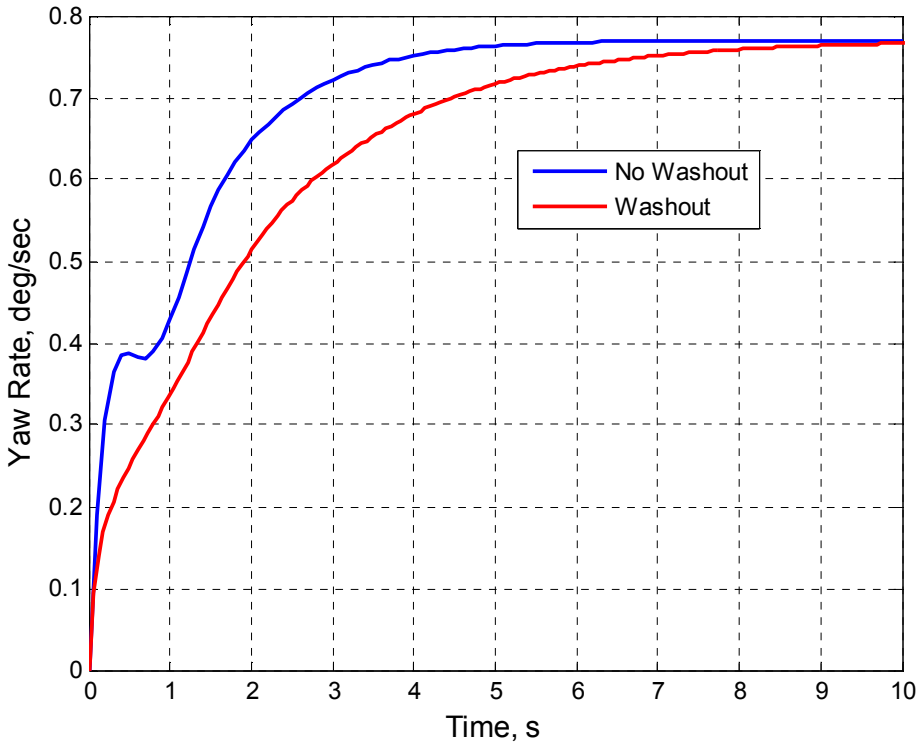

Figure 6-5: Step Response of r → δr Transfer Functions

6.3 Linear Control Law Design – Inner A1 Rate Feedback Loop

Next in the loop closure sequence is the inner A1 roll rate feedback loop. For this loop, a simple gain in the feedback path is all that will be determined. The previously closed $r \rightarrow \delta r$ washout loop will alter all of the states. By recalculating the system as discussed in section 6.1, the new open loop $p \rightarrow \delta a$ transfer function becomes:

$$\frac{p}{\delta a} = \frac{14.13\,s\,(s+9.91)\,(s^2+14.58s+111.3)}{(s+17.40)\,(s+7.96)\,(s+0.52)\,(s^2+3.02\,s+9.42)} \qquad \textbf{(6-10)}$$

The primary tool for this loop is the root locus plot as show in Figure 6-6. Increasing the gain will provide better aileron response to any induced roll rate. For this loop, a feedback gain of 2 was chosen. It was determined that this gain provided the best response by increasing the damping of the residual Dutch roll mode from 0.49 to 0.54. A gain made too high, will demand excessive control deflection rates of ailerons.

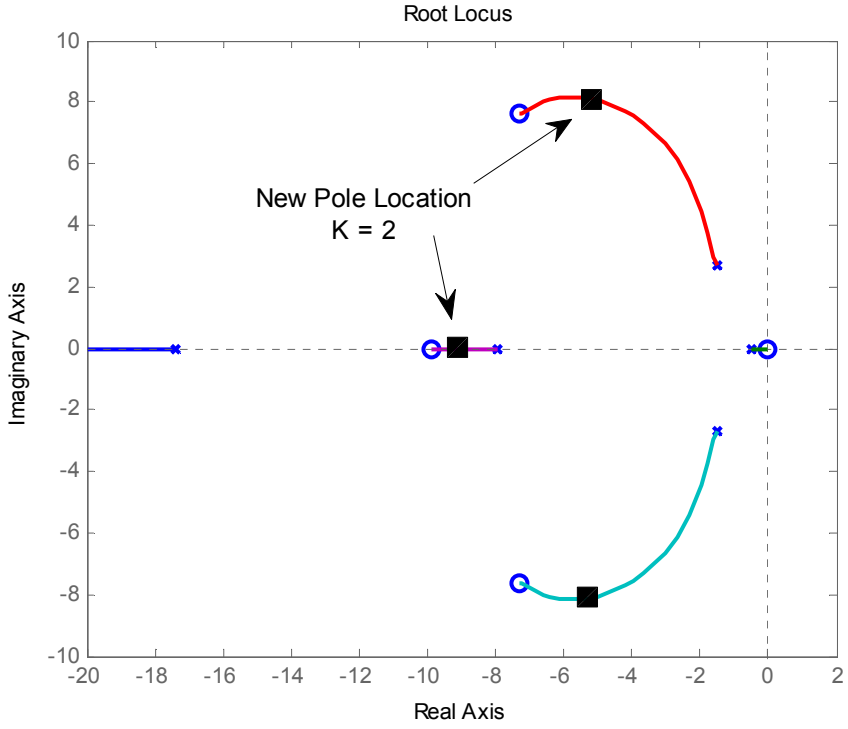

Figure 6-6: Root Locus of the p → δa Transfer Function

The step response of the $p \rightarrow \delta a$ system shows the most dramatic changes from the addition of the roll rate feedback loop. Roll rate is very quickly attenuated and held at the commanded value. Figure 6-8 shows the block diagram of the two inner loops.

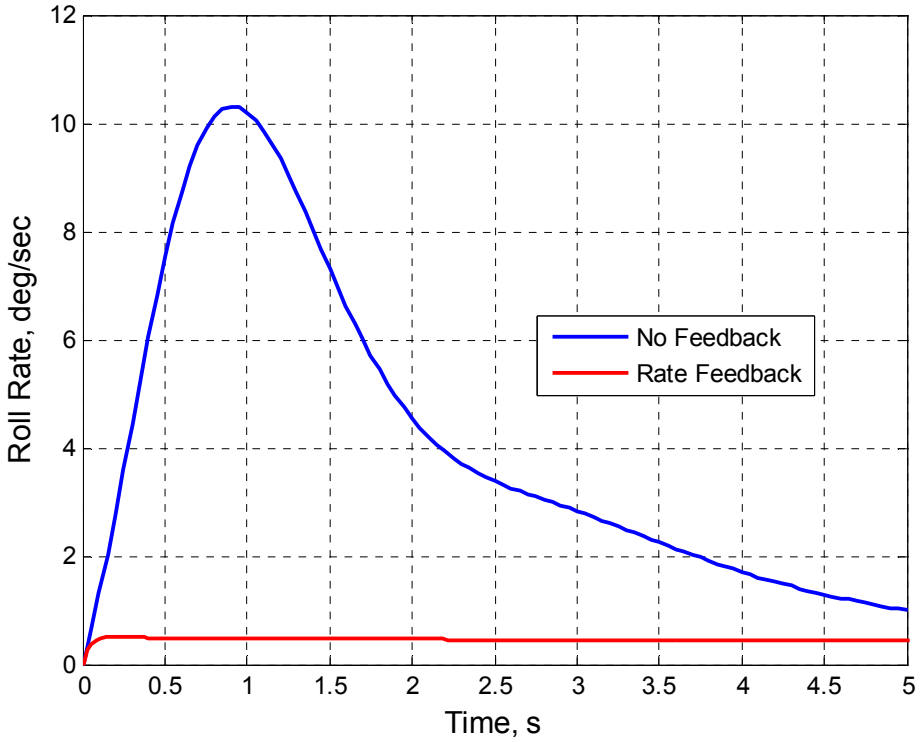

Figure 6-7: Step Response of the p → δa Transfer Function

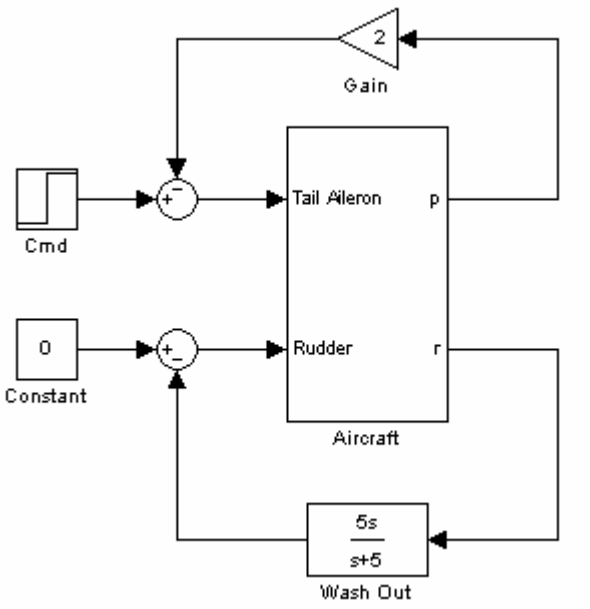

Figure 6-8: Block Diagram of the A1 and R1 Inner Loop Closures

6.4 Linear Control Law Design – Outer A2 Bank Angle Feedback Loop

One of the most important loop closures is the A2 outer loop bank angle control. This particular loop is the heart of the control system and enables the NXT UAV to accomplish wings level skid turns. The open loop $\phi \rightarrow \delta a$ transfer function is given by integrating the $p \rightarrow \delta a$ closed loop transfer function.

$$\frac{\phi}{\delta a} = \frac{14.13\,(s+9.91)(s^2+14.58s+111.3)}{(s+37.32)(s+9.46)(s+0.02)(s^2+10.36s+92.46)} \qquad \textbf{(6-11)}$$

The transfer function above shows that $\phi \rightarrow \delta a$ is a type 0 system, thus it will have a steady state error. This is undesirable since the requirements specify that the bank angle must return to zero. Subsequently, some from of integral compensation must be used to cancel out any steady state error.

The initial idea for the compensator was to design a lead-lag system and convert this to an equivalent PID controller. From a programming standpoint, since the Cloud Cap autopilot is based off of PID compensation, this form of a controller might be the easiest to implement. Four iterations of lead-lag compensators were designed in an attempt to gain the best step response. Table 6-1 below shows a listing of the lead-lag compensator specifications that were evaluated.

Lead Lag Compensator	Gain	Zeros	Poles
Comp 1	161	[-0.9 ; -2.0]	[-44 ; 0]
Comp 2	59	[-2.5 ; -2.0]	[-57 ; 0]
Comp 3	84	[-2.5 ; -0.6]	[-102 ; 0]
Comp 4	49	[-2.5 ;-0.2]	[-102 ; 0]

Table 6-1: Lead-Lag Design Iterations

The initial compensator design, Lead-Lag 1 started with placing a pure integrator at the origin. This provides the necessary integral to eliminate any steady state error. To remove the ill effects of the integrator on the phase curve, a zero was placed

approximately two decade before crossover. Another zero was placed one decade before the crossover to provide additional phase that would increase bandwidth. Finally, a pole was placed one decade after crossover to cancel the effects of the zero. This last pole acts as a means to roll the magnitude curve off at higher frequency, subsequently providing attenuation of noise. Figure 6-9 below shows the step response of this first iteration, along with the subsequent lead-lag designs.

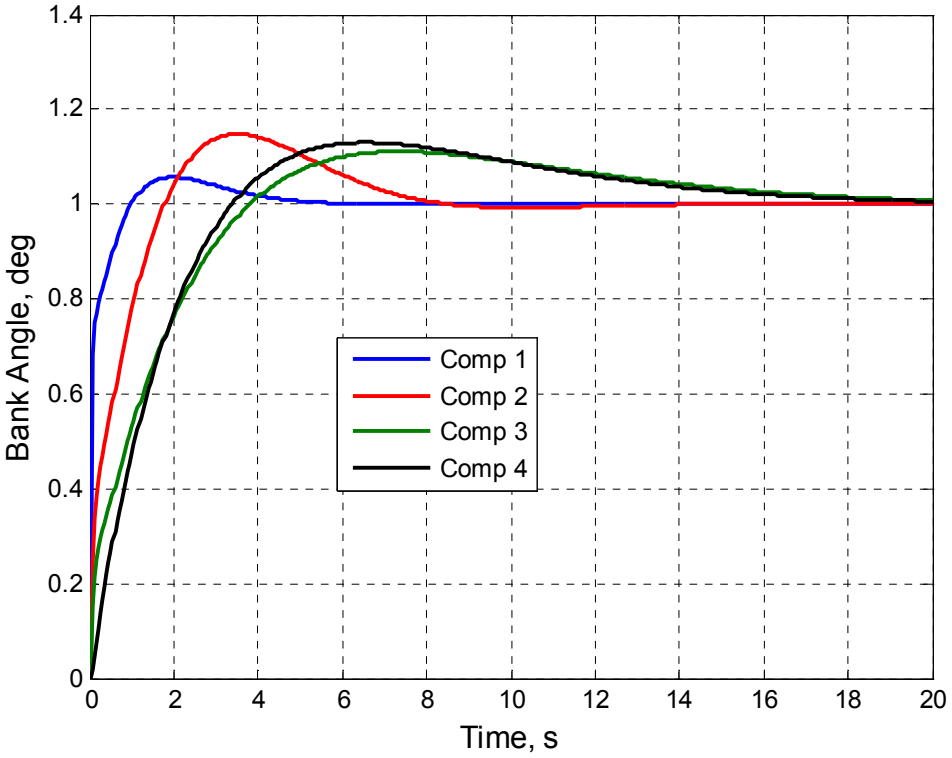

Figure 6-9: Step Responses to φ→δa Transfer Function with Lead-Lag Comp.

This first design imposes a very steep instantaneous demand at the beginning of the response. Such a demand is not suitable for the control surfaces. To soften this demand, the zeros in the compensator were moved closer together near crossover and the gain was reduced. This decreased the instantaneous demand by half, but allowed a larger overshoot. Compensator 3 separated the poles by a decade and increased the gain. While

this design was better, it still was not suitable. Compensator 4 essentially took the previous design and reduced the gain. This particular compensator looks to have a smooth input, little overshoot and virtually no oscillation. It might seem that this would be an excellent compensator; however, the control deflection demand is still excessively large for this system. The gain of 49 causes an unacceptable sharp spike in instantaneous control deflection that exceeds the physical limits of the system.

The sharp control response demanded from the lead-lag combination is not suitable for this option. Another possibility is to remove the lead compensator from the design and just use a lag compensator; which translates into a simple Proportional-Integral (PI) controller rather than a PID controller. PI controllers do have the disadvantage of the possibility of integrator windup (see next section). However, it is not intended for the system to have too large of bank angle deviations. This will safely allow the use of a PI controller.

Lag Compensator	Gain	Zeros	Poles
Comp 5	1.5	-0.15	0
Comp 6	0.7	-0.15	0
Comp 7	1.6	-0.06	0

Table 6-2: Lag Compensator Design Iterations

Table 6-2 above shows the design iterations for the integral lag compensator. The design was started by placing a pure integrator at the origin. A zero was placed one decade before crossover to counteract the effects of the pole. Figure 6-10 shows this step response with the lag compensator. This design has a little too much overshoot and takes a while before settling. A smaller gain was tried in Compensator 6, but this produced an even larger overshoot. The final lag compensator design, Comp 7, had a fairly quick response and limited overshoot.

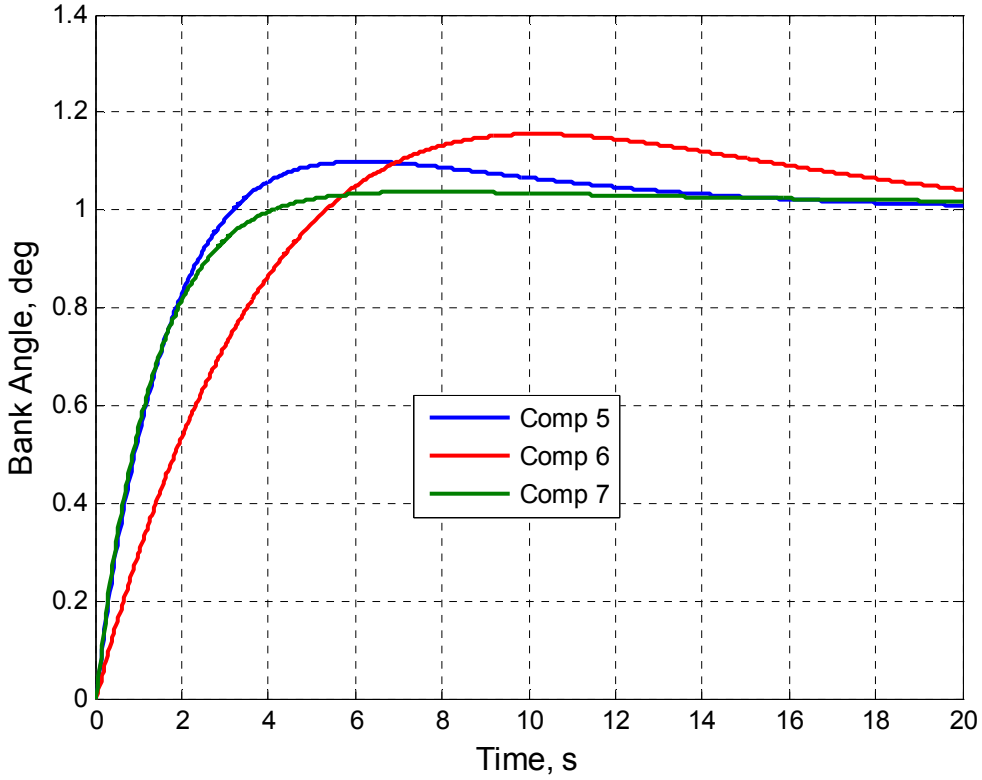

Figure 6-10: Step Responses to φ→δa Transfer Function with Lag Compensators

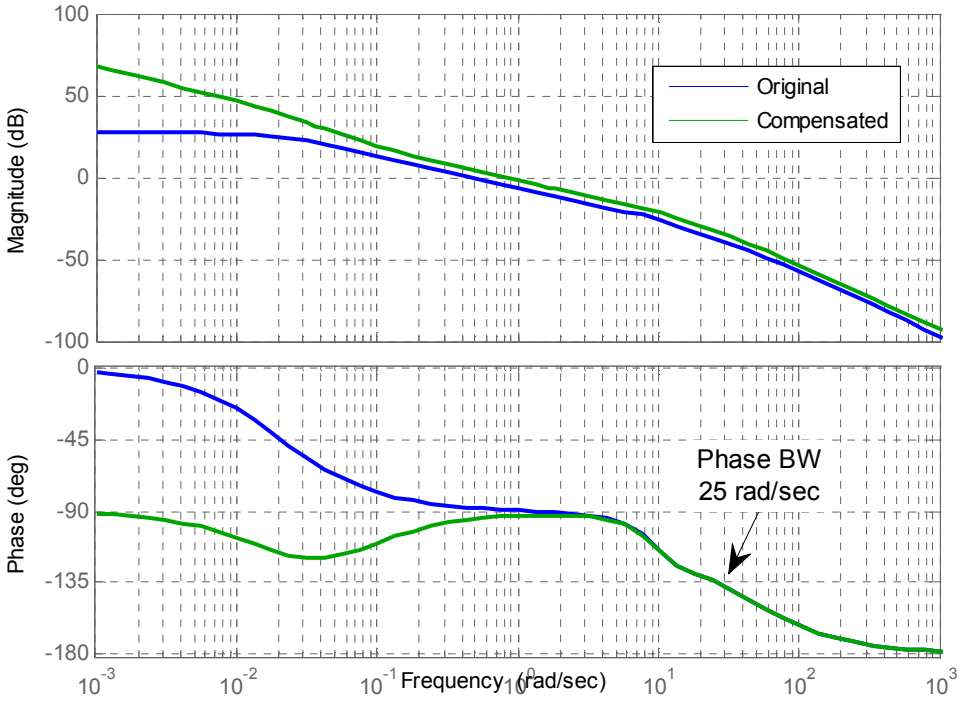

Figure 6-11: Bode Plot of the φ→δa TF with and without Compensation

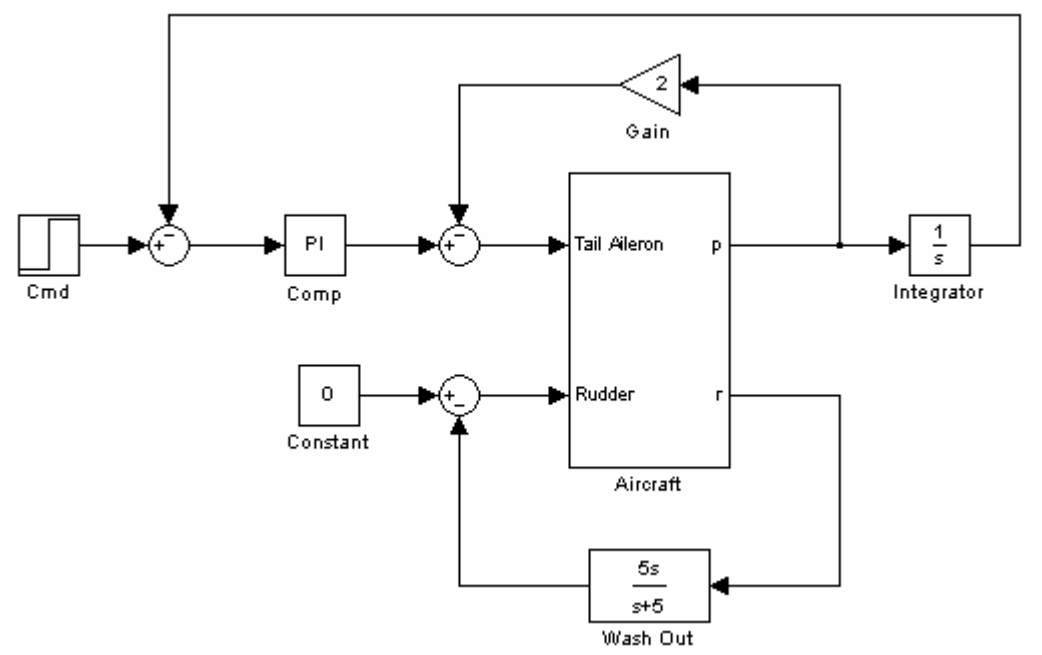

Figure 6-12: Block Diagram for the A2 Loop Closure

One last parameter must be checked to ensure that the compensator will be acceptable in the linear model. Using the definition of bandwidth from MIL-STD-1797, the A2 loop bandwidth is 25 rad/sec. This system is considered to be phase limited since the gain bandwidth of this loop is infinity.

6.5 Linear Control Law Design – Outer R2 Heading Angle Feedback Loop

The final loop closure that must be completed is the R2 heading angle outer loop. This loop's intended purpose is to be designed to accept any third part guidance system that controls navigation through heading. Closing the loop starts with the $\psi \rightarrow \delta r$ transfer function as given below:

$$\frac{\psi}{\delta r} = \frac{2.26(s+5)(s+45.05)(s+0.02)(s^2+1.74s+1.57)}{s(s+36.8)(s+9.43)(s+0.06)(s^2+10.14s+93.36)} \qquad \textbf{(6-12)}$$

In deciding the best compensator for this loop, a key distinction must be made from the previous loops. This particular loop will be accepting heading commands that can range

from 0º to 359º. If the turns will be made in an optimal manner, then the theoretical maximum input will be 180º. In either case, large inputs could possibly be commanded through this loop; subsequently leading to performance saturation and lengthy amounts of time that the vehicle would be generating an error through the feedback loop.

Any compensation that includes an integration gain, such as an ILC, PI or PID controller, is not suitable for this control task. A problem arises during the period of performance saturation where the integrator continues to integrate the error during the saturation. As the vehicle approaches the commanded heading, the controller must then integrate all of the accumulated error back to zero. This phenomenon is known as integrator windup. In the time it takes for the controller to integrate out the error, the system has significantly overshot the commanded value and large oscillations will occur. Because of this problem, a Proportional-Derivative (PD) controller will be used for the heading control system. One drawback to this setup is that the system will only reach the commanded value at infinity. However, relatively small errors from the commanded heading can be tolerated.

A PD controller is simply a gain that is multiplied by a zero. To start the PD controller design, a real zero is introduced into the system. Figure 6-13 below shows the effect of this zero on the root locus. As the zero moves from the origin with increasing frequency in the left half plane, the complex branches of the root locus break off from the real axis and merge. If this happens, then there will always be a set of complex poles in the system. Unfortunately, nearly any amount of gain in the compensator will cause some second order behavior from complex poles that will form near the origin. Minimization of the effect will become critical, especially when working with the nonlinear simulation.

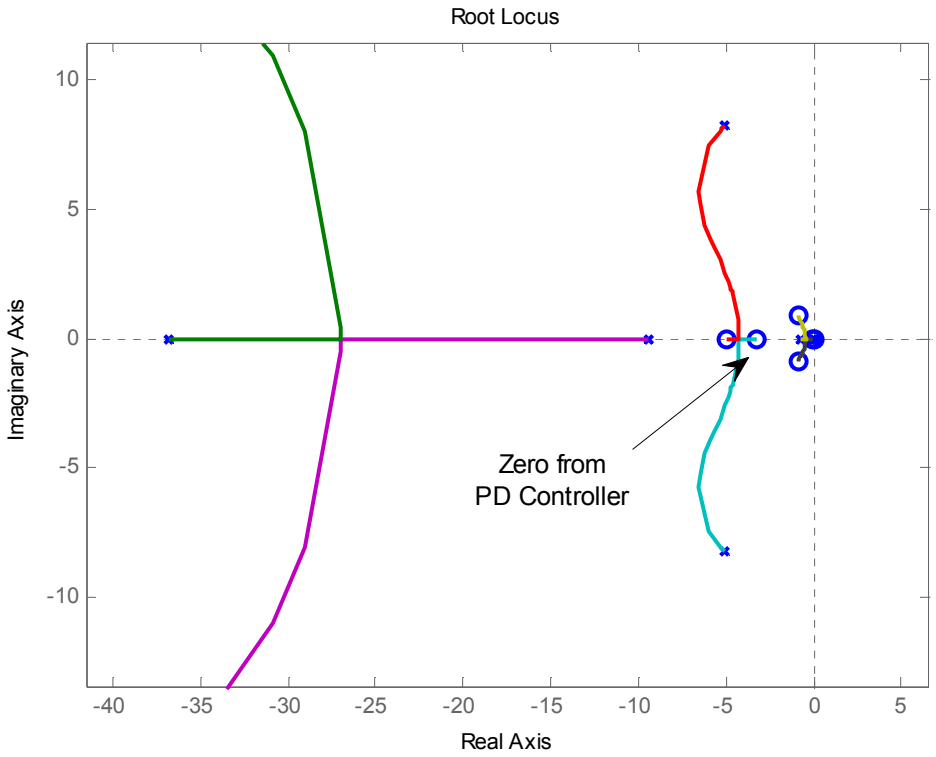

Figure 6-13: Open Loop Root Locus with Zero at -3.3

With the zero of the PD controller placed, a series of different gains were tried to see the effects on the step response. Table 6-3 below shows a selection of the gain iterations with Figure 6-14 showing the step responses. In each of the cases, there is an initial spike in the system, and subsequent demand on the rudder. The first three compensators that are shown appear to be the best candidates for the final design since they reach their steady state value fairly quickly. Unfortunately, the initial demand on the rudder from the first three compensator designs is fairly excessive with PD compensator 3 requiring 4.5 degrees of instantaneous deflection.

PD Compensator	Gain	Zero
Comp 1	250	-3.3
Comp 2	50	-3.3
Comp 3	15	-3.3
Comp 4	1	-3.3

Table 6-3: PD Gain Design Iterations

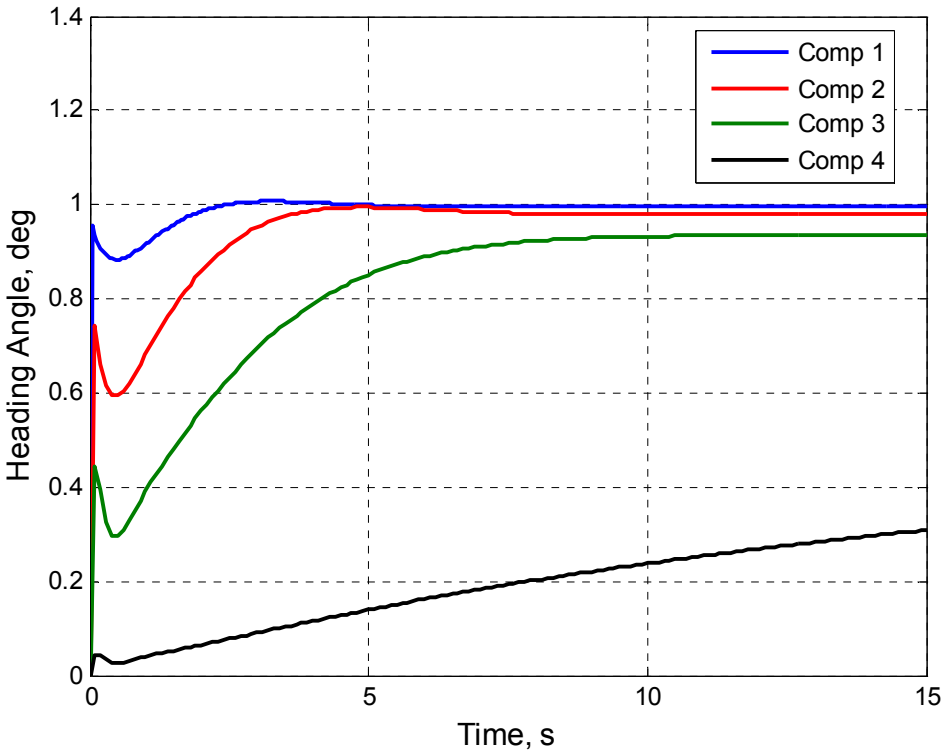

Figure 6-14: Step Responses to ψ→δr Transfer Function with PD Compensators

The last compensator design might prove to be the best controller for this particular loop. While it does have a very long response time, it must be considered that only a unity step input is used in designing the PD compensator. In reality, it is unreasonable for the NXT UAV to make a 180º turn in just a few seconds. It also should be recognized that the linear model greatly underestimates the STT dynamics of the UAV. Keeping these considerations in mind, PD Compensator 4 might prove to be the best option when fully integrated into the nonlinear model.

Figure 6-15 shows the Bode plot of the original and compensated open loop systems. As expected, the low frequency portion of the Bode remains the same, while the higher frequency portion of the system rolls off 20 dB less per decade. It should also be noted that this system exhibits an infinite amount of bandwidth per the MIL-STD-1797 definition. The figure also shows that significant attenuation is present. When placed into

the nonlinear system, this should not pose a problem since the linear system under predicts performance. When placed in the nonlinear system, the compensator is effective being multiplied by a large gain.

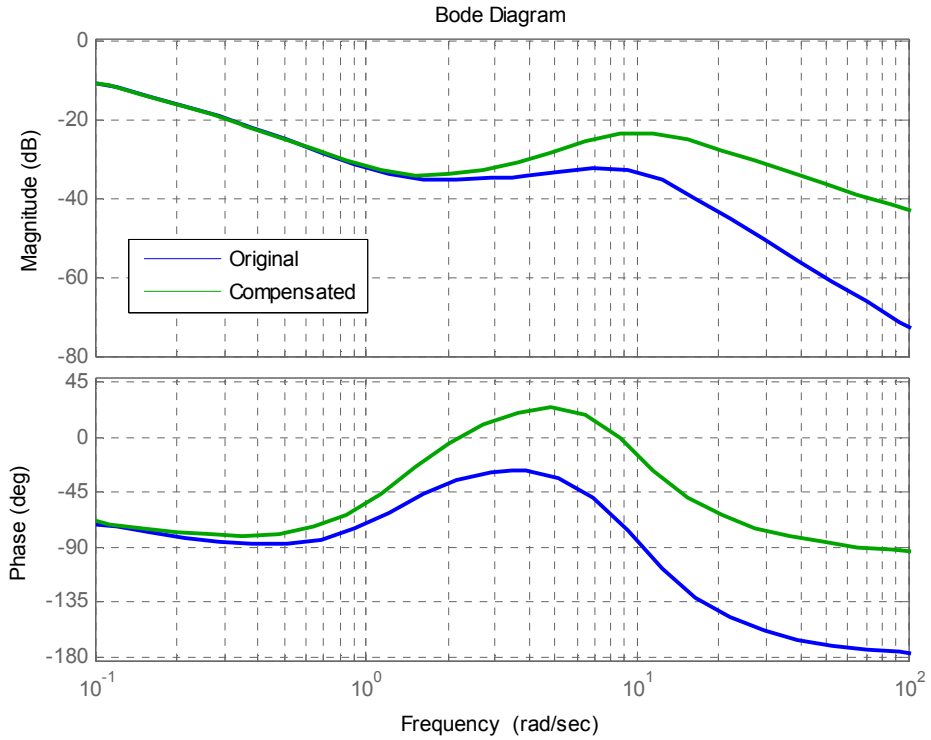

Figure 6-15: Bode Plot of the ψ→δr TF with and without Compensation

Lastly, the entire set of control laws must be analyzed together to verify that all of the loops work properly. This is an important step since SISO design techniques were used to design a MIMO system. A unit ψ step input was applied to the system with the bank angle being commanded to zero. Figure 6-16 shows the block diagram of the completed system. Primarily of interest is the initial transient response of the control inputs to insure that these deflections are reasonable. Figure 6-17 shows that the control laws immediately respond to the commanded input with most of the transitory behavior being excited by the Dutch roll washout filter. Additionally, the bank angle of the UAV quickly corrects itself back to the commanded value as shown in Figure 6-18.

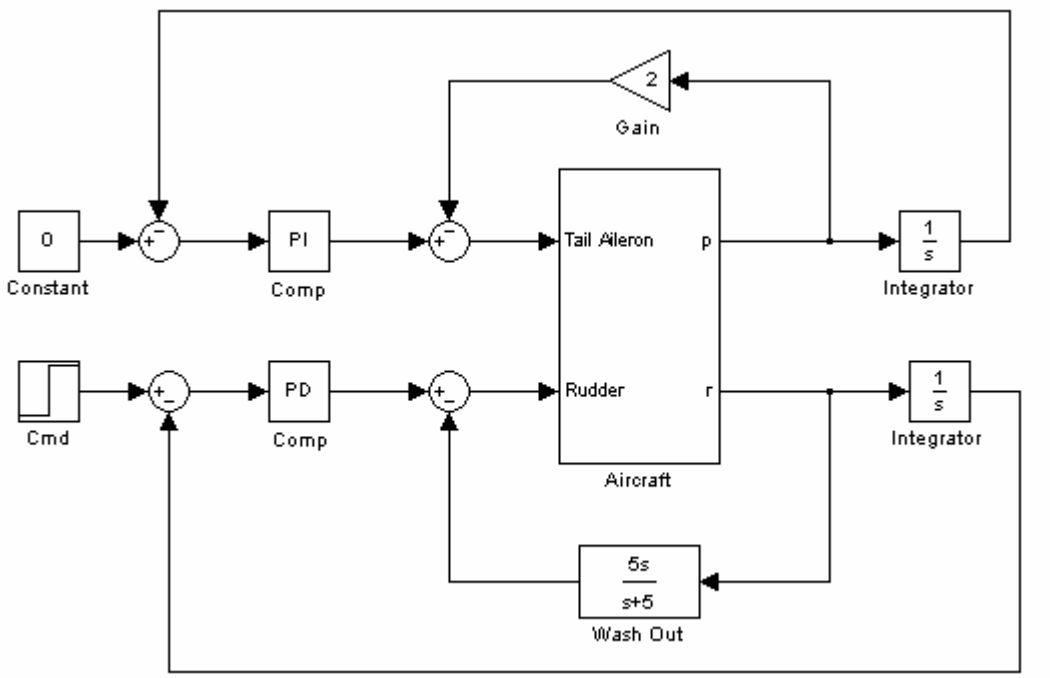

Figure 6-16: Block Diagram of Completed STT Linear Control System

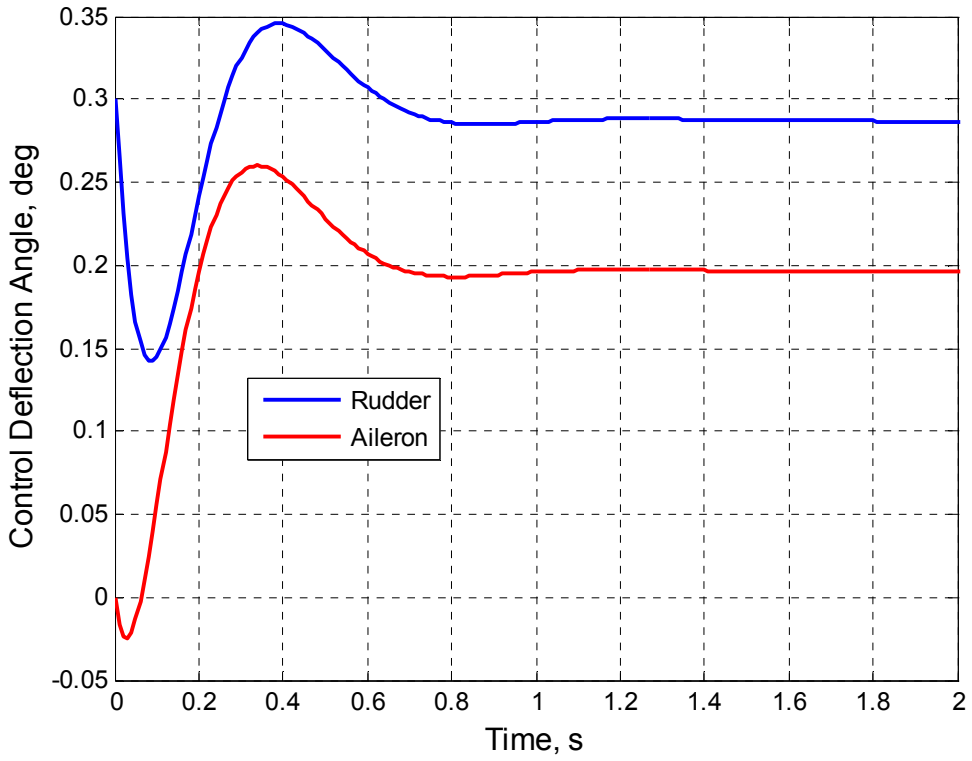

Figure 6-17: Control Surface Deflection (Linear Model) due to Unit ψ Step Input

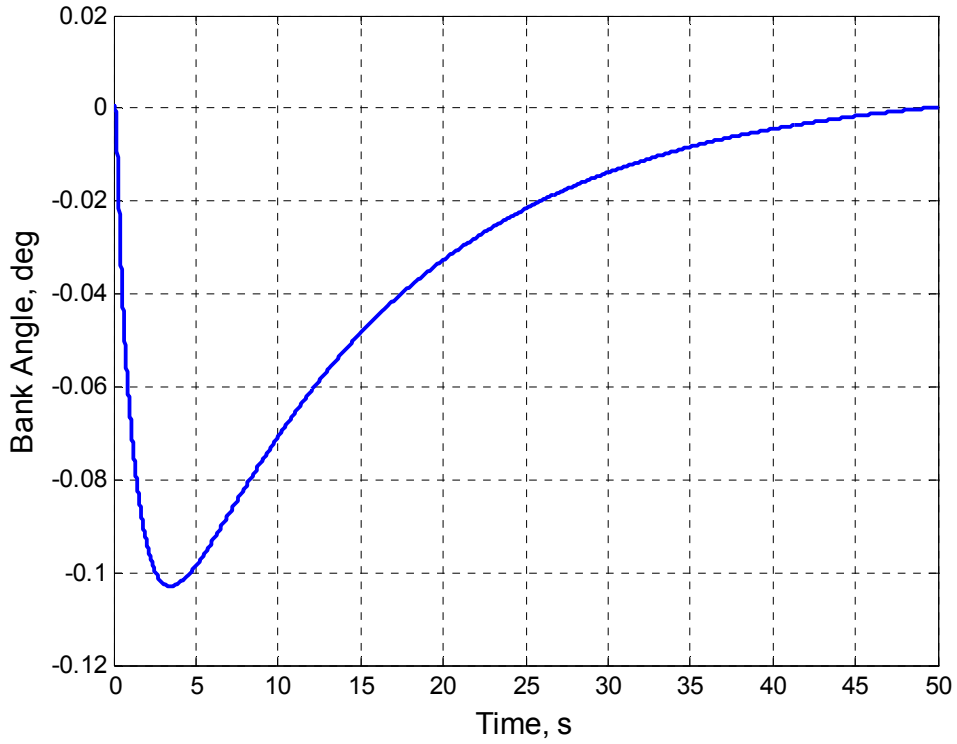

Figure 6-18: Bank Angle (Linear Model) due to Unit ψ Step Input

6.6 Control Law Application to Nonlinear Simulation

Section 5.2 showed that the linear analysis under predicts the performance of the system. It is reasonable to expect that the control laws designed for the linear simulation will require some tuning when applied to the full 6 DOF nonlinear simulation of NXT2. The control laws as designed by the linear analysis are applied to the nonlinear simulation without alteration. Appropriate deflection limits were applied to the control surfaces, ensuring that the UAV did not have unreasonable control authority.

The first area of concern is the possibility that the UAV will tumble if the horizontal stabilizer is saturated. An initial simulation proved that this was the case. A full rudder application is capable of yawing the aircraft fast enough to easily saturate the horizontal stabilizer. Previous sections of this thesis have shown that the rudder

deflection is proportional to the steady state yaw rate and required aileron deflection. From tests using the nonlinear simulation, it was determined that a 1.6º rudder deflection provides the maximum allowable steady state skidding turn without exceeding the three limits discussed in Section 5.2. Subsequently, it would be appropriate to limit the rudder deflection to 1.6º at airspeeds around 400 knots.

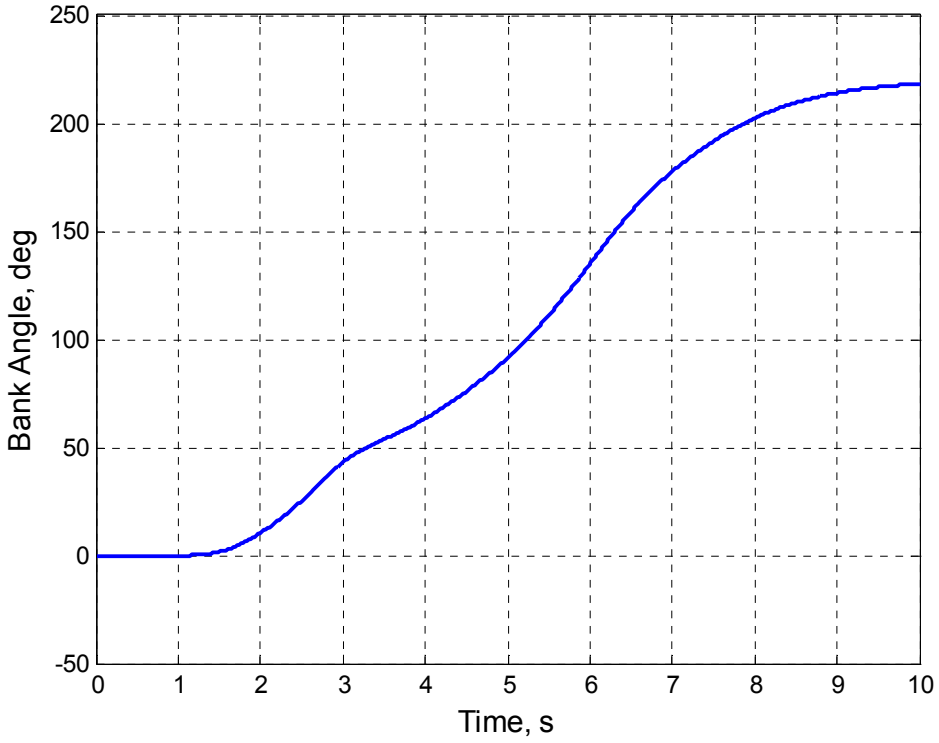

Figure 6-19: Bank Angle Using Linear Design PI Controller

The next two problems encountered are not mutually exclusive since the solutions for each problem depend on each other. For the first part of the problem, even through the steady state STT value is limited by the maximum rudder deflection, the initial transient response could produce high enough yaw rates to once again saturate the ailerons. Primarily, this becomes an issue when large heading commands are issued to the autopilot, or if a pilot on the ground reverts to manual STT control. This effect can be minimized, without having to sacrifice the maximum steady state value, by limiting the

rate at which the rudder can be actuated. Iterative testing determined that applying a rate limit of 2 deg/sec was appropriate to minimizing the initial transient response.

The second part of the problem is that the gain on the PI controller is not adequate to maintain wings level. Figure 6-19 shows that the UAV flips if the linear PI controller is used. However, the rudder rate limiter also affects controller performance. Limiting the angular rate on the rudder requires that the Kp/Ki ratio changes. In other words, the amount of proportional gain to integral gain must change in order to properly account for the lag introduced by the rudder rate limitation.

An iterative approach, using the nonlinear simulation, was used to determine a new set of gains for the bank angle PI controller. Six different PI controllers were tested until adequate performance was found. Table 6-4 below shows the list of compensators that were tried. The best Kp/Ki ratio was found to be 2 versus the original ratio of 90. Additionally, the gain for the entire controller had to be significantly raised to insure that the bank angle maintained the ± 5º limits. A 180º heading change step response was applied during each iteration, with the resulting bank angle plotted in Figure 6-20. The final compensator for the bank angle controller was chosen to be PI 6, which has a proportional gain of 40 and an integral gain of 20.

PI Compensator	Kp	Ki
PI 1	2	0.5
PI 2	2	1
PI 3	4	2
PI 4	8	4
PI 5	20	10
PI 6	40	20

Table 6-4: PI Compensator Iteration

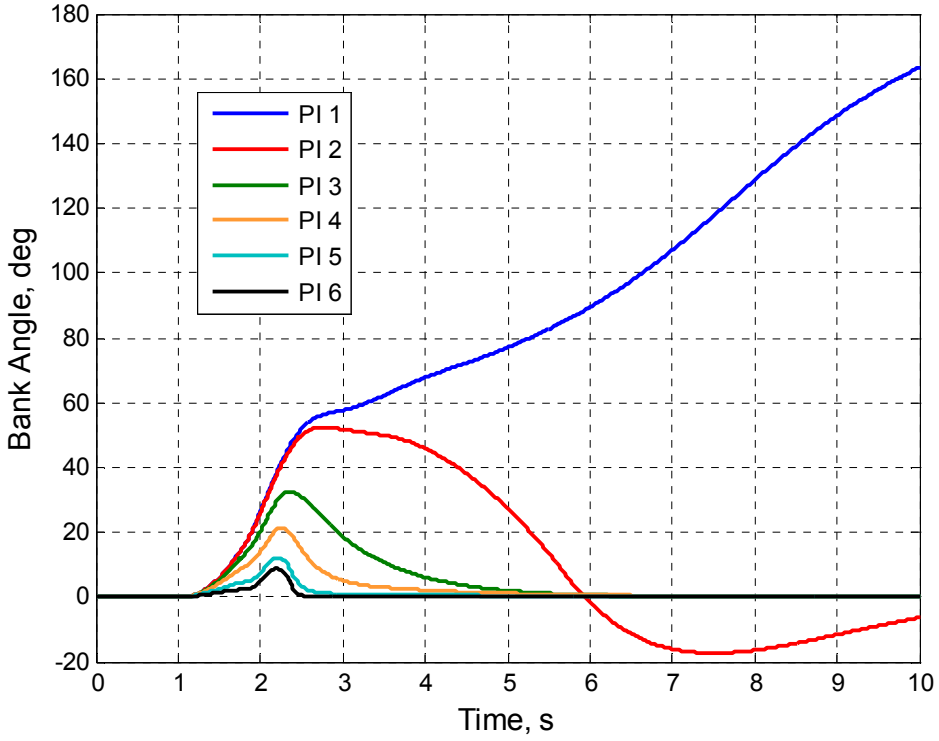

Figure 6-20: Bank Angle PI Controller Iteration

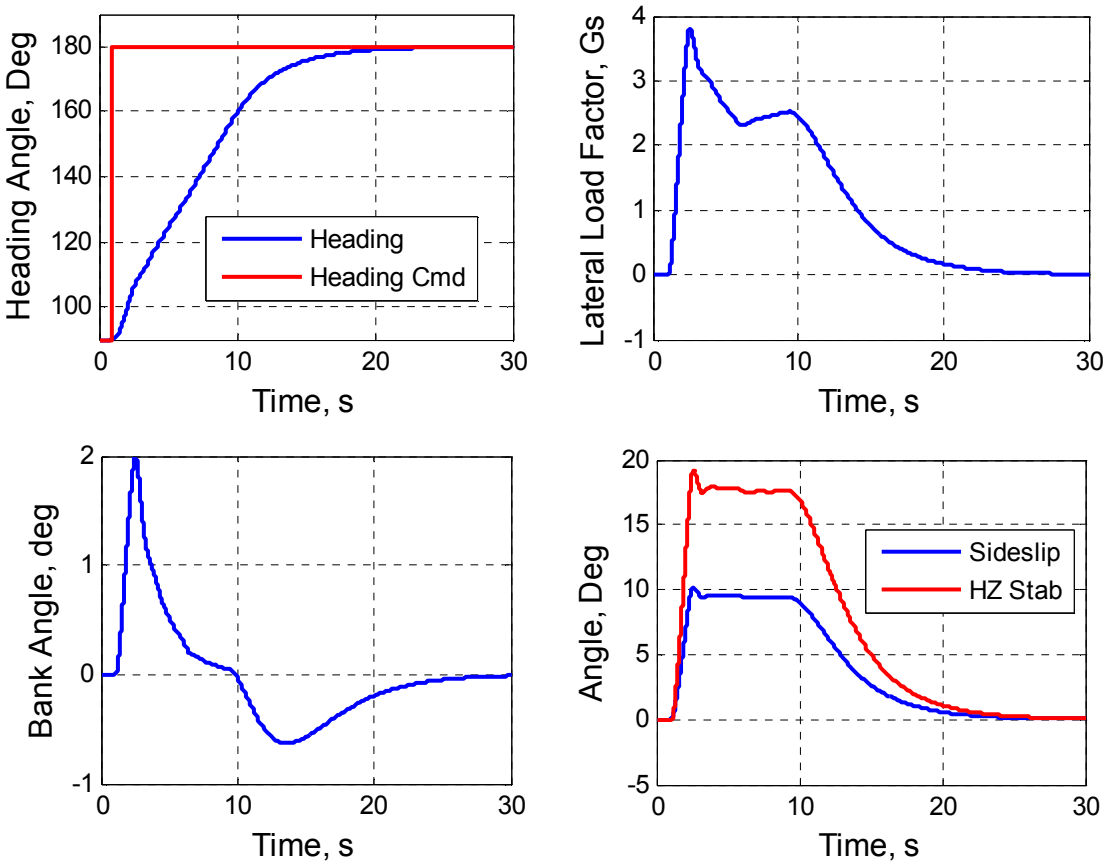

Figure 6-21: Critical Dynamic Parameters for 180º STT Using Final PI Controller

Final verification of the performance of the STT control system as applied to the nonlinear system can be seen in Figure 6-21. This test was a simple right handed turn with a change in heading of 90º. The heading angle tracked very nicely using the PD controller as designed in the linear analysis. No modifications were necessary for this compensator. Bank angle was quickly and smoothly corrected back to zero. Most importantly, the control system maintained a sideslip angle less than 10º and did not saturate any of the control surfaces. There is also approximately 3º degrees of control authority left in the horizontal stabilizers that can be used for pitch control as necessary.

6.7 Skidding S-Turn Profile

The last step in attempting to meet the design requirements is to demonstrate that the STT control system is capable of flying skidding S-Turns. For this particular demonstration, an S-Turn will be defined as having 180º heading changes. Shallower S-Turns can be accomplished by limiting the heading variations; however, the 180º heading change scenario is considered to be worst case. To simulate heading command information from a guidance controller, a square wave was used to simulate the required 180º heading changes. The step commands issued at the proper frequency will simulate a minimum radius skid turn profile.

Figure 6-22 through Figure 6-25 show the dynamics of the NXT2 UAV while flying the S-Turn profile. The ground track shows that the vehicle is flying a very well defined set of S-Turns with the heading angle being responsive to the commands. Once again the bank angle is quick to return to zero. This simulation shows that the NXT2 vehicle design is capable of accomplishing nearly 3 G skidding S-Turns.

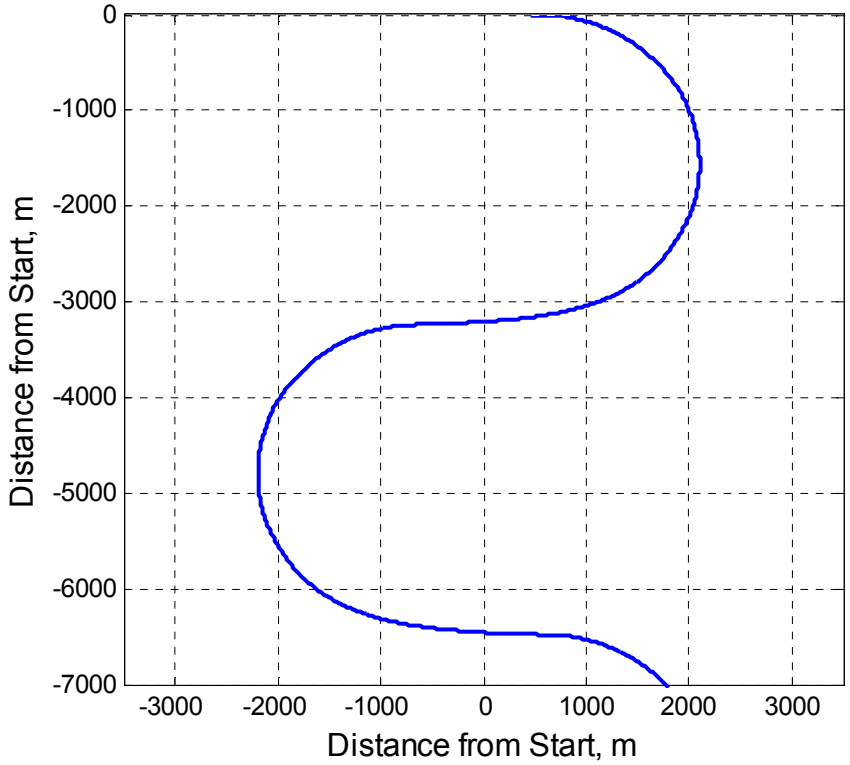

Figure 6-22: Overhead View of UAV Path during S-Turns (1 Period)

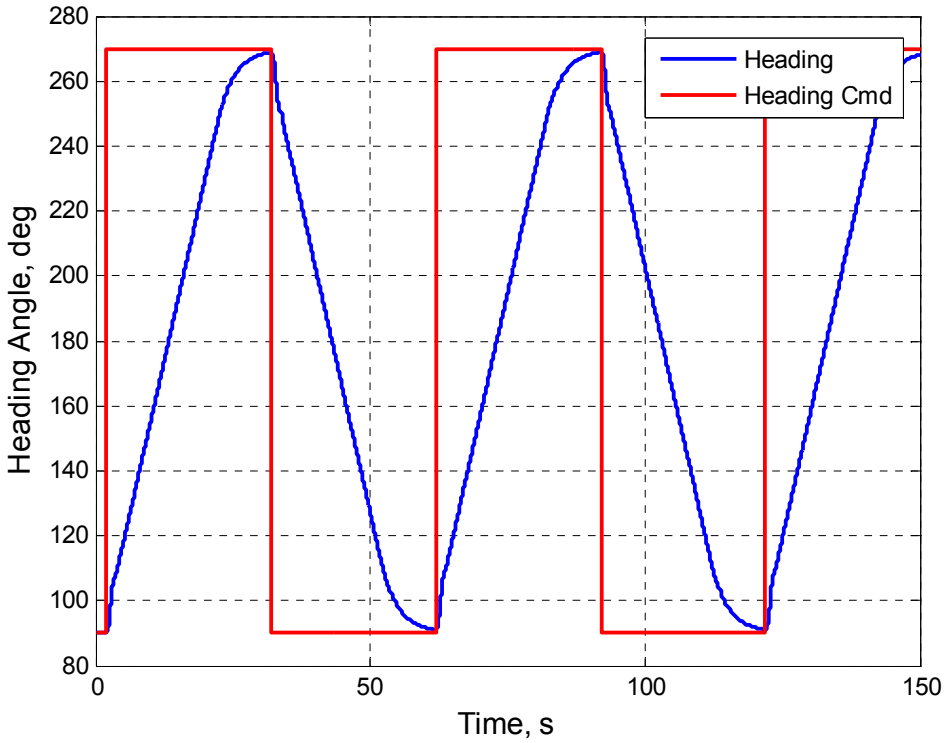

Figure 6-23: Heading Angle during S-Turn Profile

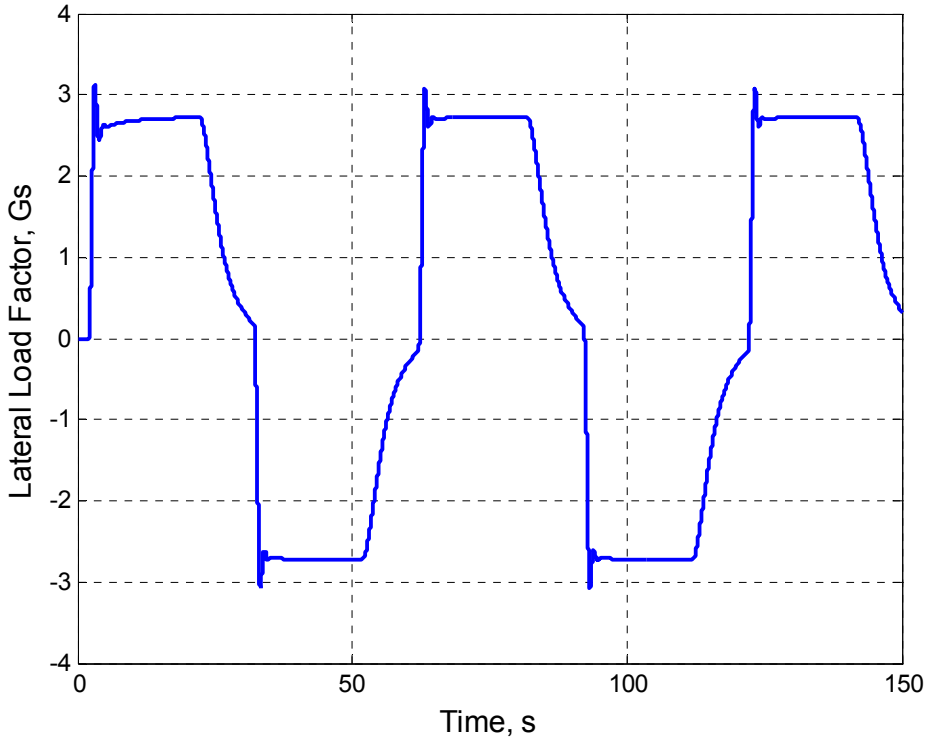

Figure 6-24: Lateral Load Factor during S-Turn Profile

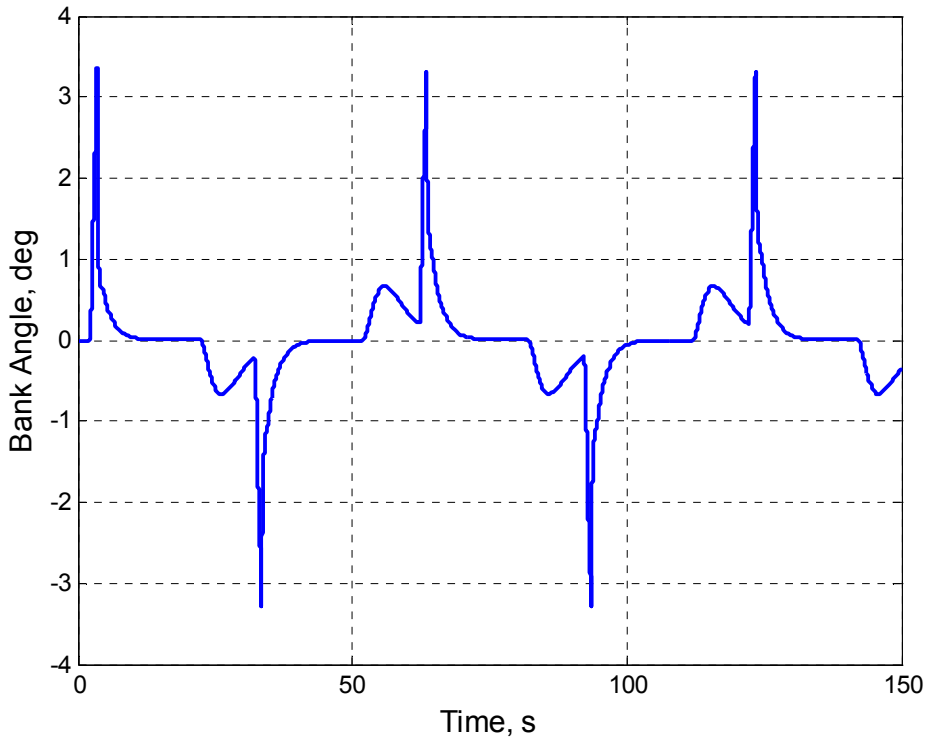

Figure 6-25: Bank Angle during S-Turn Profile

Chapter 7: Pilot in the Loop Simulation

7.1 Pilot in the Loop Control Law Considerations

The control law architecture designed in the previous chapter is excellent for fully autonomous control. However, there might be situations in which the pilot might want to hand fly the UAV from the ground station. In this case, the pilot would be making the appropriate corrections to maintain heading control; subsequently rendering the outer R2 heading loop useless. Bank angle control would still be maintained by the A1 and A2 loop closures.

There are two possible control schemes that would enable a pilot to maneuver using skidding turns. The first would be direct control of the rudder without using any feedback control with the rudder. While this would provide the simplest means of yaw control, the pilot might not find the resulting handling qualities acceptable. The Dutch roll mode would inhibit a smooth turn to heading flight profile.

A more logical solution would be to have the pilot command lateral acceleration rather than rudder deflection directly. While turning an aircraft, a pilot is attempting to maintain a constant heading rate. Fundamentally for skidding turns, a pilot is actually trying to maintain a constant yaw rate or lateral acceleration. The inner R1 washout loop provides an excellent foundation for acceleration control. Section 2.2 showed that the lateral acceleration is proportional to a gain multiplied by yaw rate. Control inputs from the pilot would only need to be multiplied by a gain and fed into the yaw rate loop. In reality, this gain is a function of airspeed; however, the simulations performed are at a constant airspeed for this research. Figure 7-1 shows the block diagram for the pilot in the loop control system.

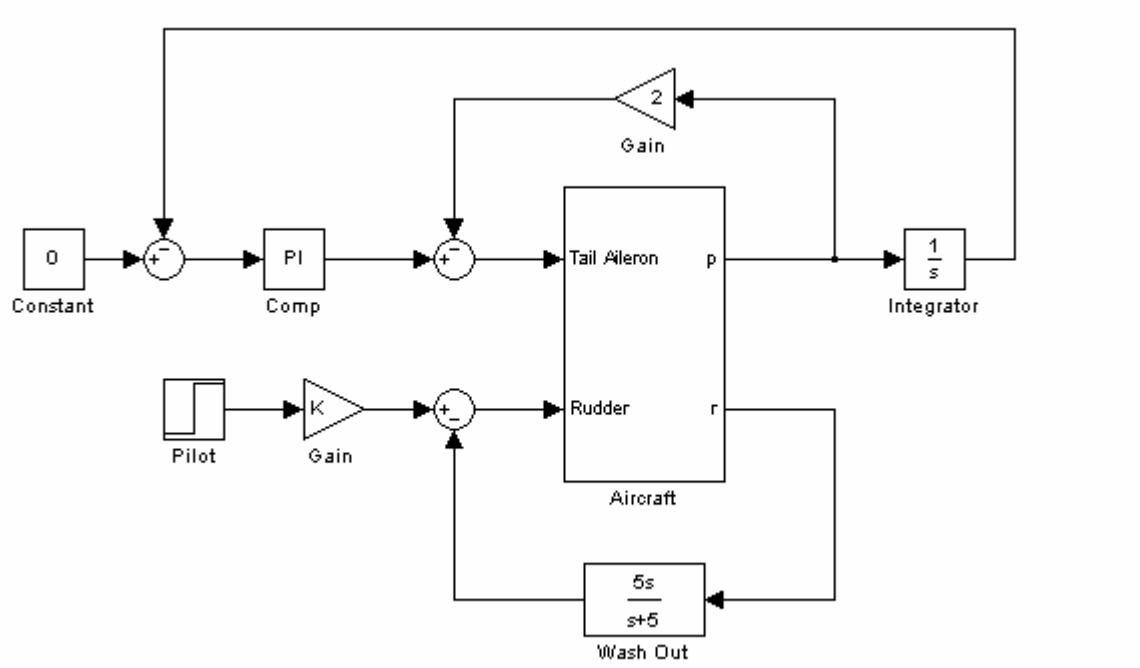

Figure 7-1: Pilot in the Loop Control Architecture

A pilot friendly interface must be established to appropriately close the heading loop with the pilot. The first step is a graphical representation of flight data to provide the pilot with situational awareness. A set of instruments that are rendered through Simulink were used to represent the information provided by the standard six cockpit gauges.

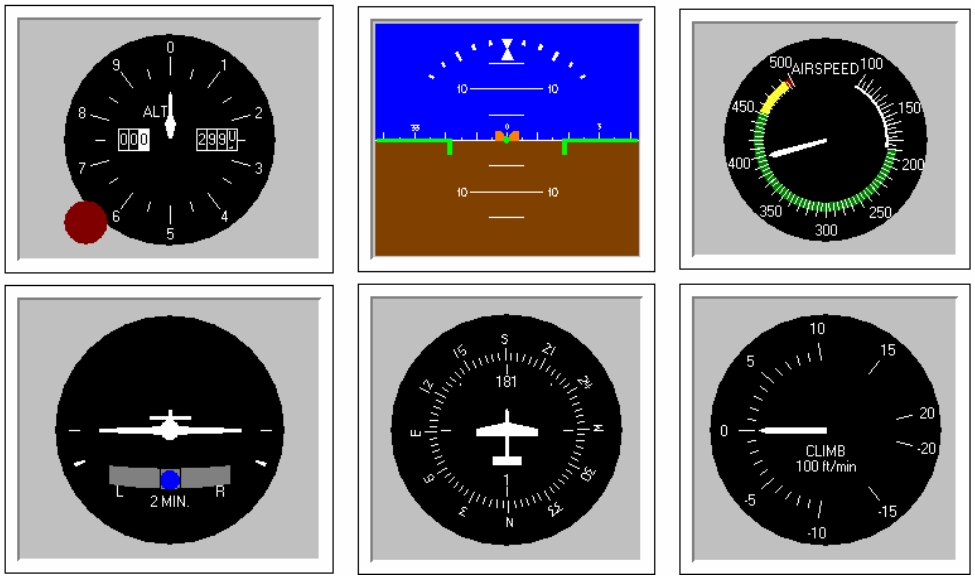

Figure 7-2: Pilot Instrument Interface

The second step is providing a set of controls for the pilot. A standard three axis joystick was interfaced with the nonlinear simulation. Skid-to-turn control was commanded by the yaw axis through the twist-stick in the hand grip. All of the rate and saturation limits that were established in section 6.6 were also implemented to prevent the pilot from over controlling the UAV.

7.2 Pilot Simulation and Evaluation

A simple piloting task was used to evaluate handling qualities of the control laws while the pilot is flying in the loop. For the task, the pilot made a right 180º turn to a heading. Three separate control situations were evaluated; using the two possible control methods described earlier and the effects of time delay on the system. Figure 7-3 through Figure 7-5 show the results of the piloted tests. These figures plot the heading angle, lateral load factor and rudder control deflection which show the interaction between the pilot and the aircraft.

The first test conducted controlled the skidding turn using lateral acceleration by utilizing the R1 washout loop. Full control was smoothly applied with the UAV entering a steady skid turn. As the 180º heading was approached, the pilot eased off the control to anticipate intercepting the desired heading angle. This configuration was very easy to fly and intercept any heading angle. In addition, the control is not overly aggressive and the pilot was able to make very shallow and precise heading changes during the evaluation. Unfortunately, this scenario is not as realistic as possible, but it does provide a nice baseline to compare the other two simulations against.

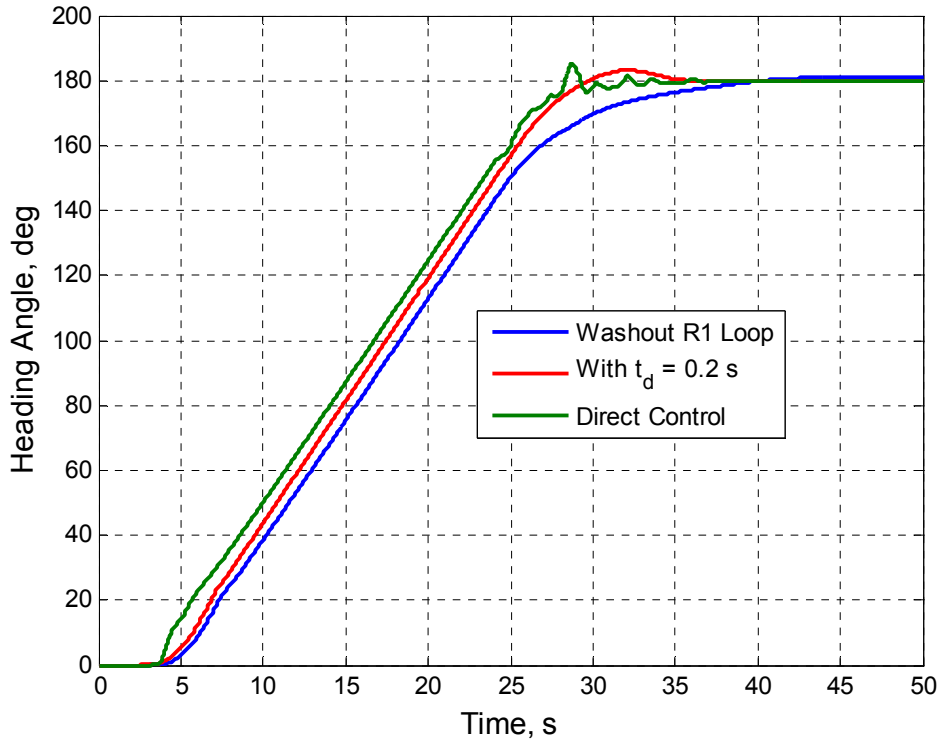

Figure 7-3: Pilot Controlled Heading Angle

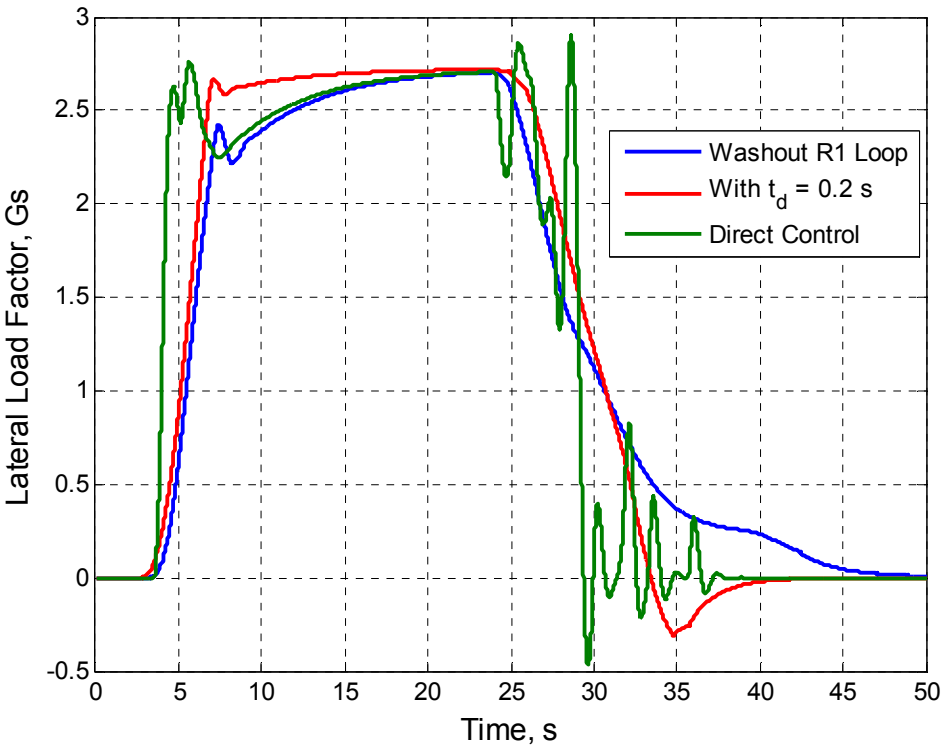

Figure 7-4: Lateral Load Factor during Pilot Controlled Simulation

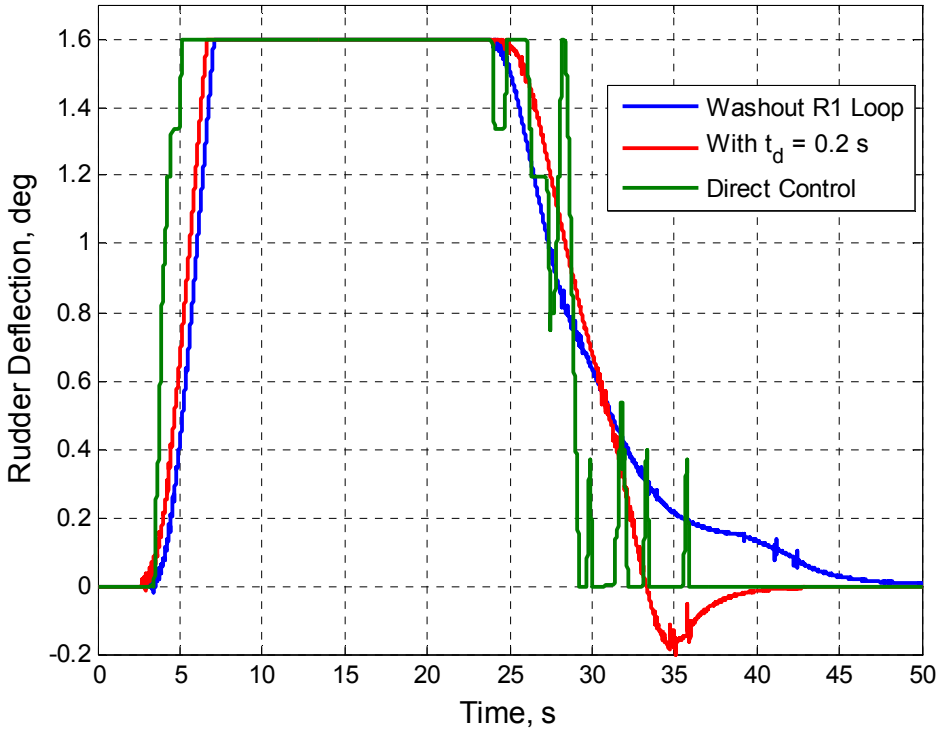

Figure 7-5: Rudder Control Activity during Pilot Controlled Simulation

The second piloted case used the control scheme as the first scenario, except that time delay was added into the system at two separate points. When piloting a UAV, latency is introduced through the uplink and downlink. This affects a pilot by delaying their control commands to the aircraft and also delays the transmission of telemetry back to the ground station for presentation to the pilot.

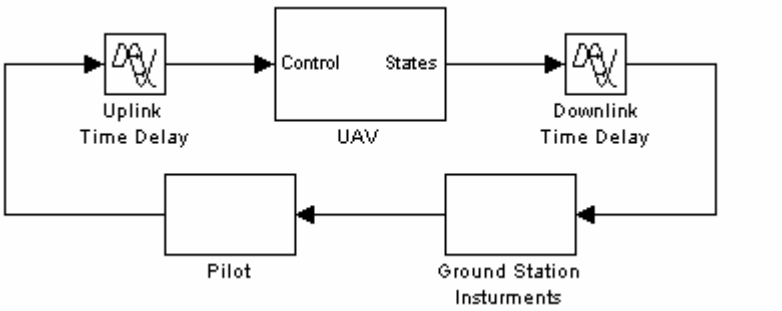

Figure 7-6: Representation of Time Delay in the Command and Control System

In accordance with the parameters of the Cloud Cap system, a worst case 0.1 second time delay was added just after the joystick input and before the data was sent to the instruments. In total 0.2 seconds of delay was introduced into the system. Figure 7-6 shows the relation between the pilot, ground station and the UAV.

Adding time delay to the system provided a very characteristic response for a system that has a human in the loop. Even though the pilot was aware of the time delay, the heading was still over shot slightly causing the pilot to have to start a small turn in the opposite direction to regain the desired heading. This slight overshoot can easily be seen in Figure 7-3 through Figure 7-5. It is interesting to note that the heading overshoot peaks at about 32 seconds where as the corrective control action does not peak until 35 seconds. The good thing about this simulation is that the pilot was easily able to track back to the heading angle without any subsequent overshoots. The pilot determined that this amount of time delay in the system did not adversely affect the handling qualities.

The last piloted controlled scenario tested the concept of direct rudder control (no washout loop). This scenario did not include any time delay. As predicted, the Dutch roll is very prevalent during the entry and exit for the turn. Any slight movement in the control from the pilot resulted in the Dutch roll mode being excited. Smooth rollout onto the desired heading was not achievable. The pilot had to apply aggressive control inputs to manually dampen out the oscillations. This behavior is most prevalent between 25 and 40 seconds in the simulation. Overall, this control scenario is completely unacceptable to present to a pilot.

Chapter 8: Robustness Analysis

8.1 Turbulence, Wind and Sensor Noise

The fundamental principle behind feedback control is to wash out the plant dynamics of a system. Robustness is the last metric that must be evaluated to determine the adequacy of the control laws. Three scenarios are used to test the system and observe how it responds to environmental and internal changes.

Wind and turbulence are always present in the real world. It is important that the control system be able to maintain proper attitude control of the UAV even through the worst environmental challenges. A simple model was developed that simulated turbulence by injecting bandwidth limited noise into the roll, pitch and yaw rates of the aircraft (Figure 8-1). The noise was set to a significantly high enough level that it would simulate moderate to severe turbulence. This type model could also be considered to simulate noise that comes from the sensors.

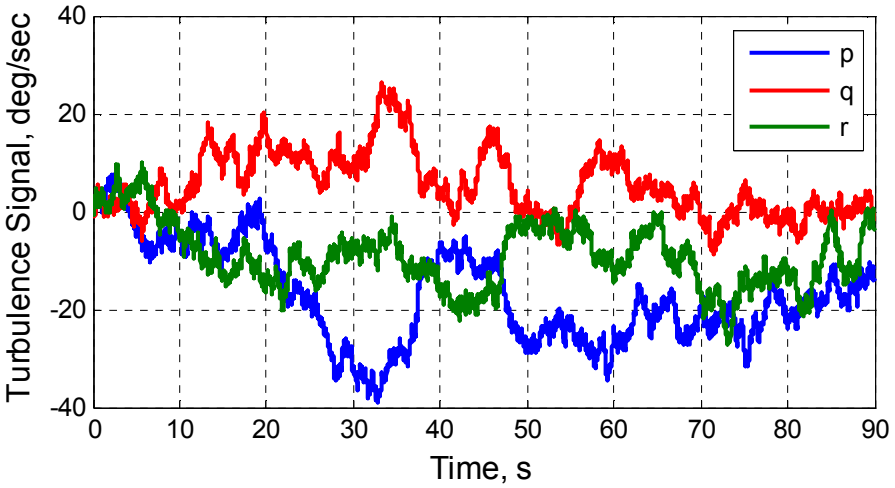

Figure 8-1: Angular Rate Input used to Simulate Turbulence or Sensor Noise

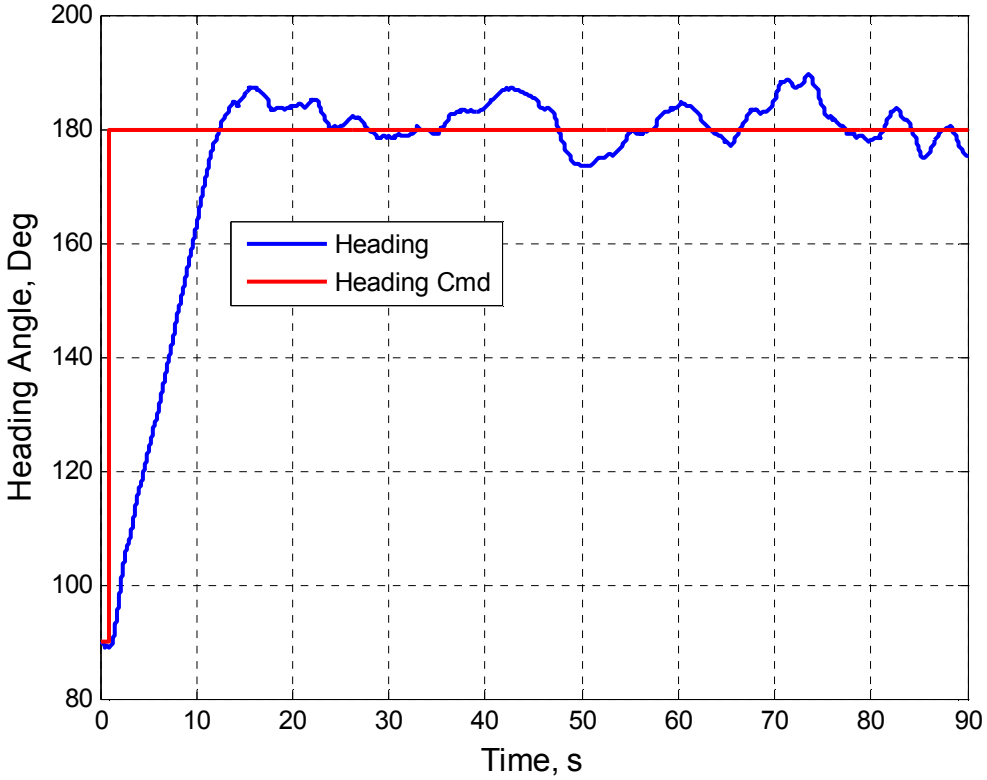

Figure 8-2: Heading Angle during Turbulence

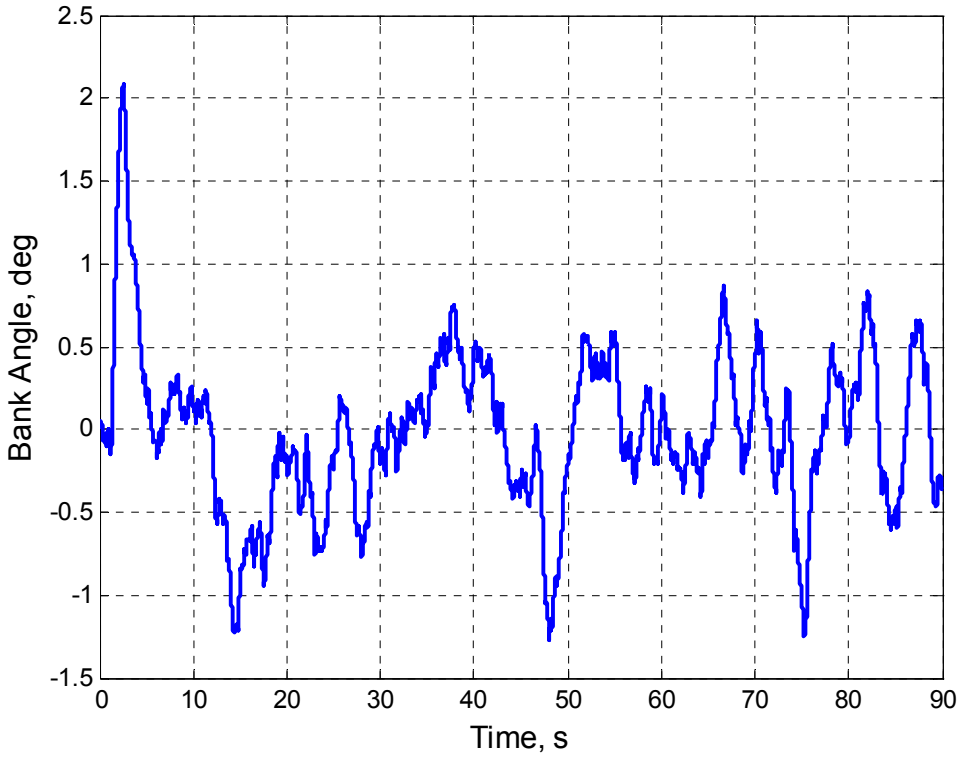

Figure 8-3: Bank Angle with Turbulence

For this simulation, the heading controller commanded a 90º right turn to a heading of 180º. The turbulence and sensor noise was applied throughout the entire time of the simulation. This forced the UAV to intercept and follow the commanded heading while always being buffeted by turbulence. Figure 8-2 and Figure 8-3 show the results of the turbulence study.

Remarkably, the STT control system performed very well. The control laws had no problem intercepting the commanded heading or sustaining that track for an indefinite period of time. Additionally, the bank angle was very well maintained and never came close to exceeding the ± 5º requirement. This simulation proves that this set of control laws can easily handle severe turbulence or very noisy sensors. Most likely, the NXT2 UAV would never be flown under these weather conditions.

8.2 Plant Sensitivity Analysis

The second scenario is designed to determine the sensitivity of the control system to changes in the plant. A robust set of control laws will have the capability to tolerate changes and variations with the plant dynamics. This scenario was designed to modify each of the lateral-directional stability derivatives by increasing or decreasing them by 25%. As each stability derivative was modified one at time, significant changes in the vehicle behavior, such as instabilities, were noted. Minor variations in heading or bank angle performance, along with other smaller changes were neglected.

After augmenting all of the lateral-directional stability derivatives, one distinct problem became evident. Aileron saturation that subsequently causes the UAV to flip and tumble, once again becomes an issue. Table 8-1 shows which of the stability derivatives are intolerant of a significant change. All of these derivatives, either directly or indirectly,

contribute to the increase in the roll rate of the UAV causing aileron saturation. The control system itself was very resilient to large changes in the plant. Figure 8-4 shows two example cases where the control system reacted very quickly, yet ran out of control authority to maintain the proper bank angle.

Stability Derivative	Required Change for Instability	Reason
$C_{l\beta}$	+7%	Increased Roll Rate during High Beta Angles
$C_{n\delta r}$	+7%	Increased Yaw Rate which Produces an Increased Roll Rate
$C_{n\delta a}$	-7%	Decreased Aileron Effectiveness
$C_{n\beta}$	-7%	Decreased Damping from Vertical Tail Increases Yaw Rate which Increases Roll Rate
C_{nr}	-7%	Decreased Damping from Vertical Tail Increases Yaw Rate which Increases Roll Rate

Table 8-1: Listing of Sensitive Stability Derivatives

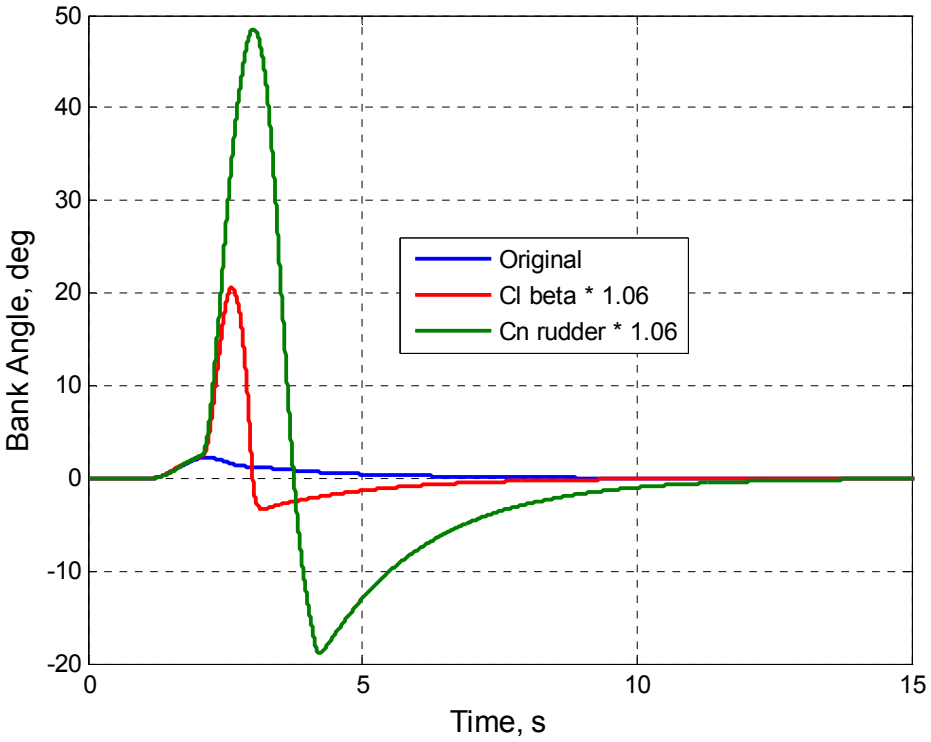

Figure 8-4: Bank Angle with Increases in Clβ & Cnδr

8.3 Control Loop Tolerance

Finally, the last study conducted analyzed the effectiveness of the system if any of the control loops failed and a STT maneuver was initiated. By individually breaking loops, the performance of the system was observed while commanding a 180º turn. In a digital system, the chances of these failures happening is extremely small; however, any loss of attitude control can not be tolerated at 400 knots.

Simulation results show that the system is not capable of loosing the outer A2 bank angle control loop under any circumstances. The UAV very quickly becomes unstable, flips and tumbles. A failure of the outer R2 loop mathematically converts the system to piloted control as discussed in the last chapter. The system is very tolerant of failures of the inner rate loops as shown in Figure 8-5. Essentially this means that the outer loops are tuned well enough that they do not have to rely on rate feedback.

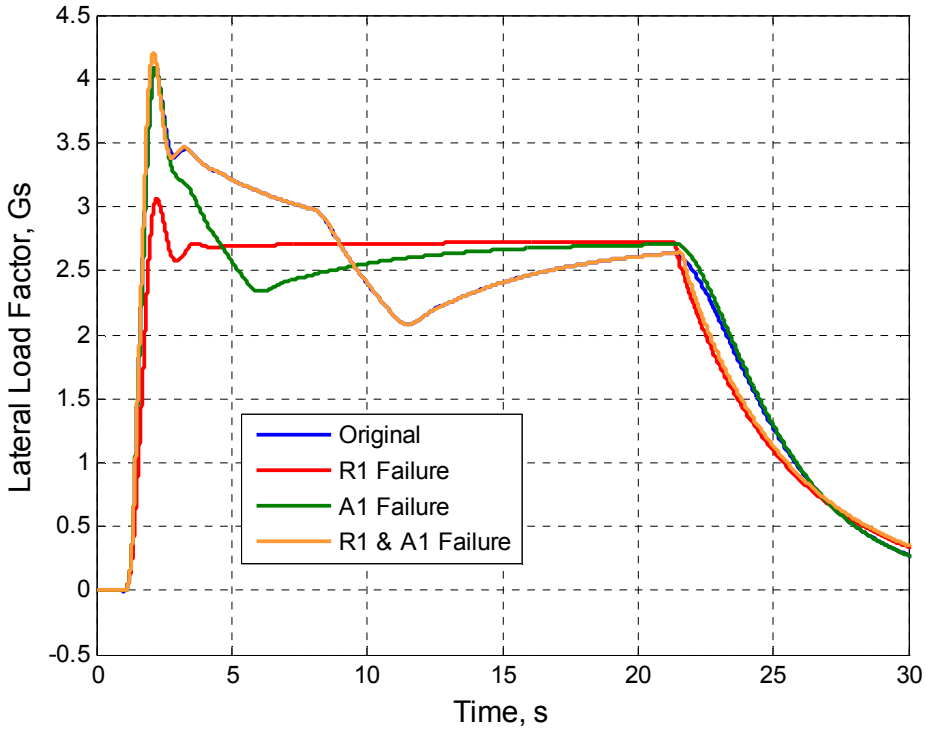

Figure 8-5: Lateral Load Factor after Loop Failure

Chapter 9: Conclusions and Future Work

9.1 Conclusions

Creating an unmanned aerial vehicle that is capable of performing high G skid turns is a challenge in both aerodynamic modeling and flight dynamics simulation. Skidding turns present problems in which small winged missiles do not have to contend. In general, the biggest issue is simply having enough control authority to overcome the induce roll moment.

Modeling the forces and moments on the NXT proved to be very challenging. The well established linearized equations of motion greatly under estimated the dynamics of STT maneuvers. While the linear equations model the proper trend, the overall magnitude of the states was poorly modeled. To compensate for this, a nonlinear simulation was developed as a final testing platform for the control laws.

Combining the results from the linear and nonlinear simulation, there are three suggested improvements to the NXT that will enable better performance in skidding turns. First is replacing the inverted V tail with a traditional horizontal stabilizer. With the tail now horizontal, additional rolling moment can be generated by making the aileron/elevator surfaces full chord rather than the original 20% chord. The third suggestion is to increase the vertical stabilizer area to 0.09 m^2 to account for the slight loss in lateral stability by removing the inverted V tail.

Skid-to-Turn control laws were then developed with the modified design. Initial loop closures were modeled using the linear model since the trends were still predicted correctly. A four loop architecture was chosen that would turn the UAV to a heading; all while maintaining a bank angle of zero. The inner R1 $r \rightarrow \delta r$ loop was chosen to have a

washout filter placed at 5 rad/sec to dampen out the Dutch roll mode through the rudder. The next loop closed was the inner A1 $p \rightarrow \delta a$ loop. A simple feedback gain of 2 was chosen for this loop. Bank angle was ultimately controlled with the outer $\phi \rightarrow \delta a$ loop. Since only minimal bank angle excursions were anticipated, a PI controller with gains of Kp = 40 and Ki = 20 was ultimately chosen through nonlinear simulation. Finally, the outer R2 $\psi \rightarrow \delta r$ loop was closed using a PD controller with gains of Kp = 0.3 and Kd = 1.0. The PD controller provided a desirable response over concerns with integrator windup. These control laws provide Level 1 handling qualities and exceed the 1.25 rad/sec bandwidth criteria specified by MIL-STD-1797.

These control laws were then applied to the nonlinear simulation to determine the maximum performance of the modified NXT2 design. Initial testing showed that the vehicle could quickly saturate the control power of the ailerons and cause the vehicle to tumble. Limiting the rudder deflection to 1.6º and the deflection rate to 2 deg/sec eliminates the chance the vehicle will tumble when initiating a skid turn. The vehicle showed very smooth and crisp responses to the commanded heading. The vehicle proved that it is capable of performing up to 3 G skidding S-Turns during one simulation. Additionally, a pilot was easily able to control the UAV using the designed control laws; even with a worst case scenario of 0.2 seconds of system latency in the command and control system.

Robustness analysis was performed to verify that the control laws are tolerant of environmental, sensor, plant and control architecture changes. A moderate to severe turbulence model was implemented in the nonlinear simulation with the control laws successfully intercepting and tracking a heading. The control system is also very tolerant

of most changes to the plant. Unfortunately, the aileron saturation problem is the most sensitive to plant changes. However, this is a control geometry issue and not a problem with the designed control laws. As a final test of robustness, the performance of the vehicle was observed as loops were broken to simulate failures. The only loop that must remain in tact during a STT maneuver is the outer A2 bank angle control loop. This system can still remain stable with both of the inner R1 and A1 rate feedback loops broken.

This research has demonstrated that it is possible to create a set of simple and robust STT control laws for a UAV. As expected, the aerodynamics of the airplane are ill suited for STT maneuvering. Massive amounts of control authority are required from both the aileron and rudder to maintain attitude control at all times during high speed skidding turns.

9.2 Future Work

Continued research is still needed to fully investigate the high G skid-to-turn problem for aircraft. In relation to this particular analysis, the nonlinear flight simulation needs to be augmented with flight test or experimental data. Computational data is good for this proof of concept study; however, a better understanding of all the nonlinear effects needs to be investigated. Specifically, problems arising due to flow separation from the fuselage could greatly affect the flow over the wing. The fuselage could even mask one of the wings at higher sideslip angles and generate an unpredictable rolling moment. Additionally, drag effects are significant for this problem and require additional thrust to overcome the large drag rise. Before any control law should be applied to the

NXT vehicle at 400 knots, comprehensive testing at slower speeds or even on less agile platforms should be conducted to have a better understanding of the dynamics involved.

Bibliography

[1] Pearson, Lee. "Developing the Flying Bomb". *Naval Aviation in World War I.* Chief of Naval Operations, Government Printing Office. Washington DC. 1969.

[2] Navel Air Systems Command. United States Navy. www.navair.navy.mil [retrieved April 2009]

[3] Federal Aviation Administration, *Airplane Flying Handbook,* Department of Transportation, Oklahoma City, 2004.

[4] Siouris, George M., Airborne Missile Guidance and Control Systems, Springer-Verlag, New York, 2004.

[5] United States Air Force. www.af.mil [retrieved April 2009]

[6] Cloutler, J. R., and Stansbery, D. T., "Nonlinear, Hybrid Bank-to-Turn/Skid-to-Turn Missile Autopilot Design," AIAA Guidance, Navigation, and Control Conference, AIAA, Montreal, Canada, 2001

[7] Department of Defense, *Flying Qualities of Piloted Aircraft.*, MIL-STD-1797., 1997

[8] Nelson, Robert C., Flight Stability and Automatic Control., 2nd ed., McGraw-Hill, 1998

[9] Cloud Cap Technology, *Crista Sensor Head Interface Control Document.*, Hood River, OR., March 2006

[10] Hitec RCD Korea Inc., *General Specification of HSR-5990TG Coreless Digital Robot Servo*., June 2006

[11] Cloud Cap Technology, *Piccolo System User's Guide*., Hood River, OR., January 2009

[12] Drela, Mark, *AVL 3.26 User Primer,* Massachusetts Institute of Technology. www.mit.edu [retrieved April 2009]

[13] Ashkenas I., Graham D., and McRuer D., *Aircraft Dynamics and Automatic Control,* Princeton University Press, Princeton NJ, 1973.

[14] Blakelock, J., *Automatic Control of Aircraft and Missiles.* John Wiley & Sons. New York. 1965.

[15] Bryson, Arthur, *Control of Spacecraft and Aircraft,* Princeton University Press, Princeton NJ, 1994.

[16] Connolly, T., Dommasch, D., Sherby, S., *Airplane Aerodynamics,* 4th ed., Pitman Publishing Corp., New York, 1967.

[17] Cronvich, Lester, "Aerodynamics Considerations for Autopilot Design," *Tactical Missile Aerodynamics,* edited by M. Summerfield, Progress in Astronautics and Aeronautics, AIAA, Washington, DC, 1986.

[18] Etkin, Bernard., *Dynamics of Atmospheric Flight.,* John Wiley & Sons Inc., 1972.

[19] Lewis, F., and Stevens, B., *Aircraft Control and Simulation,* 2nd ed., John Wiley & Sons Inc., 2003.

[20] McLean, Donald, *Automatic Flight Control Systems,* Prentice Hall (UK), Cambridge, 1990.

[21] Ogata, Katsuhiko, *Modern Control Engineering,* 4th ed., Prentice-Hall, Upper Saddle River, New Jersey, 2002.

[22] Phillips, Warren, *Mechanics of Flight,* John Wiley & Sons Inc., 2004.

Appendix A: MIL-STD-1797 Definition of Bandwidth

The bandwidth frequency, ω_{BW}, to be used…is defined from the frequency response plot of heading or lateral flight-path angle to cockpit direct-force control input. Specifically, it is the lower of two frequencies: the frequency at which the phase margin is 45 deg, or the frequency for a gain margin of 6 dB (Figure A-1). In order to apply this definition, first determine the frequency for neutral closed-loop stability (180 deg phase angle) from the phase portion of the Bode plot (ω_{180}). The next step is to note the frequency at which the phase margin is 45 deg. This is the bandwidth frequency defined by phase, ω_{BW} phase. Then, note the amplitude corresponding to ω180 and add 6 dB to it. The frequency at which this value occurs on the amplitude curve is ω_{BWgain}. Finally, the bandwidth, ω_{BW}, is the lesser of $\omega_{BWphase}$ and ω_{BWgain}.

If $\omega_{BW} = \omega_{BWphase}$, the system is said to be phase-margin limited. On the other hand, if $\omega_{BW} = \omega_{BWgain}$ the system is gain-margin limited; that is, the aircraft is driven to neutral stability when the pilot increases his gain by 6 dB (a factor of 2). Gain-margin-limited aircraft may have a great deal of phase margin, ϕ_M, but then increasing the gain slightly causes ϕ_M to decrease rapidly. Such systems are characterized by frequency-response amplitude plots that are flat, combined with phase plots that roll off rapidly, such as shown on Figure A-1.

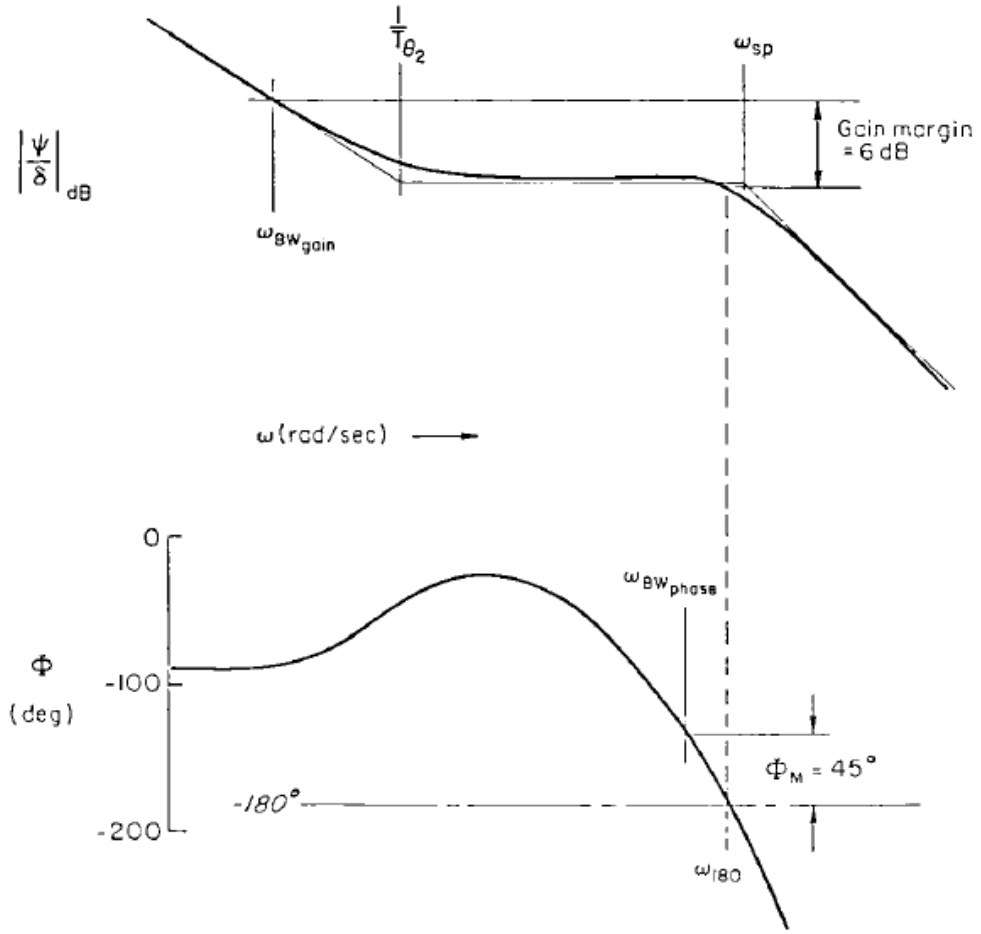

Figure A-1: Definition of Bandwidth Frequency

Appendix B: AVL Geometry File

```
NXT_lateral_model
#  Original File by Aeromech Engineering
#  Modified by Tanner A. Sims
#==============================================================
#  Lateral model:
#  all measurements in this model are:
#    referenced to the nose
#    done in metric units (meters, degrees)
#==============================================================
0.6                                  | Mach
0           0            0           | iYsym  iZsym  Zsym
0.567013    0.372131    1.524        | Sref   Cref   Bref
1.2707        0        0.0187        | Xref   Yref   Zref
0.05                                 | CDp  (optional)
#==============================================================
SURFACE
LeftWing
#Nchordwise Cspace
8           1
INDEX
1
ANGLE
0
TRANSLATE
#DX             DY             DZ
#1.037627    -0.177800    0.160794   #Actual widths
1.037627     0    0.210511    #adjusted width, and height
#Tip-------------------------------------------------------
SECTION
#Xle        Yle           Zle            Chord        Ainc    Nspan
Sspace
0.364598    -0.670700     -0.025247      0.372131     0       18
1
CONTROL
lwf  1.0  0.8   0 0 0   1.0  | name, gain,  Xhinge,  XYZhvec,  SgnDup
AFILE
n0813s.dat
#Root------------------------------------------------------
SECTION
#Xle        Yle           Zle            Chord        Ainc    Nspan
Sspace
0            0            0              0.372131     0       5
1
CONTROL
lwf  1.0  0.8   0 0 0   1.0  | name, gain,  Xhinge,  XYZhvec,  SgnDup
AFILE
n0813s.dat
##Wing Body Seal-----------------------------------------------
#SECTION
##Xle        Yle           Zle            Chord        Ainc    Nspan
Sspace
#0            0            -0.128083      0.372131     0       0
0
#==============================================================
```

```
SURFACE
RightWing
#Nchordwise Cspace
8           1
#
INDEX
1
ANGLE
0
TRANSLATE
#DX            DY            DZ
#1.037627    0.177800    0.160794   #Actual widths
1.037627    0    0.210511    #adjusted width, and height
SECTION
#Xle        Yle           Zle            Chord        Ainc    Nspan
Sspace
0           0             0              0.372131     0       18
1
CONTROL
rwf  1.0  0.8   0 0 0   1.0  | name, gain,  Xhinge,  XYZhvec,  SgnDup
AFILE
n0813s.dat
#Tip-------------------------------------------------------------
SECTION
#Xle        Yle           Zle            Chord        Ainc    Nspan
Sspace
0.364598    0.670700      -0.025247      0.372131     0       0
0
CONTROL
rwf  1.0  0.8   0 0 0   1.0  | name, gain,  Xhinge,  XYZhvec,  SgnDup
AFILE
n0813s.dat
#==============================================================================
SURFACE
LeftHzTail
#Nchordwise Cspace
8           1
INDEX
1
ANGLE
0
TRANSLATE
#DX            DY            DZ
#2.096590        -0.126387    -0.029166   #actual width
2.096590         0    0.032711    #adjusted width, and height
#Tip-------------------------------------------------------------
SECTION
#Xle        Yle           Zle            Chord        Ainc    Nspan
Sspace
0.199634    -0.39     -0.142553      0.248075     0       18        1
CONTROL
lht  1.0  0.8   0 0 0   1.0  | name, gain,  Xhinge,  XYZhvec,  SgnDup
AFILE
t05s.dat
#Root------------------------------------------------------------
SECTION
```

```
#Xle        Yle           Zle            Chord        Ainc    Nspan
Sspace
0            0            0              0.248075     0       5
1
CONTROL
lht  1.0  0.8   0 0 0   1.0  | name, gain,  Xhinge,  XYZhvec,  SgnDup
AFILE
t05s.dat
#==============================================================
SURFACE
RightHzTail
#Nchordwise Cspace
8           1
INDEX
1
ANGLE
0
TRANSLATE
#DX            DY            DZ
#2.096590        0.126387    -0.029166   #actual width
2.096590         0    0.032711    #adjusted width, and height
##Tail Body Seal-----------------------------------------------------
---
#SECTION
##Xle        Yle           Zle            Chord        Ainc    Nspan
Sspace
#0            0            0.061877       0.248075     0       5
1
#Root----------------------------------------------------------
SECTION
#Xle        Yle           Zle            Chord        Ainc    Nspan
Sspace
0            0            0              0.248075     0       18
1
CONTROL
rht  1.0  0.8   0 0 0   1.0  | name, gain,  Xhinge,  XYZhvec,  SgnDup
AFILE
t05s.dat
#Tip-----------------------------------------------------------
SECTION
#Xle        Yle           Zle            Chord        Ainc    Nspan
Sspace
0.199634    0.39      -0.142553      0.248075     0       0         0
CONTROL
rht  1.0  0.8   0 0 0   1.0  | name, gain,  Xhinge,  XYZhvec,  SgnDup
AFILE
t05s.dat
#==============================================================
SURFACE
VtTail
#Nchordwise Cspace
8           1
INDEX
1
ANGLE
0
TRANSLATE
```

```
#DX             DY             DZ
2.117940    0            0.131148
#Root-------------------------------------------------------
SECTION
#Xle        Yle           Zle            Chord        Ainc    Nspan
Sspace
0            0            0              0.248066    0        8       1
CONTROL
vt  1.0  0.8   0 0 0   1.0  | name, gain,  Xhinge,  XYZhvec,  SgnDup
AFILE
vt05s.dat
#Vtbody2_top------------------------------------------------------------
SECTION
#Xle        Yle           Zle            Chord        Ainc    Nspan
Sspace
0.05557     0             0.079362808    0.248066    0        8
1.0
CONTROL
vt  1.0  0.8   0 0 0   1.0  | name, gain,  Xhinge,  XYZhvec,  SgnDup
AFILE
vt05s.dat
#Tip---------------------------------------------------------
SECTION
#Xle        Yle           Zle            Chord        Ainc    Nspan
Sspace
0.188239    0             0.268833       0.248066    0        0
0
CONTROL
vt  1.0  0.8   0 0 0   1.0  | name, gain,  Xhinge,  XYZhvec,  SgnDup
AFILE
vt05s.dat
#=============================================================================
SURFACE
VtBody1
#Nchordwise Cspace    Nspanwise Sspace
24          1         18        1.0
#
INDEX
1
ANGLE
0
TRANSLATE
#DX             DY             DZ
0.912156         0             0.159711
#-------------------------------------------------------------
SECTION
#Xle    Yle    Zle    Chord    Ainc    Nspanwise    Sspace
-0.1524    0    -0.3048    0.889    0    0    0
#-------------------------------------------------------------
SECTION
#Xle    Yle    Zle    Chord    Ainc    Nspanwise    Sspace
-0.4856226    0    -0.2794    1.4925548    0    0    0
#-------------------------------------------------------------
SECTION
#Xle    Yle    Zle    Chord    Ainc    Nspanwise    Sspace
-0.788455548    0    -0.2286    2.02344528    0    0    0
#-------------------------------------------------------------
```

```
SECTION
#Xle    Yle    Zle    Chord    Ainc    Nspanwise    Sspace
-0.9271    0    -0.1778    2.316895798    0    0    0
#------------------------------------------------------------
SECTION
#Xle    Yle    Zle    Chord    Ainc    Nspanwise    Sspace
-0.871638567    0    -0.127    2.395638592    0    0    0
#------------------------------------------------------------
SECTION
#Xle    Yle    Zle    Chord    Ainc    Nspanwise    Sspace
-0.805761863    0    -0.089210642    2.21714568    0    0    0
#------------------------------------------------------------
SECTION
#Xle    Yle    Zle    Chord    Ainc    Nspanwise    Sspace
-0.644964649    0    -0.028562808    2.0988147    0    0    0
#============================================================================
SURFACE
VtBody2
#Nchordwise Cspace    Nspanwise Sspace
24          1         8         1.0
#
INDEX
1
ANGLE
0
TRANSLATE
#DX            DY            DZ
0.912156        0            0.159711
#------------------------------------------------------------
SECTION
#Xle    Yle    Zle    Chord    Ainc    Nspanwise    Sspace
-0.644964649    0    -0.028562808    1.85075322    0    0    0
#------------------------------------------------------------
SECTION
#Xle    Yle    Zle    Chord    Ainc    Nspanwise    Sspace
-0.396866516    0    0.0254    1.35274558    0    0    0
#------------------------------------------------------------
SECTION
#Xle    Yle    Zle    Chord    Ainc    Nspanwise    Sspace
-0.127    0    0.0508    0.8636    0    0    0
```

Appendix C: Non-Linear Simulation Block Diagrams

System Root View

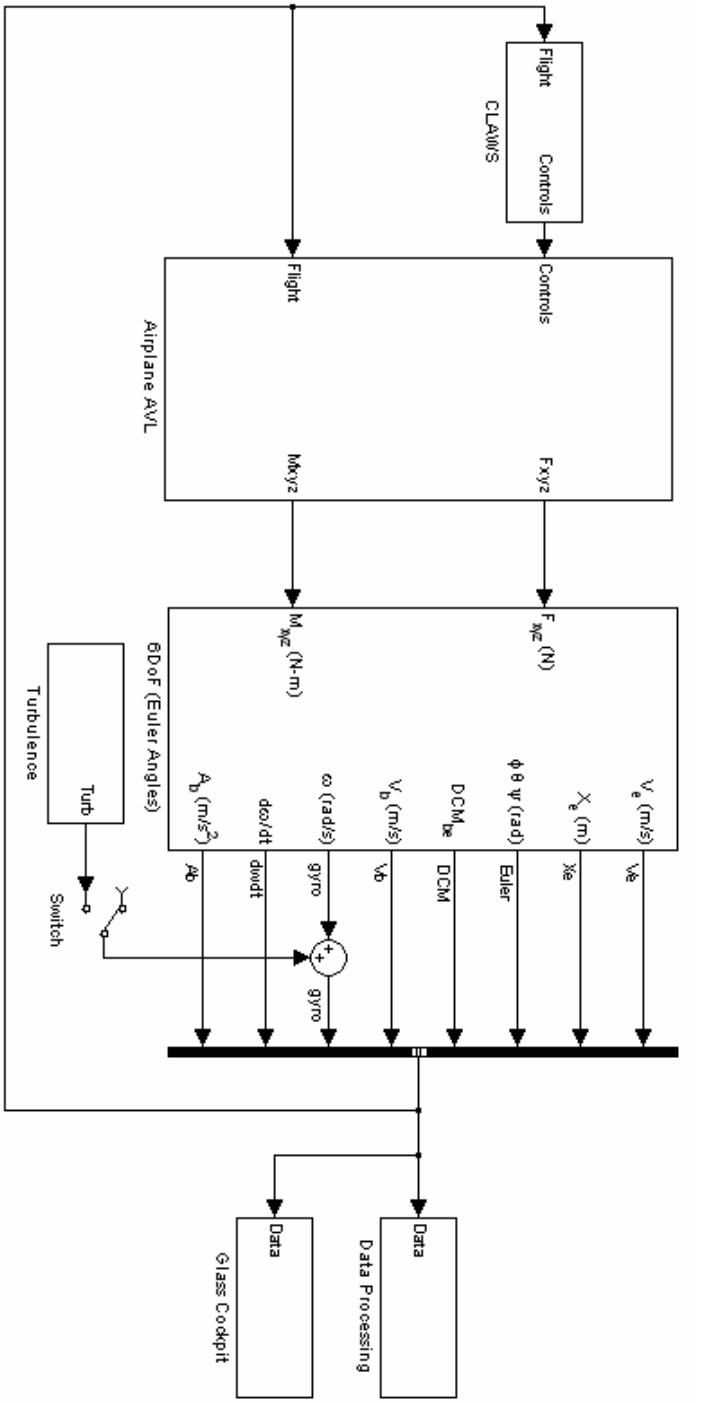

Control Law Interface

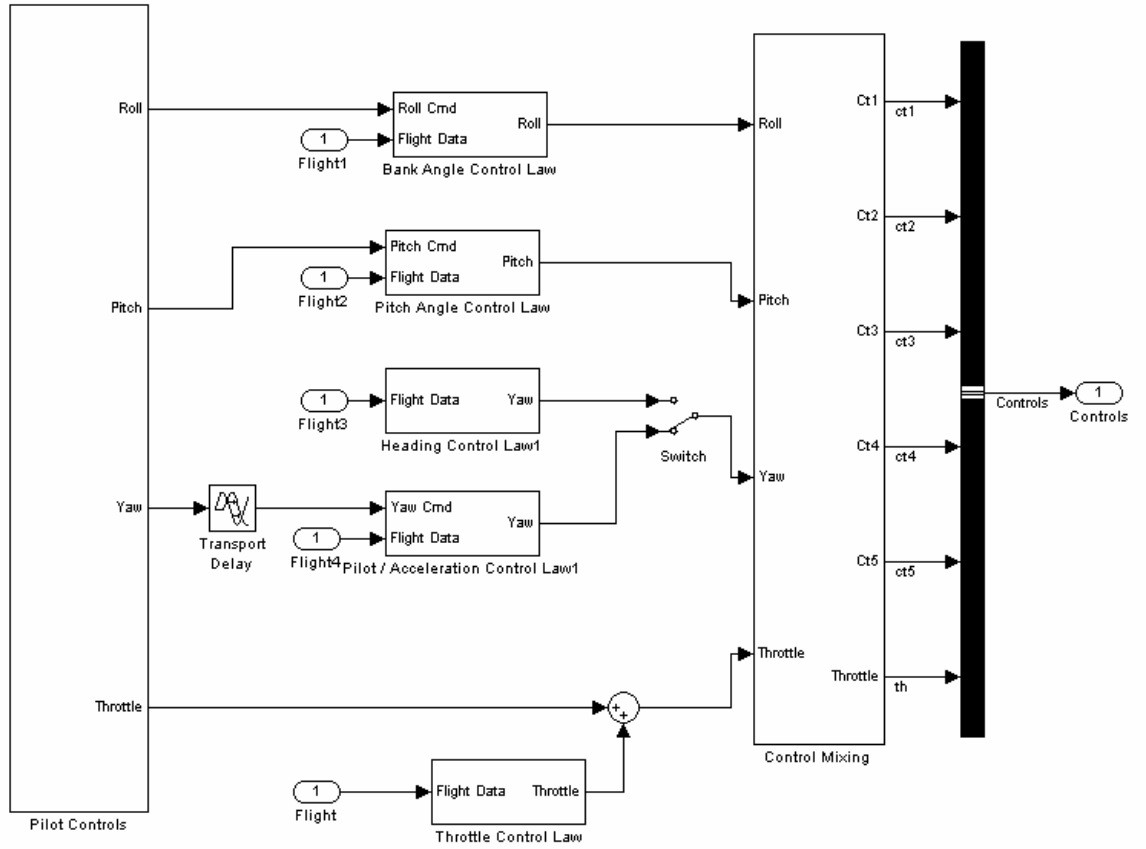

Pilot Control Interface

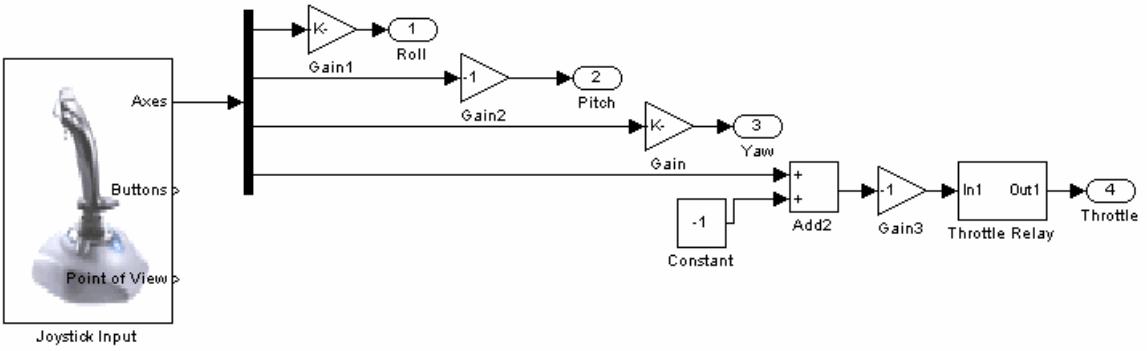

Bank Angle Control Law

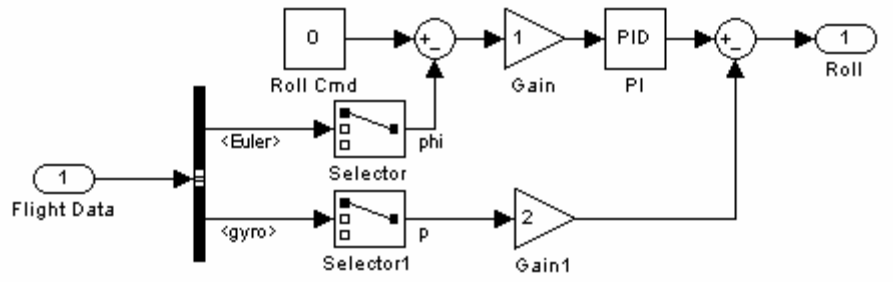

Heading Angle Control Law

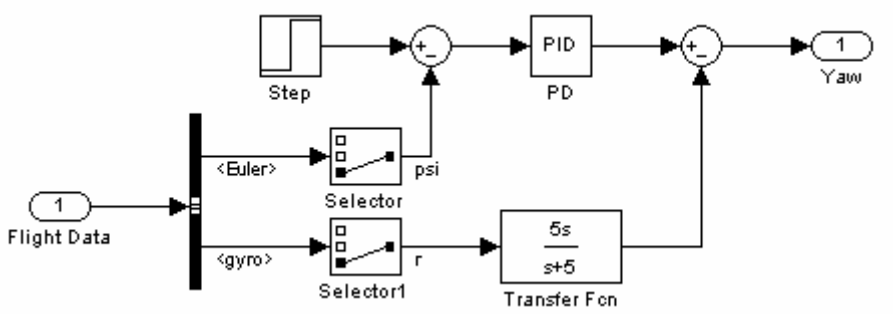

Pilot-in-Loop Yaw Control Law

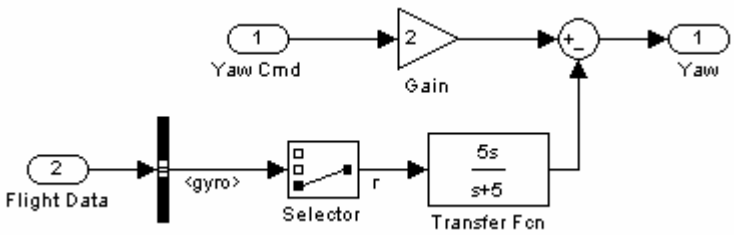

Control Mixing / Saturation / Rate Limiting

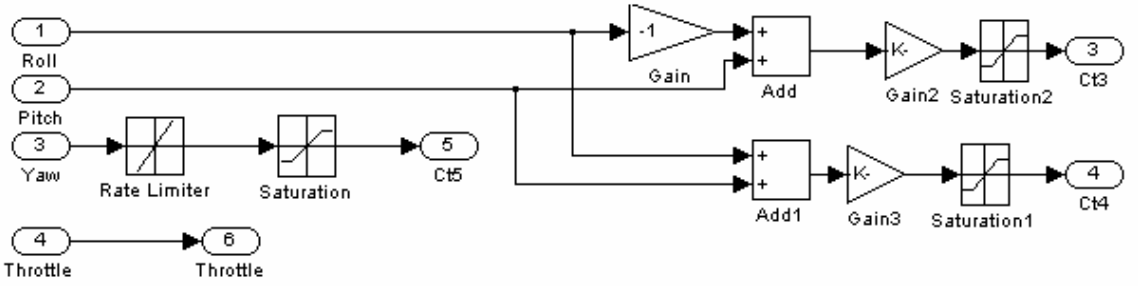

Force and Moment Calculation

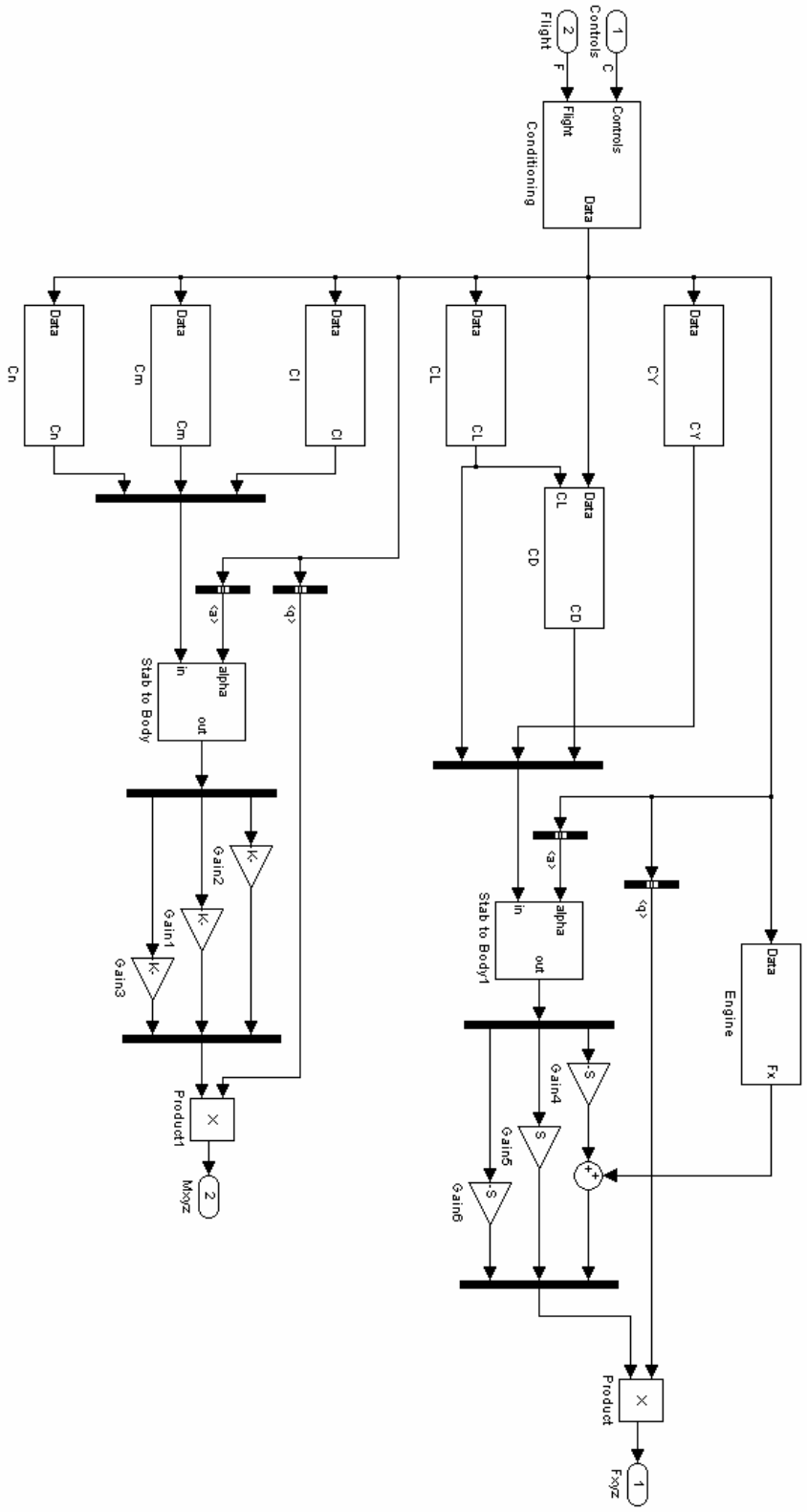

Drag Coefficient Calculation

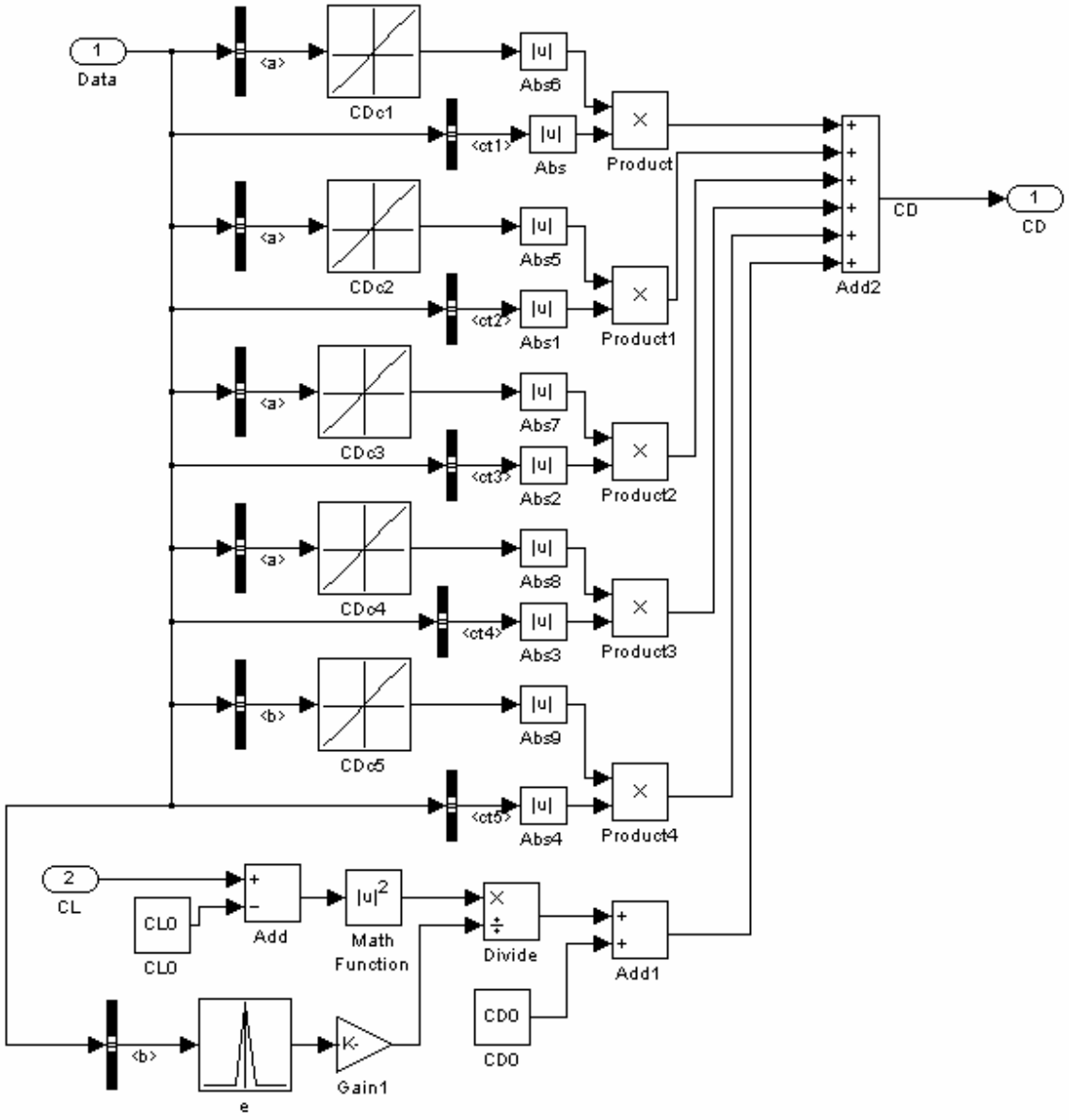

Lift Coefficient Calculation

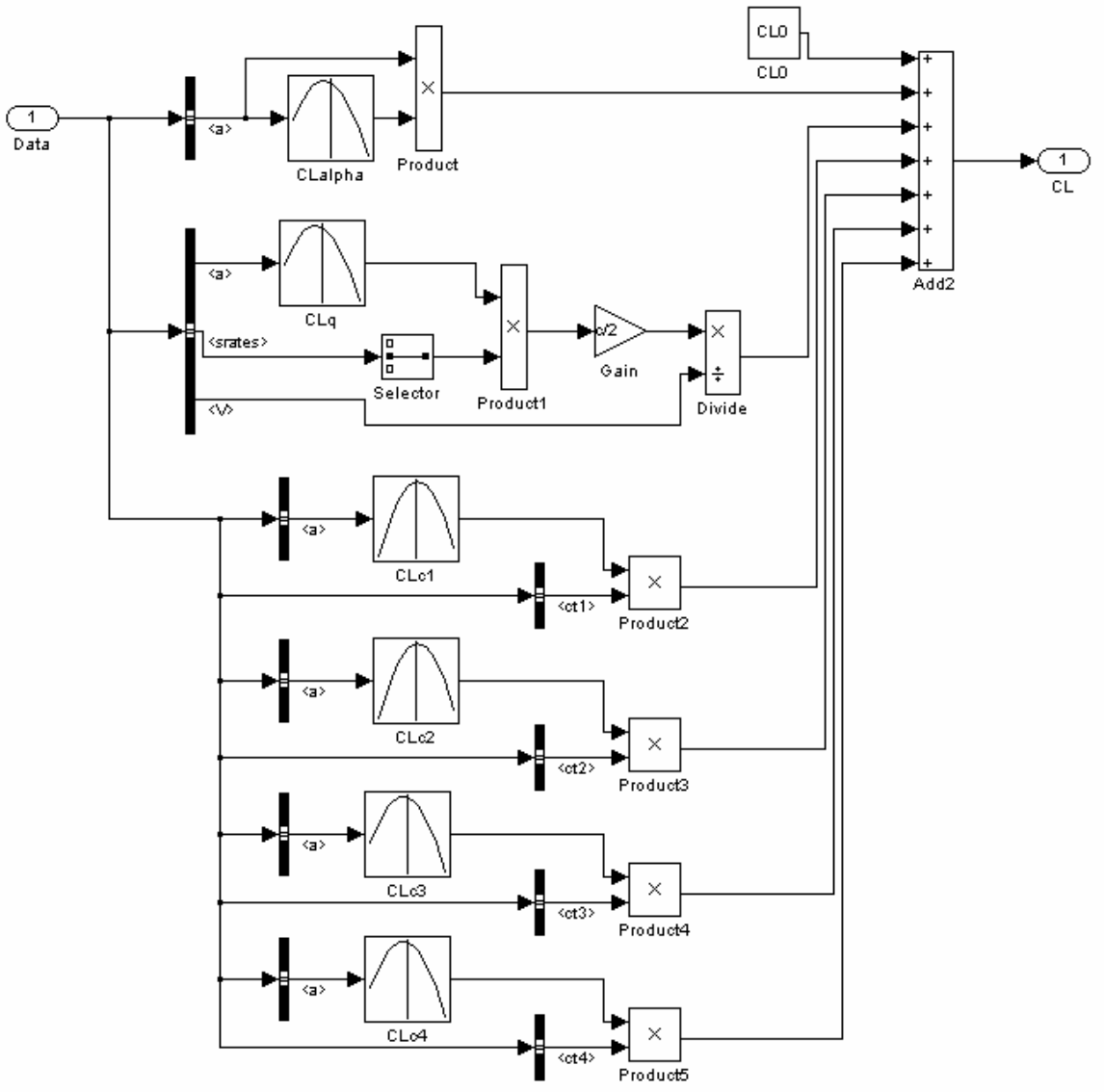

Side Force Calculation

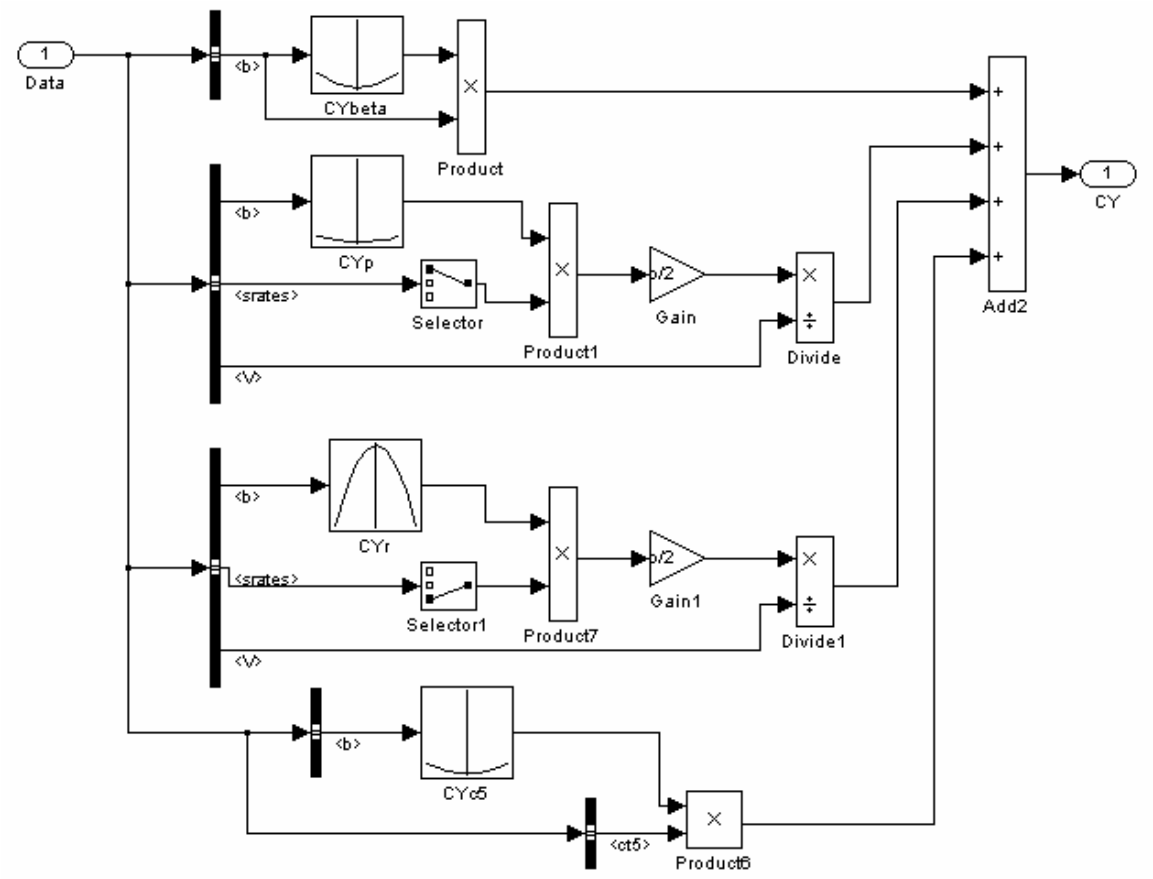

Rolling Moment Calculation

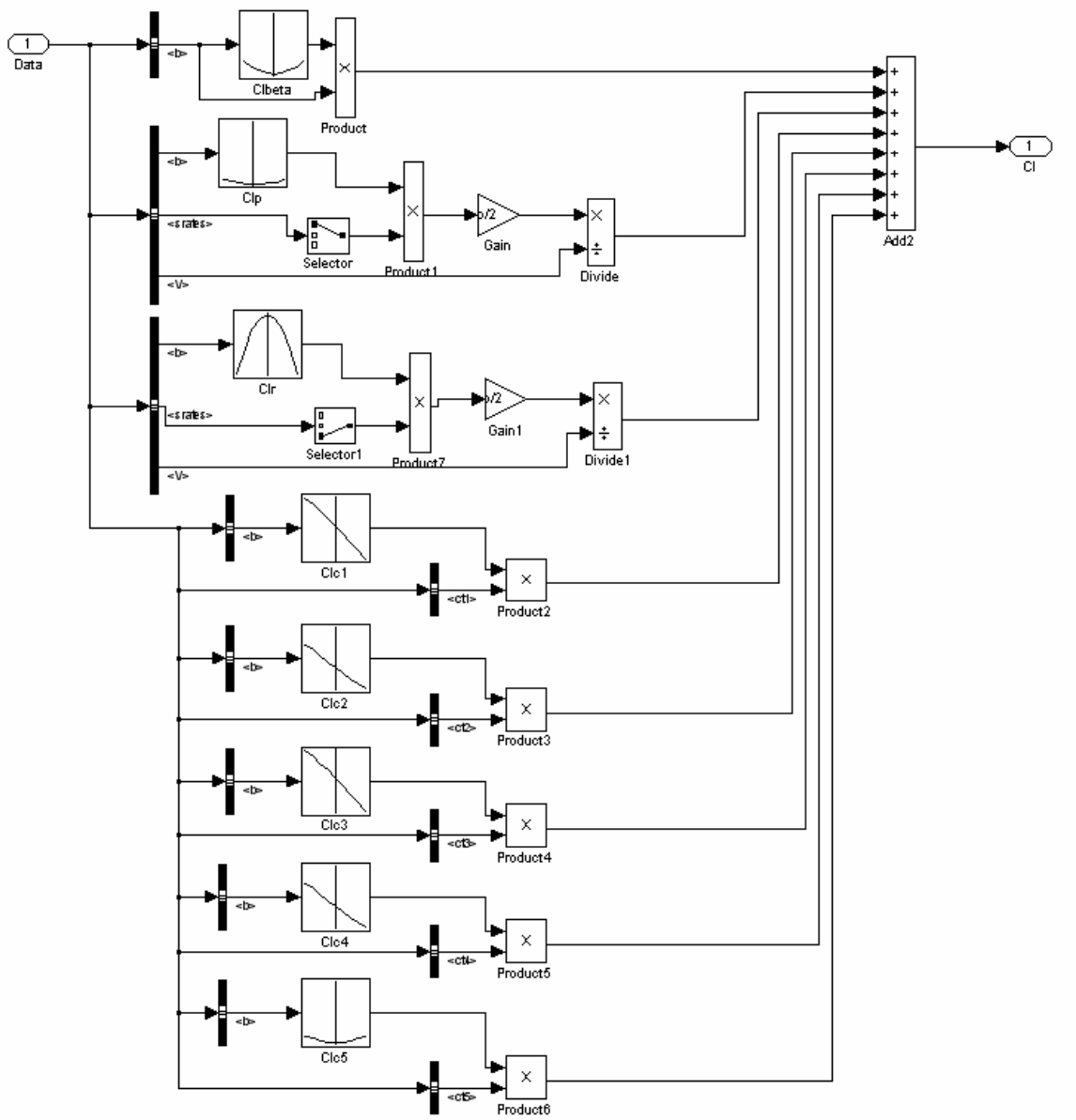

Pitching Moment Calculation

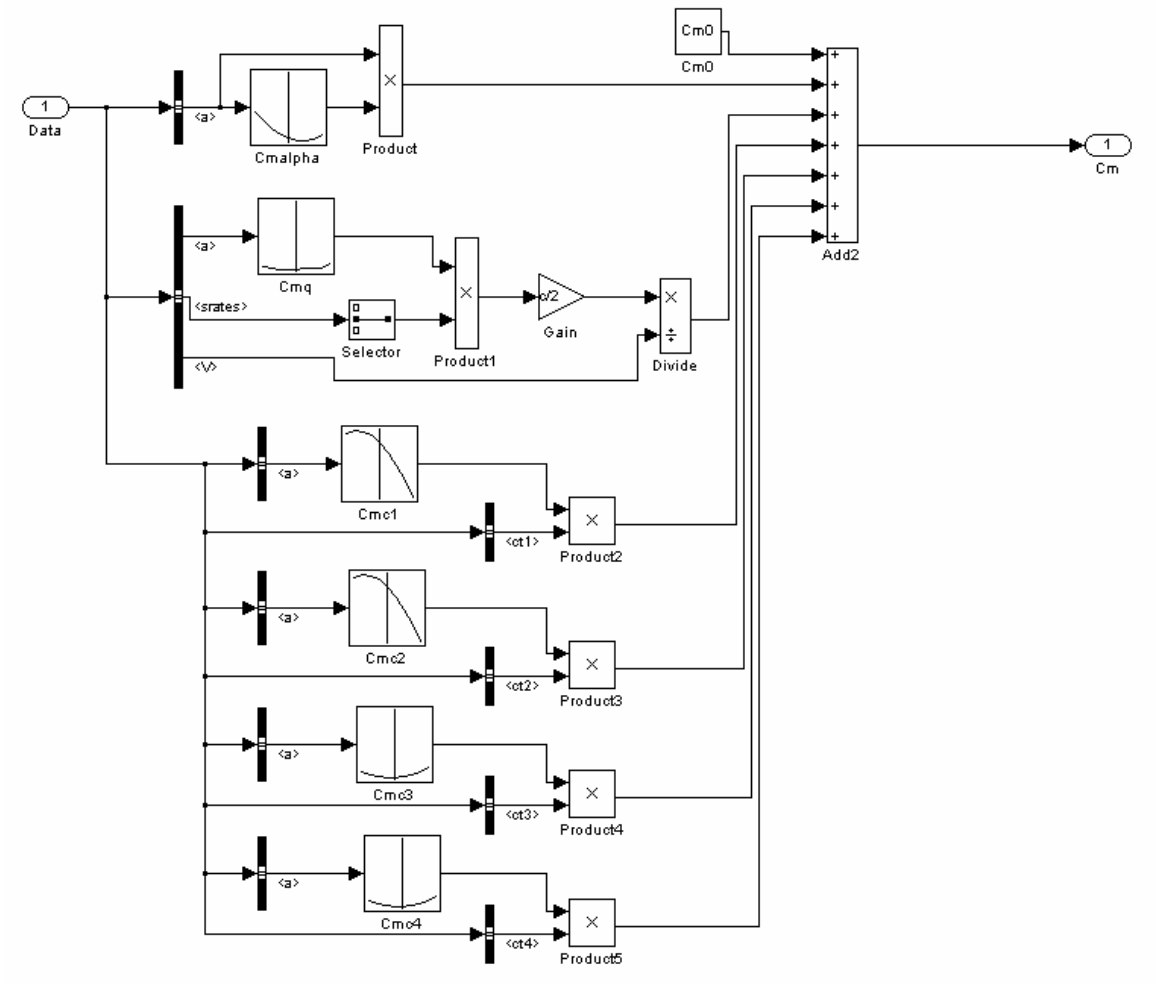

Yawing Moment Calculation

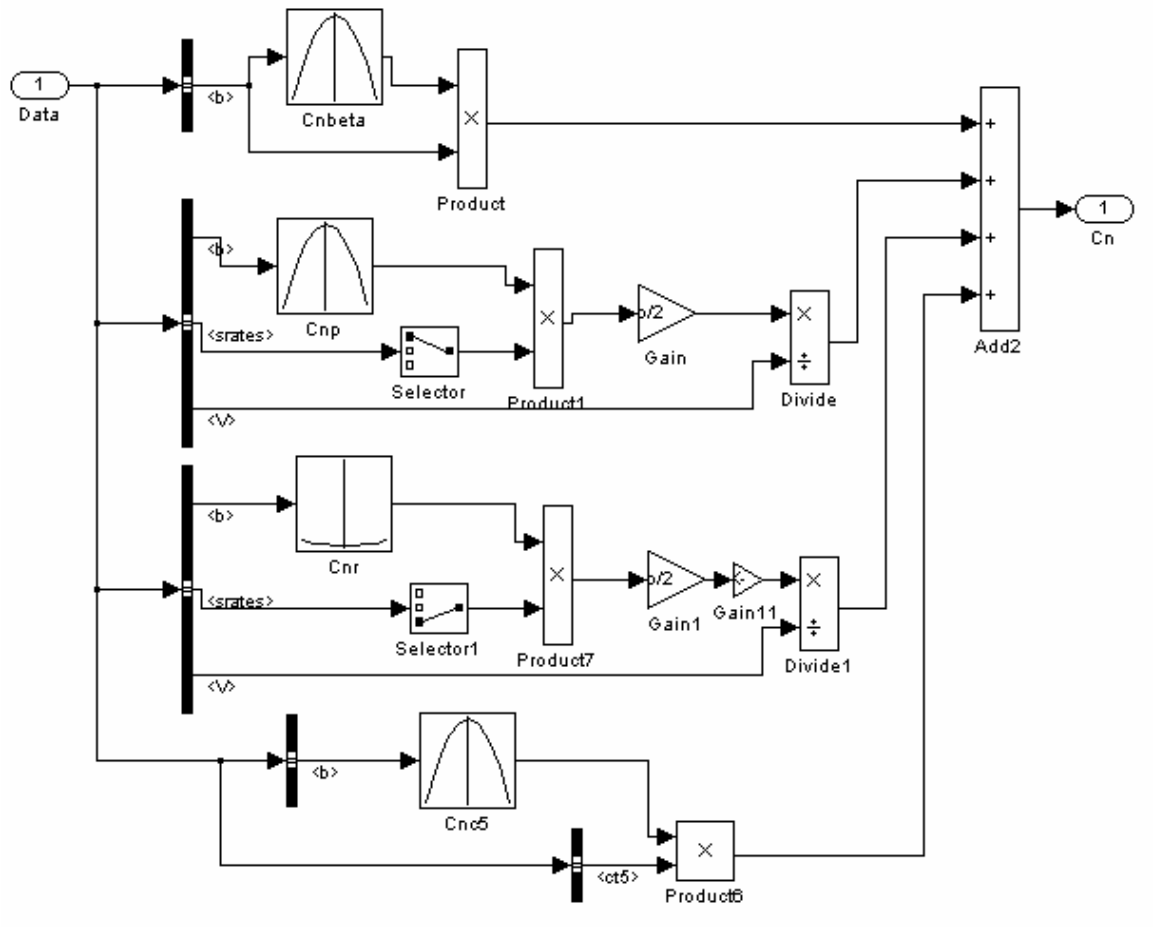

Stability to Body Coordinate Transformation

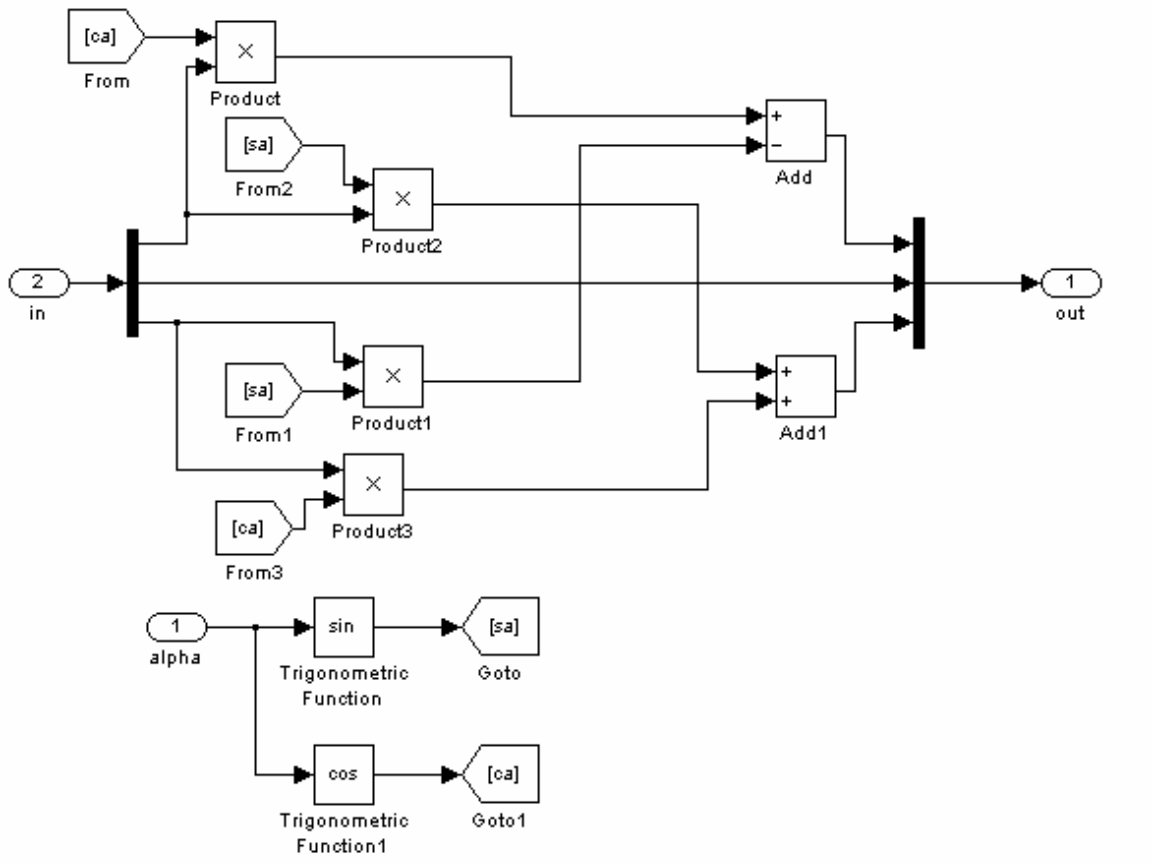

Data Conditioning

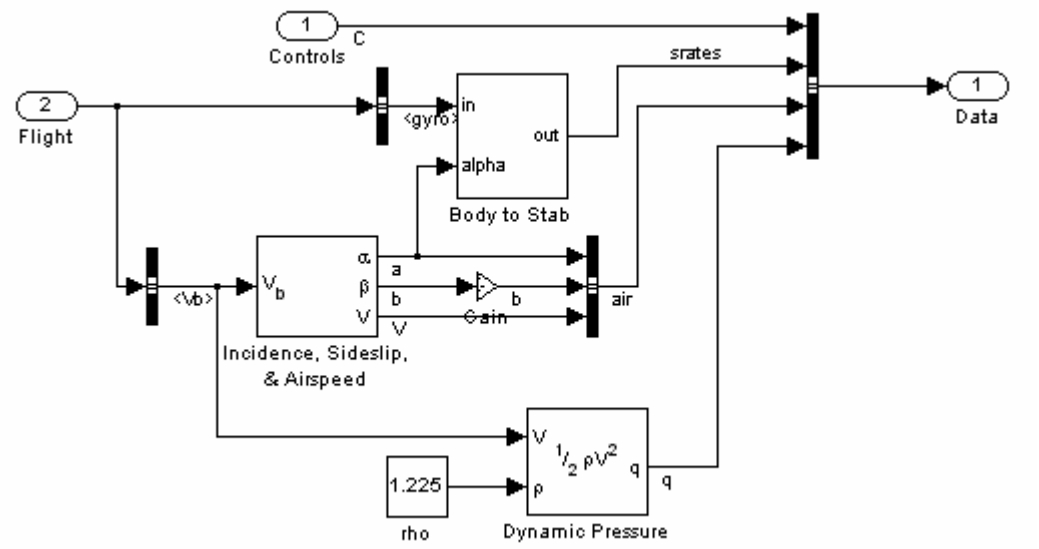

Appendix D: Non-Linear Simulation Stability Derivatives for NXT2

Note: All derivatives are per radian.

The following derivatives are functions of Alpha from -20 to 20 in 5º steps.

CLalpha	Cmalpha	CLq	Cmq
3.836858	-0.9722	14.90071	-30.5858
4.111168	-1.2097	15.1737	-31.212
4.291695	-1.41045	15.2991	-31.6008
4.370299	-1.56834	15.27309	-31.749
4.344337	-1.67858	15.09647	-31.6556
4.216822	-1.73781	14.7746	-31.3213
3.996204	-1.74425	14.31726	-30.7486
3.695804	-1.69768	13.73834	-31.212
3.332912	-1.59954	13.05545	-28.9073

CLc1	CLc2	CLc3	CLc4
0.281744	0.281687	0.585835	0.585835
0.302945	0.302888	0.617923	0.617923
0.319161	0.319104	0.639984	0.639984
0.32959	0.32959	0.650985	0.650985
0.333715	0.333715	0.65047	0.65047
0.331366	0.331366	0.638551	0.638551
0.322656	0.322656	0.615803	0.615803
0.307988	0.307988	0.583314	0.583314
0.288162	0.288104	0.542574	0.542574

Cmc1	Cmc2	Cmc3	Cmc4
0.145084	0.145084	-1.4686	-1.4686
0.14686	0.14686	-1.53593	-1.53593
0.146172	0.146172	-1.58085	-1.58085
0.143135	0.143135	-1.60205	-1.60205
0.137807	0.137807	-1.5989	-1.5989
0.130358	0.130358	-1.57145	-1.57145
0.12096	0.121018	-1.52057	-1.52057
0.110016	0.110016	-1.4478	-1.4478
0.097754	0.097754	-1.35532	-1.35532

efficiency	Cdc1	Cdc2	Cdc3	Cdc4
0.8304	-0.09122	-0.09122	-0.16583	-0.16583
0.8304	-0.07082	-0.07082	-0.12852	-0.12852
0.8306	-0.04813	-0.04813	-0.08733	-0.08733
0.8309	-0.02384	-0.02384	-0.04349	-0.04349
0.6694	0.001318	0.001318	0.001662	0.001662
0.829	0.026645	0.026645	0.046757	0.046757
0.8296	0.051284	0.051284	0.090419	0.090419
0.8298	0.07449	0.07449	0.131332	0.131332
0.8299	0.095634	0.095634	0.168233	0.168233

The following derivatives are functions of Beta from -20 to 20 in 5º steps.

CYbeta	Clbeta	Cnbeta	CYp
-0.80267	-0.07665	0.013099	-0.16806
-0.90266	-0.08666	0.014812	-0.17279
-0.97631	-0.09404	0.016075	-0.1762
-1.02142	-0.09856	0.016849	-0.17826
-1.03664	-0.10008	0.017112	-0.17898
-1.02149	-0.09857	0.016854	-0.17833
-0.97644	-0.09405	0.016085	-0.17632
-0.90284	-0.08669	0.014827	-0.17297
-0.80291	-0.07668	0.013118	-0.1683

Clp	Cnp	CYr	Clr	Cnr
-0.23452	0.025613	1.017826	0.088138	-0.63494
-0.24107	0.026341	1.046239	0.090599	-0.65266
-0.24578	0.026868	1.066689	0.09237	-0.66542
-0.24863	0.027191	1.079021	0.093438	-0.67311
-0.24958	0.027307	1.083141	0.093795	-0.67568
-0.24863	0.027215	1.079018	0.093438	-0.6731
-0.2458	0.026916	1.066682	0.09237	-0.66541
-0.24109	0.026413	1.046229	0.090599	-0.65265
-0.23454	0.025708	1.017813	0.088138	-0.63492

CYc1	CYc2	CYc3	CYc4	CYc5
0.07025	-0.06607	-0.09208	0.087554	-0.29458
0.074777	-0.07157	-0.09781	0.094316	-0.31125
0.077985	-0.07575	-0.10188	0.099473	-0.32352
0.079704	-0.07856	-0.10411	0.102911	-0.33108
0.079876	-0.07988	-0.10446	0.104458	-0.3336
0.078558	-0.0797	-0.10291	0.104114	-0.33108
0.075751	-0.07799	-0.09947	0.101879	-0.32352
0.071568	-0.07483	-0.09432	0.097811	-0.31125
0.066124	-0.07031	-0.08755	0.092081	-0.29458

Clc1	Clc2	Clc3	Clc4	Clc5
0.15534	-0.04103	0.078157	-0.00579	-0.03134
0.144453	-0.05552	0.069963	-0.01369	-0.03306
0.131733	-0.07094	0.060967	-0.02246	-0.03438
0.11758	-0.08669	0.051455	-0.03192	-0.03518
0.102395	-0.1024	0.041657	-0.04166	-0.03547
0.086695	-0.11758	0.031916	-0.05146	-0.03518
0.070937	-0.13173	0.022462	-0.06097	-0.03438
0.055524	-0.14445	0.013695	-0.06996	-0.03306
0.041027	-0.15534	0.005787	-0.07816	-0.03134

Cnc1	Cnc2	Cnc3	Cnc4	Cnc5	Cdc5
0.014612	-0.00372	0.05455	-0.05896	0.187256	-0.08412
0.013523	-0.00504	0.059306	-0.06274	0.197857	-0.06544
0.01232	-0.00653	0.06303	-0.06538	0.205707	-0.04475
0.010944	-0.00802	0.065494	-0.0667	0.210463	-0.02269
0.009512	-0.00951	0.066755	-0.06675	0.212067	0
0.008022	-0.01094	0.066697	-0.06549	0.210463	0.022748
0.006532	-0.01232	0.065322	-0.06297	0.205707	0.044751
0.005042	-0.01352	0.062744	-0.05931	0.197857	0.065437
0.003667	-0.01461	0.058962	-0.05455	0.187256	0.084116